U.S. Department of Transportation

Federal Railroad Administration

Advanced Cushioning Devices for Freight Locomotives

Office of Research,
Development,
and Technology
Washington, DC 20590

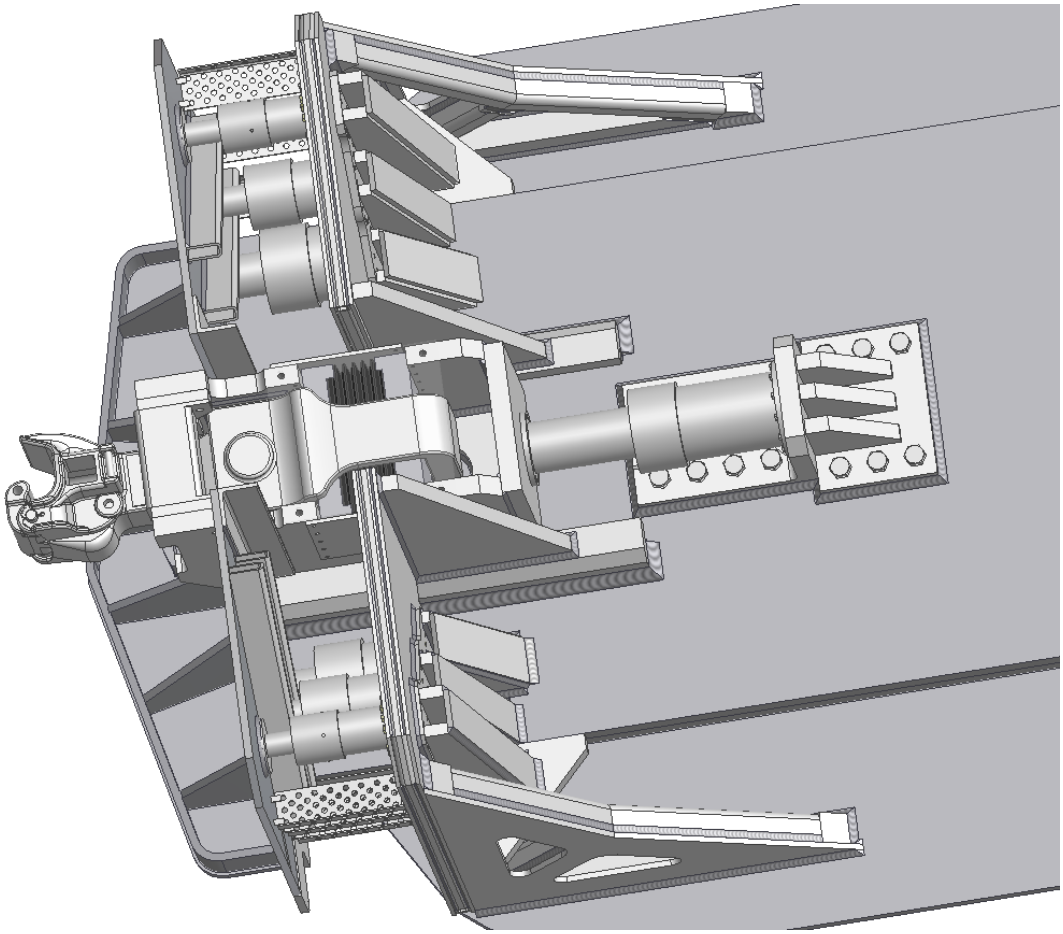

DOT/FRA/ORD-16/27

Final Report
July 2016

REPORT DOCUMENTATION PAGE

Form Approve
OMB No. 0704-0188

1. AGENCY USE ONLY (Leave blank)	2. REPORT DATE	3. REPORT TYPE AND DATES COVERED
	July 2016	Technical Report – June 2011

4. TITLE AND SUBTITLE
Advanced Cushioning Devices for Freight Locomotives

5. FUNDING NUMBERS
DTFR53-07-D-00003
Task Order 011

6. AUTHOR(S)
Basant Parida, James Carter, and Abdullatif K. Zaouk

7. PERFORMING ORGANIZATION NAME(S) AND ADDRESS(ES)
QinetiQ North America
Technology Solutions Group
350 Second Avenue
Waltham, MA 02451-1196

8. PERFORMING ORGANIZATION REPORT NUMBER

9. SPONSORING/MONITORING AGENCY NAME(S) AND ADDRESS(ES)
U.S. Department of Transportation
Federal Railroad Administration
Office of Railroad Policy and Development
Office of Research, Development, and Technology
Washington, DC 20590

10. SPONSORING/MONITORING AGENCY REPORT NUMBER
DOT/FRA/ORD-16/27

11. SUPPLEMENTARY NOTES
Program Manager: John Punwani

12a. DISTRIBUTION/AVAILABILITY STATEMENT
This document is available to the public online through the FRA Web site at http://www.fra.dot.gov.

12b. DISTRIBUTION CODE

13. ABSTRACT (Maximum 200 words)

This report describes the design and analysis of an advanced cushioning device for freight locomotives. The device, or crash energy management system, minimizes the risk of locomotive override in the event of an in-line collision. As part of the system, energy dissipative elements integrated with locomotive structures reduce the speed over a portion of impact. In doing so, the overall post-impact kinetic energy is reduced, and the locomotive remains on the rails for a longer duration following collision. Controlling the deformation in the front end eliminates the formation of a ramp that will allow the locomotive front-wheels to climb over the impacted car wheels.

Researchers propose a system that decouples the pilot plate from the main locomotive sill and provides a reinforced frontal structure just ahead of the front trucks. Energy dissipative elements installed between the two parallel plate structures provide a means of controlling the movement of the pilot plates during impact and transferring loads directly to the locomotive sill. This process couples the stiffest portions of the impacted car with the stiffest portions of the locomotive. The system has three important features: (1) it provides improved load transfer between the locomotive and the impacted car, (2) it controls deformation at the time of impact and dissipates a significant amount of kinetic energy, and (3) it uses the mass associated with a stationary consist to its best advantage as the locomotive comes to a stop.

14. SUBJECT TERMS

15. NUMBER OF PAGES
81

16. PRICE CODE

17. SECURITY CLASSIFICATION OF REPORT	18. SECURITY CLASSIFICATION OF THIS PAGE	19. SECURITY CLASSIFICATION OF ABSTRACT	20. LIMITATION OF ABSTRACT
Unclassified	Unclassified	Unclassified	

NSN 7540-01-280-5500 Standard Form 298 (Rev. 2-89)

METRIC/ENGLISH CONVERSION FACTORS

ENGLISH TO METRIC	METRIC TO ENGLISH
LENGTH (APPROXIMATE)	**LENGTH (APPROXIMATE)**
1 inch (in) = 2.5 centimeters (cm)	1 millimeter (mm) = 0.04 inch (in)
1 foot (ft) = 30 centimeters (cm)	1 centimeter (cm) = 0.4 inch (in)
1 yard (yd) = 0.9 meter (m)	1 meter (m) = 3.3 feet (ft)
1 mile (mi) = 1.6 kilometers (km)	1 meter (m) = 1.1 yards (yd)
	1 kilometer (km) = 0.6 mile (mi)
AREA (APPROXIMATE)	**AREA (APPROXIMATE)**
1 square inch (sq in, in^2) = 6.5 square centimeters (cm^2)	1 square centimeter (cm^2) = 0.16 square inch (sq in, in^2)
1 square foot (sq ft, ft^2) = 0.09 square meter (m^2)	1 square meter (m^2) = 1.2 square yards (sq yd, yd^2)
1 square yard (sq yd, yd^2) = 0.8 square meter (m^2)	1 square kilometer (km^2) = 0.4 square mile (sq mi, mi^2)
1 square mile (sq mi, mi^2) = 2.6 square kilometers (km^2)	10,000 square meters (m^2) = 1 hectare (ha) = 2.5 acres
1 acre = 0.4 hectare (he) = 4,000 square meters (m^2)	
MASS - WEIGHT (APPROXIMATE)	**MASS - WEIGHT (APPROXIMATE)**
1 ounce (oz) = 28 grams (gm)	1 gram (gm) = 0.036 ounce (oz)
1 pound (lb) = 0.45 kilogram (kg)	1 kilogram (kg) = 2.2 pounds (lb)
1 short ton = 2,000 pounds (lb) = 0.9 tonne (t)	1 tonne (t) = 1,000 kilograms (kg) = 1.1 short tons
VOLUME (APPROXIMATE)	**VOLUME (APPROXIMATE)**
1 teaspoon (tsp) = 5 milliliters (ml)	1 milliliter (ml) = 0.03 fluid ounce (fl oz)
1 tablespoon (tbsp) = 15 milliliters (ml)	1 liter (l) = 2.1 pints (pt)
1 fluid ounce (fl oz) = 30 milliliters (ml)	1 liter (l) = 1.06 quarts (qt)
1 cup (c) = 0.24 liter (l)	1 liter (l) = 0.26 gallon (gal)
1 pint (pt) = 0.47 liter (l)	
1 quart (qt) = 0.96 liter (l)	
1 gallon (gal) = 3.8 liters (l)	
1 cubic foot (cu ft, ft^3) = 0.03 cubic meter (m^3)	1 cubic meter (m^3) = 36 cubic feet (cu ft, ft^3)
1 cubic yard (cu yd, yd^3) = 0.76 cubic meter (m^3)	1 cubic meter (m^3) = 1.3 cubic yards (cu yd, yd^3)
TEMPERATURE (EXACT)	**TEMPERATURE (EXACT)**
[(x-32)(5/9)] °F = y °C	[(9/5) y + 32] °C = x °F

QUICK INCH - CENTIMETER LENGTH CONVERSION

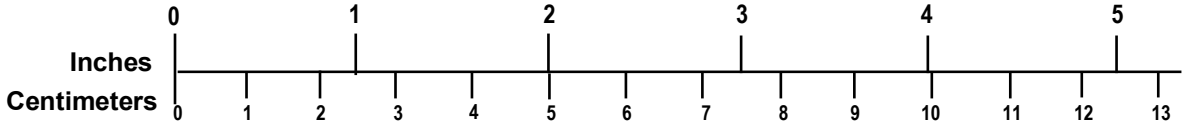

QUICK FAHRENHEIT - CELSIUS TEMPERATURE CONVERSIO

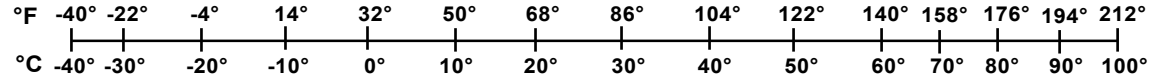

For more exact and or other conversion factors, see NIST Miscellaneous Publication 286, Units of Weights and Measures. Price $2.50 SD Catalog No. C13 10286

Updated 6/17/98

Acknowledgments

The authors would like to thank and acknowledge the continued support and guidance that the Office of Research and Development of the Federal Railroad Administration provided. In particular, the authors extend their gratitude to the Contracting Officer's Representative (COR), Mr. John Punwani.

Contents

Illustrations

Tables

Executive Summary

This report describes the design and analysis of an advanced cushioning device for freight locomotives that may constitute a crash energy management (CEM) system. The device minimizes the risk of locomotive override in the event of an in-line collision.

After assessing alternative high-capacity shock absorbers, QinetiQ North America (QNA), Technology Solutions Group (TSG), designed and evaluated a compact shock energy absorber (SEA) system. This device has potential applications in CEM within the restricted space of a freight locomotive's fore-body. Researchers performed a series of laboratory scale tests to understand and evaluate the deformation and energy absorption behavior of cylindrical bars of ultrahigh molecular weight–polyethylene (UHMWPE) material. UHMWPE was placed within the confines of a steel cylinder and subjected to high-speed impact by a plunger with a conical front. An Instron servo-hydraulic test machine performed a quasi-static compression test. For a dynamic impact test, a 175-pound (lb) pendulum impacted the plunger at a velocity of approximately 17 feet (ft) per second (s).

The test results offered insights into the deformation and energy absorption behavior of the UHMWPE material, including its phase transition from solid to viscous fluid above a critical flow stress under three-dimensional (3D) compression. Results demonstrate that the phase transition process is reversible, and the associated critical flow stress magnitude depends on the rate of material strain or the impact velocity of the plunger. Furthermore, the magnitude of peak dynamic force developed during high-speed impact depends on the velocity of impact as well as on the cross-sectional area ratio of the UHMWPE material within the cylinder and the plunger.

Through the use of the critical flow stress of UHMWPE under quasi-static compression loading as baseline data, a dynamic stress multiplying factor (DSMF) was defined and evaluated. DSMF estimates the critical flow stress and the corresponding peak dynamic force magnitude under high-speed impact conditions. On the basis of the results of several pendulum impact tests, it was possible to evaluate the high strain rate (HSR) deformation and energy absorption behavior of UHMWPE material under high-speed impact conditions.

The research team designed and fabricated a larger SEA prototype capable of absorbing about 80,000 ft-lb (60 kilojoules (kJ)) of energy. The prototype underwent a 27,000-pound drop hammer test at the ASF-Keystone facility in Pittsburgh, PA. The SEA prototype successfully absorbed the crash energy associated with a 30-inch (in) drop of the hammer. Finite element analysis (FEA) had predicted the aforementioned results for a small stroke of the plunger. The peak compression force magnitude following impact also matched the FEA prediction.

The results of this prototype validation test enabled QNA TSG to design a set of compact SEAs of varying sizes for application to a CEM system located in the front of a locomotive.

The FEA model without a SEA was validated with an earlier full-scale locomotive crashworthiness test composed of a consist of stationary hopper cars at the Transportation Technology Center (TTC) in Pueblo, CO. The simulated results of a frontal collision of a locomotive with SEAs constituting an integral part of the CEM system revealed no locomotive override up to a closing speed of 30 miles per hour (mph).

1. Introduction

Ensuring the safety of train crews and the public is a vital area for railroad research. The Federal Railroad Administration (FRA) sponsors a program of research aimed at improving the crashworthiness of locomotives and reducing the severity of rail collisions. The research addresses the structural, dynamic, and human factors related to rail safety. The work described here is part of this ongoing program.

The program's purpose is to develop and validate the use of CEM to limit the possibility of override resulting from an in-line collision. CEM absorbs a portion of the impact energy associated with an in-line collision between a locomotive and another rail vehicle. Managing the energy during a collision event is beneficial because it reduces damage from peak impact forces and decreases the potential for the locomotive to override an impacted vehicle.

Although car cushioning devices exist in the draft gear of freight cars, a SEA within the locomotive to prevent override does not exist. To address this gap in technology, QinetiQ North America Technology Solutions Group (QNA TSG) partnered with ASF-Keystone, Inc., to develop an advanced cushioning device that will operate in collision scenarios. ASF-Keystone is an internationally known manufacturer and supplier of a variety of rail car cushioning devices, draft gears, and other rail-related products. ASF-Keystone's participation included testing a prototype cushioning device at its facility, in addition to providing consulting services to QNA TSG.

Freight locomotive couplers experience large draft (tensile) forces during transit and large buff (compressive) forces in push modes. In collisions, shock loads generated along the coupling mechanisms result in extreme buff loading. Currently, locomotives are not equipped with adequate mechanisms to absorb the collision energy. This results in excessive damage to both the front-end components of the locomotive and impacted structures.

When the impacted structure is stiffer than the locomotive (or vice versa), the deformations created can cause derailment. In addition, if structures deform under the locomotive, the result may be an override of the locomotive on the other vehicle. FRA-sponsored tests at the Transportation Technology Center (TTC) conducted by QNA TSG and the Transportation Technology Center, Inc. (TTCI) showed that a locomotive can override the trailing car of a consist following a rear-end collision at 32 mph. As the locomotive climbed up the impacted hopper car, it crushed the sidewalls of the car. In addition, the wheels on the hopper car pushed the locomotive trucks backwards, puncturing the locomotive fuel tank. As evident from these tests, locomotive overrides result in hazardous vehicle crash scenarios.

This report describes the design, development, and associated testing and analysis of a CEM system for the front end of a locomotive. The system provides impact control between a locomotive and an impacted car by dissipating energy and reducing the likelihood of derailment or override. The system design limits the loads associated with a 30 mph in-line collision.

The present research used data collected during full-scale crash testing at TTC. The dynamics of the override scenario were further analyzed using advanced FEA. These analyses allowed for the study of crash dynamics at various speeds and impact conditions.

1.1 Description of In-Line Collision and Override

The following discussion provides an overview of the basic dynamics associated with collision and override. When a locomotive meets a trailing car during an in-line collision, the initial contact occurs at the draft gear. Figure 1 shows the alignment of the draft gear prior to a collision test. It is evident from the position of the draft gear that the locomotive (on the right) is slightly higher than that of the hopper car (on the left). In addition, the main structure of the hopper car is roughly level with its draft gear, whereas the main structure of the locomotive is 1-2 ft higher.

Figure 1. Mismatch between Hopper Car and Locomotive

The draft gear mismatch allows for derailment and/or override during collision in two ways. First, the height difference of the draft gears allows the locomotive gear to rise over the gear on the hopper car, lifting the front-end of the locomotive. Cushioning devices within the draft gear dissipate a small amount of impact energy, but there is insufficient capacity to accommodate all of the energy.

Second, as the draft gears retract into the structures, the pilot plate and snowplow of the locomotive impact the stiffest portion of the hopper car. As this occurs, the hopper car sill forces the relatively compliant snowplow under the locomotive sill and into the foremost wheels of the front truck. This creates a ramp for the locomotive, guiding it over the sill of the hopper car and lifting it off the rails. Figure 2 shows this ramp formation during the in-line collision test.

Figure 2. Pilot Plate Forced under Locomotive Structure

As the locomotive starts to climb the adjacent car, the locomotive protrudes into the car's frame. This generates large deformations, spilling the load and allowing the rear trucks of the hopper car to contact the forward trucks of the locomotive. Figure 3 shows the impact between the trucks and the general rise of the locomotive. Note that in this particular collision, displacement of the forward trucks created a secondary impact with the fuel tank, crushing and puncturing the tank structure.

Figure 3. Locomotive Riding the Pilot Plate over Hopper Car Wheels

These results indicate that override occurs when there is significant contact between the locomotive and the rear wheelset of the struck rail car, and the sill of the struck rail car is highly loaded and very strong. This indicates that the two most important factors in preventing override are managing the high loads from the locomotive-rail car frame contact and the contact between the rear wheel set of the impacted railcar and the locomotive.

Figure 4 is a composite of photographs from another field test that shows override in a collision between a locomotive and a lead hopper car. These figures each have a horizontal line drawn at the height of the top of the hopper car to show when the locomotive moved vertically relative to the hopper car (i.e., when it started to override). In this test, the locomotive struck a consist of several loaded hopper cars (out of the frame to the right); therefore, the inertia from the loaded cars caused substantial force within the sill of the struck hopper car.

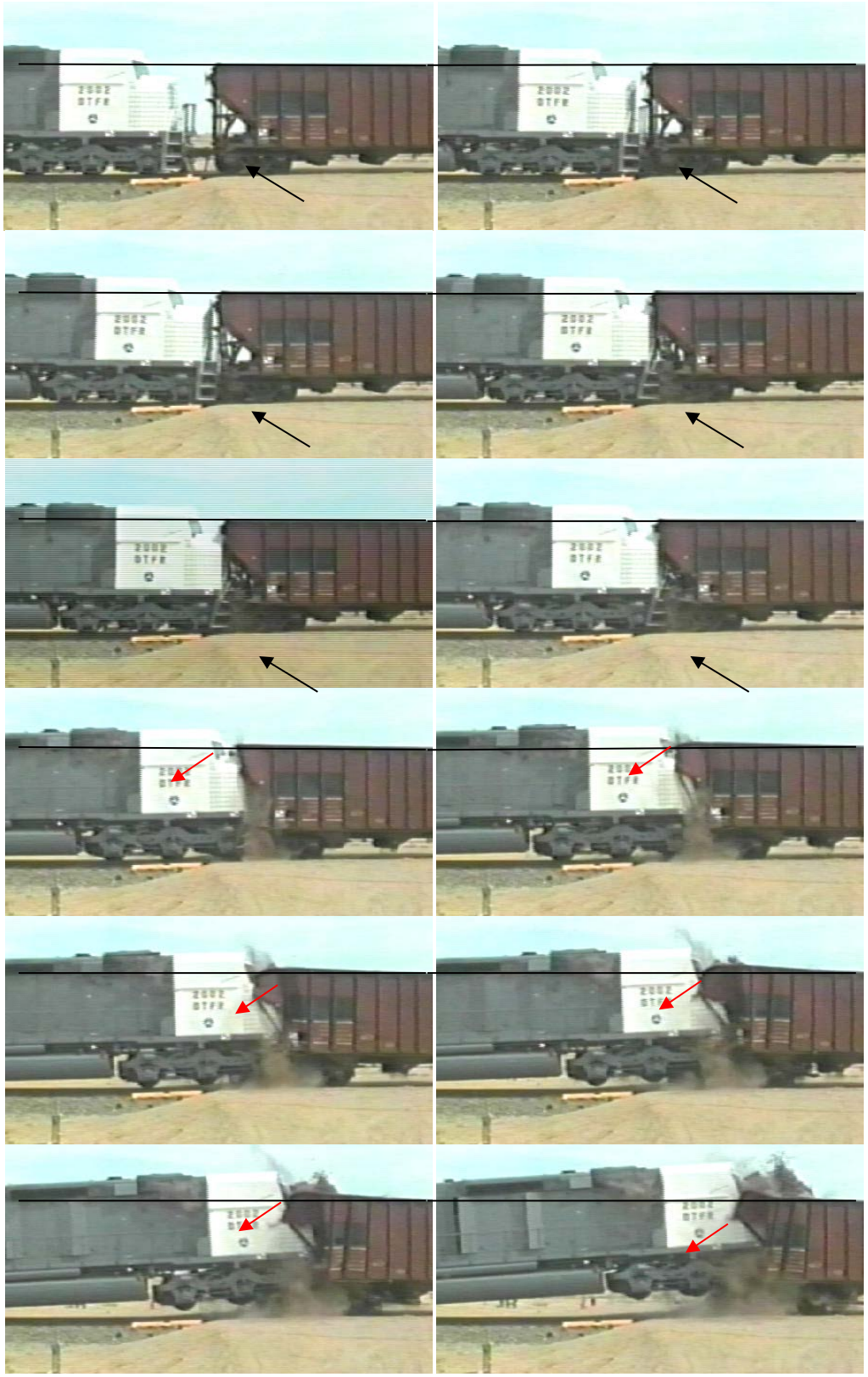

Figure 4. Video Frames Showing the Sequence that Leads to Override

1.2 Approach to CEM

To better mitigate the overall impact forces, QNA TSG proposed to retrofit the front end of a locomotive with a CEM system. The system provided a means of transferring the loads from the stiffest sections of the impacted car to the locomotive sill through an alternative force flow path. Within the force transfer elements, an area for energy dissipation and damping was included that offered both a controlled deformation and a reduction in the peak impact force magnitude. Figure 5 shows a schematic of the configuration's essential elements.

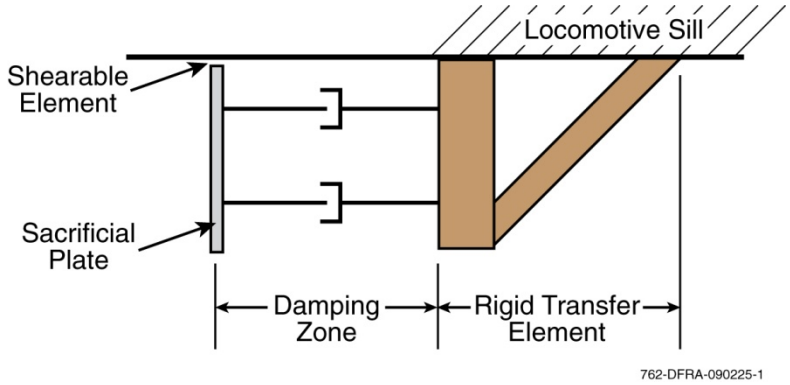

Figure 5. Schematic of Coupling Structures

Once the energy generated during the collision is dissipated and controlled, the inertia of the locomotive will continue to follow the rails, reducing the risk of override and limiting the damage to the undercarriage to predefined areas. In addition, if the energy during the collision is mitigated, the system allows for a controlled stop limiting damage to the overall consist.

1.3 Preliminary Design Approach

The overall goal of this program is to develop a means of controlling the deformation of the front end of the locomotive during an in-line collision. As part of the system, structural integration of energy dissipative elements reduces the speed of the locomotive over a portion of impact. In doing so, the overall post-impact kinetic energy (KE) is reduced, and the locomotive remains on the rails for a longer time after the collision. Controlling the deformation in the front end eliminates the possibility that the locomotive front wheels will climb over the impacted car wheels. The reduced KE limits the conversion of inertia into the upward motion required to raise the locomotive off the rails, thus mitigating the tendency to override.

To accomplish this, the researchers developed a system that decouples the pilot plate from the main locomotive sill and provides a reinforced frontal structure just ahead of the front trucks. Energy dissipative elements installed between the two parallel plate structures provide a means of controlling the movement of the pilot plates during impact and transferring loads directly to the locomotive sill. This couples the stiffest portions of the impacted car to the stiffest portions of the locomotive. The system has three desirable effects. First, it provides improved load transfer between the two cars. Second, it provides controlled deformation at the time of impact, dissipating a significant amount of KE. Last, it uses the car masses to best advantage as the consist comes to a stop. Figure 6 shows a schematic layout of the energy dissipative systems, or shock absorbers. Three shock absorbers are located between the pilot and reinforced reaction plates on both sides of the locomotive. An additional central shock absorber is located behind the draft gear.

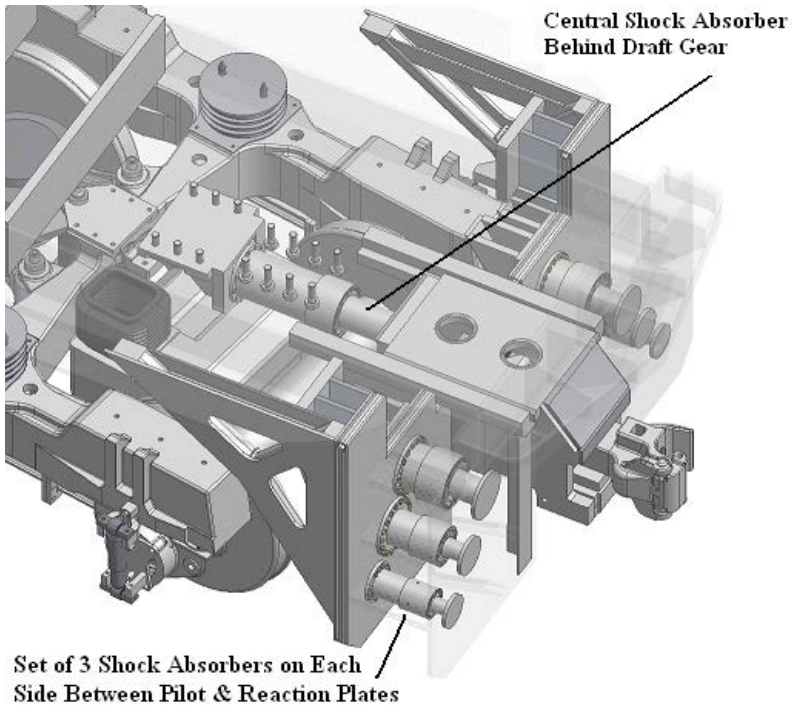

Figure 6. Schematic Layout of Energy Dissipative Systems in Locomotive Fore-Body

1.4 Scope

This report describes the design and analysis of a CEM system for a freight locomotive. The system reduces the risk of locomotive override in the event of an in-line collision. In addition, the report describes the design of a critical component of the CEM system, a high-capacity energy damper. This device is customizable to suit different configurations, and it offers shock energy dissipation capability for reducing the risk of override within the space constraints of a locomotive structure.

1.5 Organization of the Report

Section 2 describes the basic structural design of the CEM system. Section 3 describes the FEA and a description of the crash dynamics associated with an in-line railway collision. Section 4 covers the design, development, and testing of a solid-state damping element that meets the energy dissipation requirements determined through analysis. Conclusions and recommendations are provided in Section 5.

2. Design of a Locomotive CEM System

Typical rail accidents result in large amounts of rolling mass stopping in semi-controlled fashion. The energies associated with these events have a large potential to damage the right-of-way, the rolling stock, and any surrounding infrastructure. In the process, large forces influence the physical components of the locomotive and any impacted structures.

Generally, two or more locomotives power the movement of a train consist most often composed of a large number of heavily loaded or empty cars. Each locomotive is fitted with couplers and draft gears at its front and rear ends. The draft gear design provides adequate shock absorbing capacity for loads associated with typical railroad operational conditions. However, during a collision, the loads can greatly exceed the draft gear's capacity. In an in-line, frontal crash, these loads can reach several million pounds. Once the forces exceed the capacity of the draft gear, the remaining energy begins to deform the locomotive structures or those of the impacted object. Structural deformation under the locomotive sill redirects the energy, lifting the locomotive from the rails as the structure overrides the impacted object. During an in-line collision, this is typically a loaded freight car. A recent U.S. Department of Transportation (USDOT) report [1] indicates that a typical impact generates 20 million in-lb of KE. Once redirected, this energy is sufficient to lift a locomotive approximately 10 feet above the tracks during an override. Therefore, an effective CEM system must be capable of dissipating a significant portion of the energy responsible for override.

2.1 CEM Approach

The transfer of KE originating from an in-line collision between a locomotive and a trailing car begins at the coupler and transfers through the draft gear and into the rear structure of the draft gear pocket and ultimately to the sill. External structures (those outside of the draft gear) impact the pilot plate and snowplow bending these structures and finally impacting the front trucks of the locomotive. In practice, this implies that any CEM system needs to be located in this space to be effective. The overall length of travel is less than 2 ft.

Review of data from full-scale collision tests at the TTC in Pueblo, CO, indicated two primary factors are responsible locomotive override. The first factor is the deformation of structures under the locomotive sill. Effectively, this creates a ramp for the forward structure of the locomotive to ride over the rear sill of the impacted car. In one case, this deformation occurred at the pilot plate. In another, the draft gear pocket failed, allowing the rear end of the gear to drop from the pocket, and the locomotive sill rode over the coupler into the impacted car. The CEM system must control the deformation to prevent these impact phenomena.

The second important factor is the enormous momentum and KE available at the time of impact. Once the mass of the locomotive begins to climb, inertia of both the locomotive itself along with the impulse provided by trailing cars continue to drive the locomotive upward. The CEM system must be capable of dissipating a significant portion of this energy to mitigate the possibility of override.

Therefore, the CEM system design must be compact, provide controlled deformation through the majority of the event, and dissipate an appreciable quantity of energy.

To assess the viability of the energy absorption in the locomotive front end, the researchers estimated the amount of KE dissipation needed to reduce the operational speed of a locomotive

to some finite level. Figure 7 shows the relationship of KE reduction to speed change, based on closing speed at the time of collision.

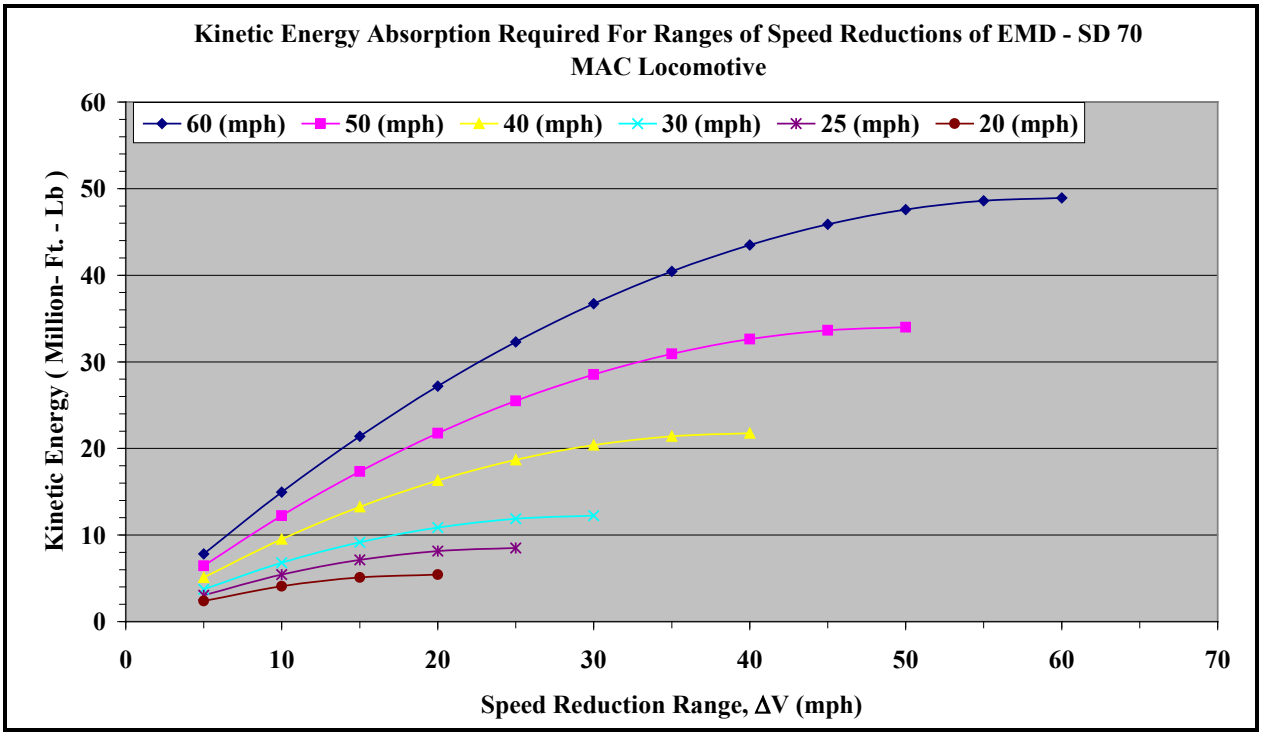

Figure 7. Change in KE Absorption Required vs. Locomotive Speed Reductions

These calculations assume that the energy is a function of the locomotive mass only and that there is little or no effect from braking. The curves in Figure 7 show that effectively slowing the locomotive requires reductions in KE of several million feet-pounds, regardless of closing speed. For example, for a closing speed of 30 mph, a 5-mile per hour speed reduction requires 4 million ft-lb of energy dissipation. To reduce speed by 20 mph, 11 million ft-lb are required. The design goal is to mitigate override in a 30 mph collision. This sets a bound on the range of energy dissipation required within the CEM.

From drawings, photographs, and field knowledge of the SD70MAC locomotive, the most viable location for the energy dissipative elements is underneath the front ladders or stairways on both sides of the cab. Figure 8 provides a schematic representation of the approach. However, this limits the permissible length of any element to approximately 18 in. The limit stems from the need to reinforce the reaction structure tied to the locomotive sill while maintaining clearance from the front trucks. There is sufficient room to place multiple elements on either side of the draft gear. Additionally, altering or adding an element allows for an increase in the capacity of the draft gear. There is space to extend the pocket rearward along the locomotive centerline before interference with the trucks becomes an issue.

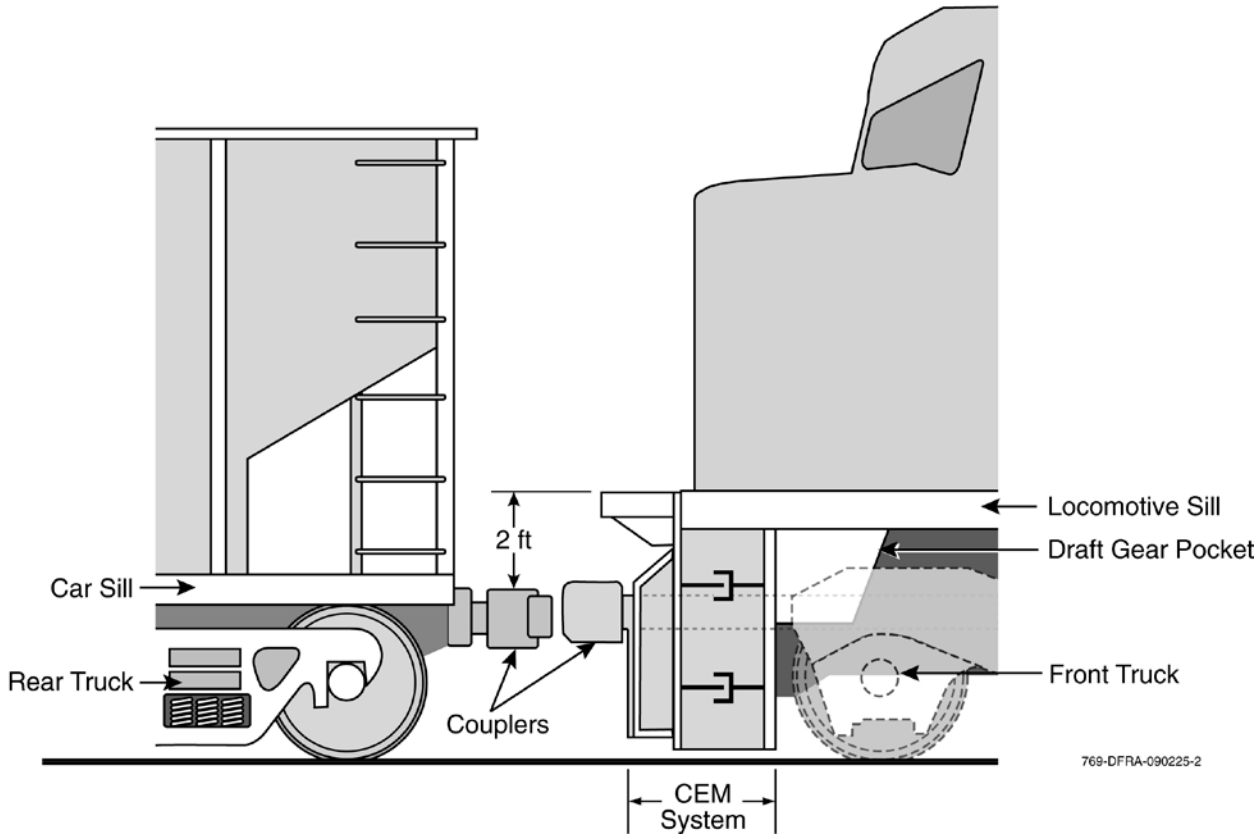

Figure 8. Side View of a Locomotive to Car Impact with CEM System

The draft gear within the locomotive has sufficient capacity to dissipate 500,000 lb (defined buff load). If loads exceed this level, the pin securing the draft gear shears. This allows the entire assembly to move backward into the pocket. Eventually, the assembly will force its way out, through the rear wall of the pocket, creating a potential ramp as described above. This dissipation and deformation reduces the overall impact energy by some amount. As the coupler and draft gear push backward, the front pilot plate and snowplow make contact with the sill of the impacted car.

In addition to energy dissipation, the CEM system must control the deformation of impacted structures during the collision. Movement of physical parts must provide a load path back to the rigid parts of the locomotive. Specifically, structures within the system must direct loads applied at or near the pilot plate by the impacted car to the locomotive sill. This allows the mass of the impacted car to help decelerate the locomotive. Coupled transfer of loads between cars minimizes the chance of derailment and override.

To accomplish this, the pilot plate on the locomotive shears away from the sill at impact. The energy dissipation system guides the plate back parallel to the rails, providing maximum control of the loads from the impacted car. A reinforced coupling plate between the trucks and the pilot plate provides a load path back to the sill.

FEA models of the locomotive allowed for simulated evaluation of the CEM system. These models provided simulated structural behavior both with and without the CEM system installed. For the non-CEM cases, results correlated well with test data collected at TTC [1].

2.2 Locomotive CEM System Design

In a frontal collision between a moving consist and an obstruction on the right-of-way, a vast amount of KE needs to be absorbed to prevent damage because of climbing or override of the locomotive. QNA TSG proposed a CEM system composed of both deformable and dissipative elements. The overall goal of the CEM is to reduce the likelihood of override resulting from an in-line collision. An examination of the locomotive fore-body indicates there is limited space to integrate a CEM system. For an EMD SD70MAC locomotive, the maximum usable distance is approximately 22 in. This represents the space from the pilot plate and snowplow to just ahead of the front trucks. Rearranging the basic structural configurations allows for integration of dissipative elements as well as controlled deformation of the impacted structures. Loads transfer from the point of impact back to the locomotive sill, with impact energy dissipated where possible.

2.2.1 Description of Structural Design

Structural space constraints within the locomotive require some distribution of dissipative and structural elements. This approach best uses the space underneath the front ladder (stairway) located in the locomotive fore-body. The designers used structural drawings of the locomotive nose of a generic EMD SD70MAC to guide the design process. EMD provided some details in the form of drawings, with the remainder developed through direct measurements of cab structure and from information from *The Car and Locomotive Cyclopedia* [2]. CAD drawings generated from this information facilitated design options and alternative structural modifications.

Crash dynamics define the required load paths. One path must pass through the coupler and draft gear pocket, because this is the first point of contact between rolling stock. This path is part of the current locomotive structure and requires only modification to be suitable for the CEM system. However, a second path is necessary to transfer load between the frame and trucks of the impacted car to the locomotive sill; this path does not exist. The pilot plate and snowplow do not have sufficient stiffness to transfer impact loads back to the locomotive sill.

To create the second load path, the designers created a relatively stiff reaction plate just forward of the front trucks. This plate is a sandwich of tubular steel sections covered by two steel faceplates. The tubes provide core reinforcements between the plates, increasing the stiffness and reducing the tendency to buckle at impact. Side gussets along the outer edge support the reaction plate. The gusset is a significant increase in stiffness over the current snowplow support and provides a direct load path to the locomotive sill. The pilot plate and snowplow remain in their current location, but the structural connection passes directly aft to the reaction plate rather than a cantilevered connection to the sill. The space between the pilot plate and reaction plate provides space for dissipative elements.

Figure 9 shows the completed arrangement. Where needed, additional box section stiffeners provide greater load-bearing capacity to the reaction plate. Placement of the reaction plate and gussets provide sufficient clearance for truck rotations under normal turning operations. Stiffening of the pilot plate provides for uniform force distribution to the dissipative elements.

In Figure 9, cylinders represent the dissipative elements between the plates. Distribution of these elements allows for maximum use of space between the point of contact (pilot plate) and the final load transfer component. A single large element provides additional capacity directly

behind the draft gear. The type of dissipation is not defined by the geometry. Rather, the total energy capacity of the distributed system must meet the 5- to 10-million feet-per-pound requirement described in Section 2.1.

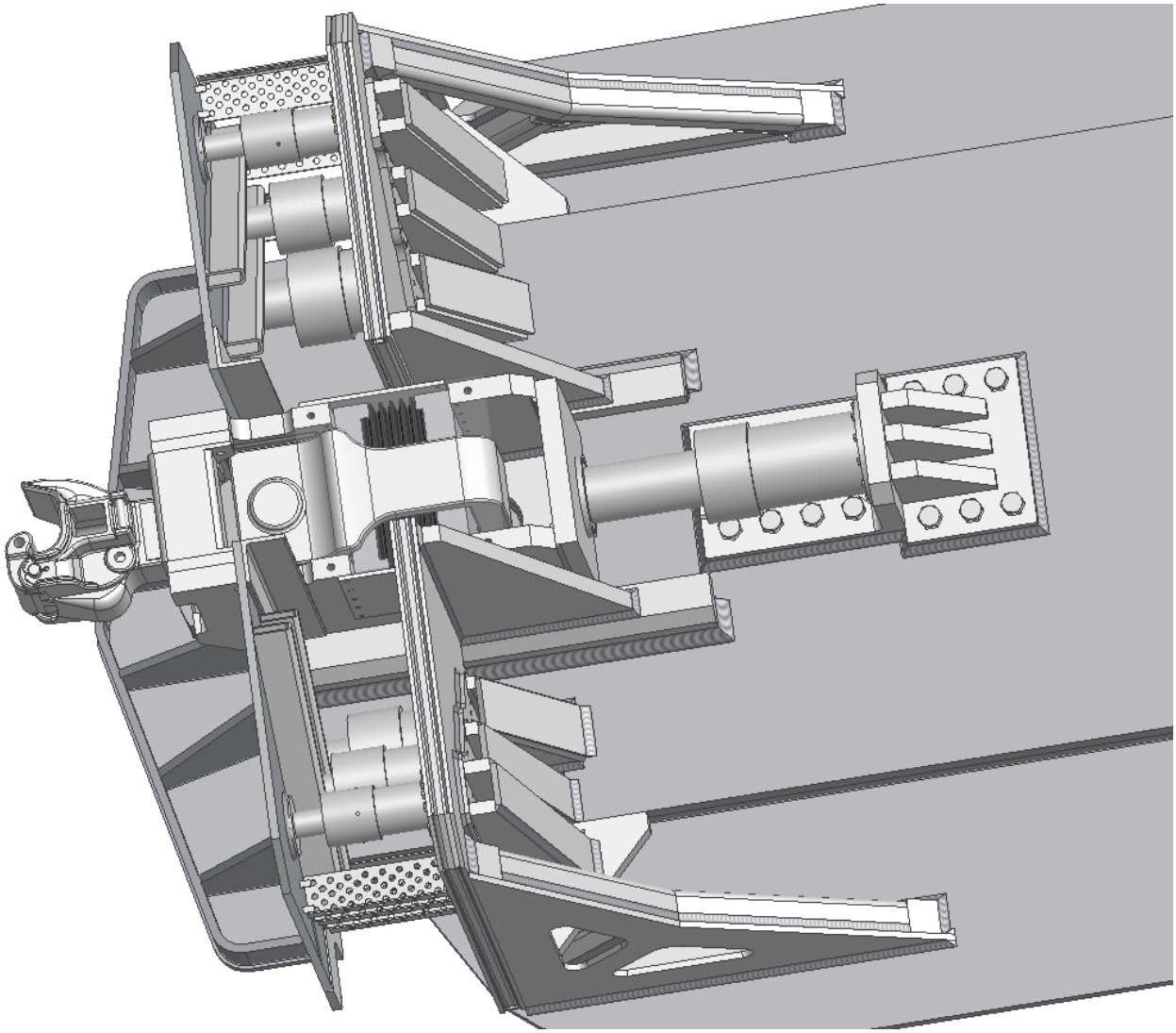

Figure 9. CAD Drawing of the CEM System

With the plates in place, the length available for the dissipation elements is 18 in. This represents the maximum separation distance available between rear face of the pilot plate and the front face of the reaction plate. The largest space available for dissipation is behind the draft gear pocket along the longitudinal axis of the locomotive. One end attaches to the rear of the draft gear, and the other attaches to the sill via a reinforced gusset. Figure 10 shows a detail of this attachment.

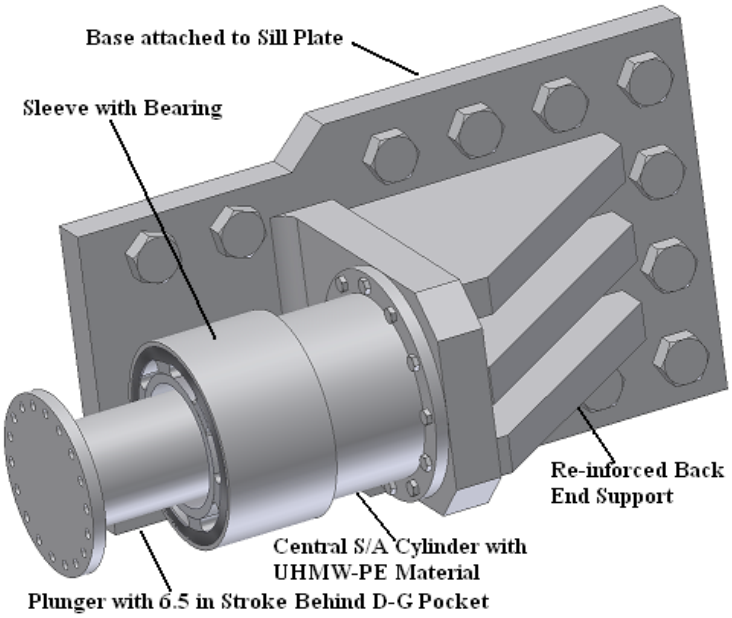

Figure 10. CAD Drawing of the Central SEA behind Draft Gear Pocket

Figure 11 shows a top view of the full CEM system. The pilot plate is transparent in the illustration to allow viewing of the energy dissipation elements. The sidewalls of the draft gear pocket slide axially rather than welding directly to the underside of sill. This allows the draft gear to shift rearward into the dissipation element during impact. The extended stroke provides for increased dissipation as well as control of impulse motion for the longest timeframe possible. This limits underbody deformation and prevents the draft gear from dislodging ahead of the trucks. Table 1 lists the specific geometric details of the various shock absorbing elements.

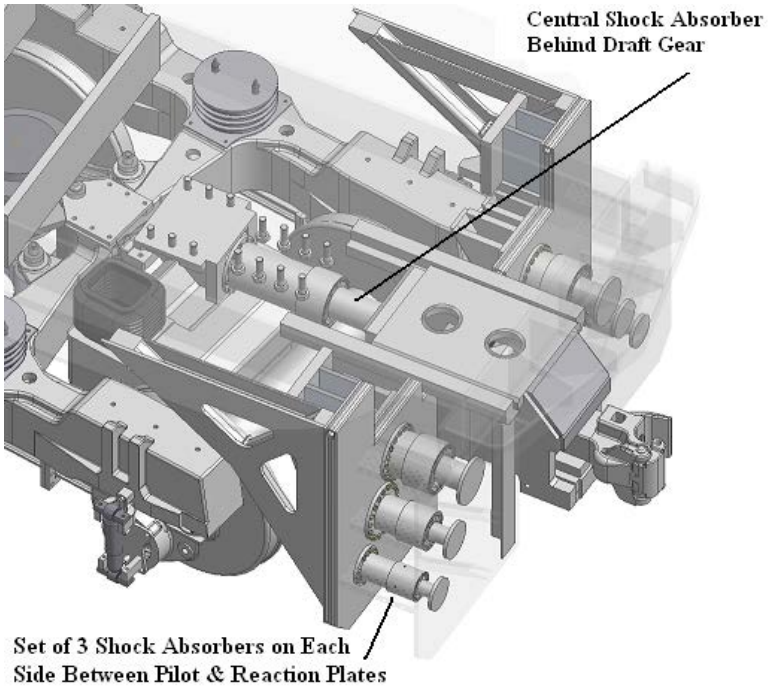

Figure 11. CAD Drawing of an EMD SD70MAC with SEAs

Table 1. Design Parameters of all SEAs Used in CEM System

SEA ID	Diameter of UHMWPE (in)	Diameter of Plunger (in)	Maximum Stroke (in)	Total SEA Length (in)	Remarks
Central SEA	8.00	5.50	6.50	19.25	Rear of draft gear pocket
LHS – small capacity SEA	4.50	2.00	6.25	17.00	Between pilot and reaction plates
LHS – medium capacity SEA	6.00	3.75	6.00	17.00	Between pilot and reaction plates
LHS – large capacity SEA	8.00	5.50	6.00	17.00	Between pilot and reaction plates
RHS – low capacity SEA	4.50	2.00	6.25	17.00	Between pilot and reaction plates
RHS – medium capacity SEA	6.00	3.75	6.00	17.00	Between pilot and reaction plates
RHS – large capacity SEA	8.00	5.50	6.00	17.00	Attached between pilot and reaction plates

The stroke of the CEM system allows the draft gear to engage the central dissipation element as the impacted car sill strikes the pilot plate. The plate dislodges, allowing the plate to push the dissipation elements below the nose stairway as the draft gear pushes the main element. Areas of maximum impact react with the largest forces by varying the size of the dissipation elements. A simplified calculation of the energy in a 30-mile per hour impact indicates a total capacity of 28 million ft-lb for all seven dissipation elements combined in the system. FEA described in Section 3 shows the effect of dissipation in these areas.

2.2.2 Structural Integration of CEM System to Locomotive

The challenge of the design is integrating the dissipation and deformation elements into the available space in the locomotive. The bracing, extensions, and dissipation elements must retrofit to the existing structure of the locomotive. For an SD70MAC locomotive, this requires the energy dissipation elements to be located underneath the front stairway on each side of the locomotive. A stiffened understructure transfers loads from these elements back to the locomotive sill. A reinforced edge-gusset ensures that the impact does not immediately buckle the structure. Figure 12 shows a side view of the integrated structure.

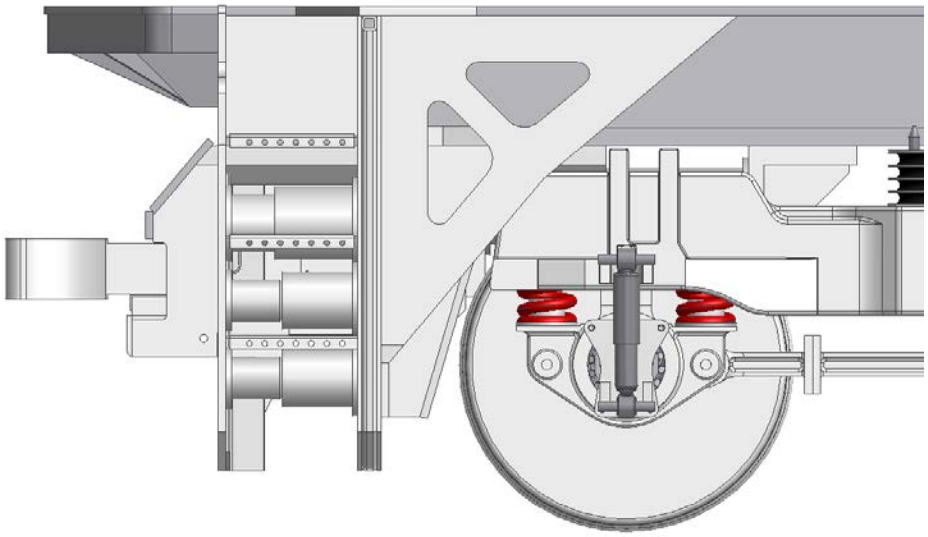

Figure 12. Structural Adaptation of CEM System Components to Locomotive Fore-Body

The central (and largest) dissipation element installs behind the draft gear pocket. This requires certain design modifications to the current method of attaching the draft gear pocket to the underside of the sill. The modified design involves welding two heavy angle sections (L–bars) to the underside of the sill plate to support the sides of the draft gear pocket while allowing the sides to shift backward during impact (Figure 11). The top plate of the draft gear pocket is "puddle-welded" at two circular cutouts to the underside of the sill plate. This provides resistance to shearing along weld lines as well as structural integrity against draft and buff loads during routine operations. However, under frontal collision scenario, buff loads in excess of 1.0-1.5 million lb shear the welds, and the draft gear pocket is then free to slide backward into the dissipation element. The rear end of the element reacts against a reinforced support fastened to the underside of the sill plate. Figure 9 above shows the complete CEM system.

2.2.3 Operational Approach

The CEM system design and integration with the fore-body of an SD70MAC locomotive enables the maximum possible crash energy absorption and dissipation. Several SEAs accomplish this by utilizing limited available space within the structure of the locomotive. The primary goal of the system is to avert a post-crash locomotive override. To achieve this, the CEM structure prevents the pilot plates from deforming under the locomotive to create a ramp that initiates override. In addition, the use of dissipation elements within the system provides a means to transfer loads to the locomotive structure while absorbing energy from the event.

In normal operations, the system behaves identically to the current locomotive understructure. The draft gear dissipates KE from coupling and braking. The locations of the additional structure do not impede turning, coupling, or other normal locomotive operations. During a frontal collision, the CEM system allows the normal buff load to transfer through the draft gear. Once the draft gear exceeds its normal stroke and the shear pin fails, the CEM system begins to operate. Weld shearing in the upper plate of the draft gear pocket allows the pocket to move axially along the locomotive frame. The central dissipation element (SEA) mitigates crash

energy as the locomotive continues forward. As the pilot plate contacts the impacted object, it shears away from the sill, and the dissipation elements under the stairway hold it parallel to the reaction plate. This prevents the plate from folding under the locomotive and forming a ramp. The dissipation elements provide additional mitigation as well as load transfer from the stiffest portion of the impacted object. If the energy dissipation elements and structural deformation absorb sufficient KE, the locomotive will continue to travel in line, not leave the rails, and minimize damage to the surrounding structures. This is evaluated through finite element modeling (FEM), simulation, and analysis presented in Section 3.

3. Analysis of Crash Dynamics and CEM

The primary goal of this program was to evaluate the feasibility of designing a CEM system for a locomotive. This system minimizes the risk of override in the event of a frontal collision with railroad rolling stock. This section describes the approach and FEA of a prototype CEM system. The analysis illustrates the effectiveness of deformation control and defines the level of cushioning required to limit override. The FEA models events in which a consist of hopper cars is impacted by an EMD SD70MAC locomotive. The actual events were performed at TTC and provided video, acceleration, and deformation data associated with a 30-mile per hour impact. The real-world impact data allowed for validation of the FEA model and prediction of CEM performance.

3.1 Analysis Approach

The initial analysis modeled an actual test event performed at TTC. This provided an initial framework for the CEM design as well as data suitable for model validation. The model simulated an on-track stationary consist of four open hopper cars impacted by a second consist of three hopper cars pulled by an SD70MAC locomotive; the model took into account the weight of these objects. The actual crash test performed by QNA TSG at TTC involved 35 stationary hopper cars. For convenience of calculation and animation, the simulation used only four stationary hopper cars. The fourth hopper car had a simulated weight and draft gear stiffness of 32 hopper cars. The hopper cars were typical “open-top” cars, modeled from dimensions provided in *The Car and Locomotive Cyclopedia* for a Union Pacific Railroad’s (UP) 3,985 cu-ft steel or aluminum quadruple-hopper coal car.

FEA of the event used an impact speed of 32.1 mph to match the actual test condition. Deformation, deceleration, and override data validated the model based on the actual event. Therefore, modifying the model provided a means to verify CEM system performance, to establish energy dissipation requirements, and to identify areas for structural modification.

All calculations of collision dynamics utilized LS-DYNA [5].

3.2 FEM a Locomotive and Hopper Car Consist

Accurate models of the structural and dynamic elements of the locomotive and hopper cars are necessary for successful FEM. Component geometry and material properties must accurately represent the structures. In these models, all components and joints are treated as elastic-plastic and not rigid. This allows for deformations in the model and estimates of energy dissipation during component fracture. Recommended practices by the American Welding Society [3] define the failure criteria at welded joints in tension and shear. FEM assumed welding stiffness per inch of weld length as a spring constant in the model. The model also included a steerable truck assembly and an improved coupler and draft gear assembly, based on an updated SD70MAC model. Figure 13 shows the elements of the locomotive model.

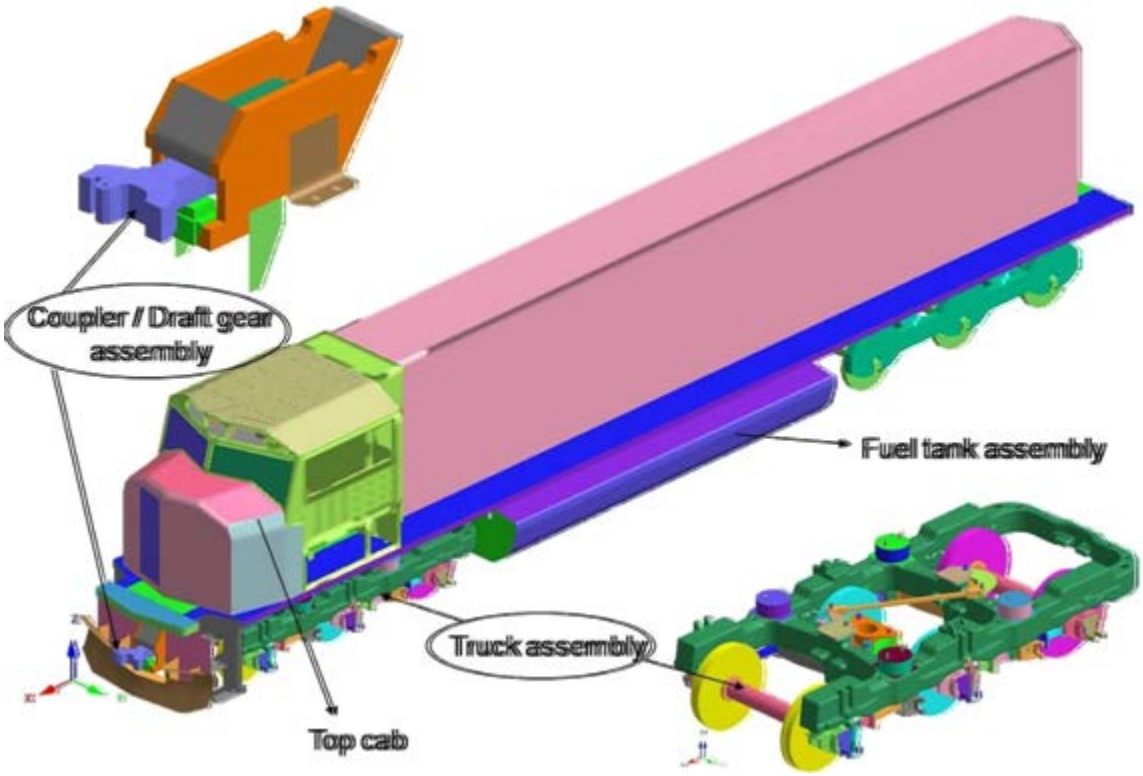

Figure 13. SD70MAC Model with Updated Coupler/Draft Gear and Steerable Truck Assembly

The model used finer meshing in the front end of the locomotive and at the striking end of the first hopper car to allow for extensive post-collision deformation. The remainder of the model used relatively coarse meshing to ease calculation requirements.

3.2.1 Modeling of SD70MAC without and with CEM System

Using data provided by EMD and measurements taken from locomotives, the researchers developed a 3D CAD model of an SD70MAC locomotive. A preprocessor, HyperMesh™ [4], generated the actual mesh suitable for calculation in LS-DYNA from the locomotive model. The FEM of the striking locomotive consist was created by adding three fully loaded hopper cars to the rear of an SD70MAC locomotive. Once assembled, LS-DYNA allows for simulated collisions with the stationary hopper car consist at different closing speeds. The following meshing details pertain to the FEM of a baseline SD70MAC without a CEM system and a modified SD70MAC with the CEM system integrated into its fore-body.

- Baseline SD70MAC without CEM system:
  - Total number of elements = 316,471
  - Total number of nodes = 386,771
  - Total number of parts = 368
  - Total weight = 415,000 lb.
- Modified SD70MAC with CEM system:
  - Total number of elements = 409,431
  - Total number of nodes = 559,972
  - Total number of parts = 508

- Total weight = 416,175 lb.

Figure 14 through Figure 20 show the meshing details of the two locomotives referenced above and the major CEM system components as represented in the FEMs.

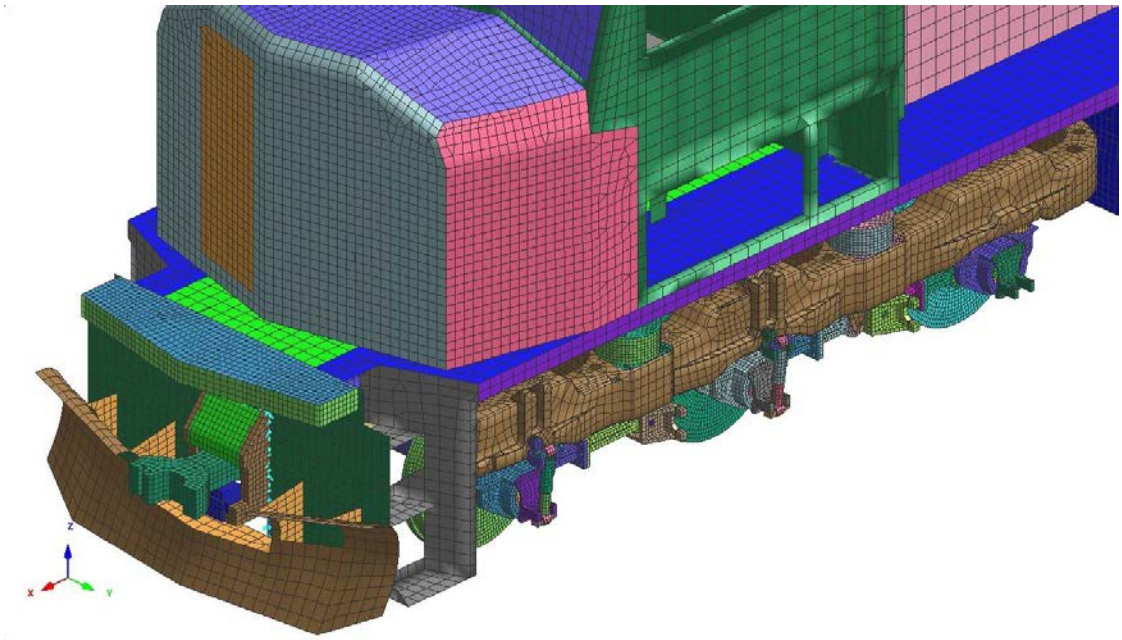

Figure 14. FEM of a Standard SD70MAC Locomotive

Integrating the CEM system adds 92,960 elements to the original SD70MAC. The modified locomotive model with the CEM consists of 559,972 nodes, 409,431 elements, and 508 parts. The total simulated weight of this model is 416,175 lb—an additional 1,175 lb compared with the base model SD70MAC.

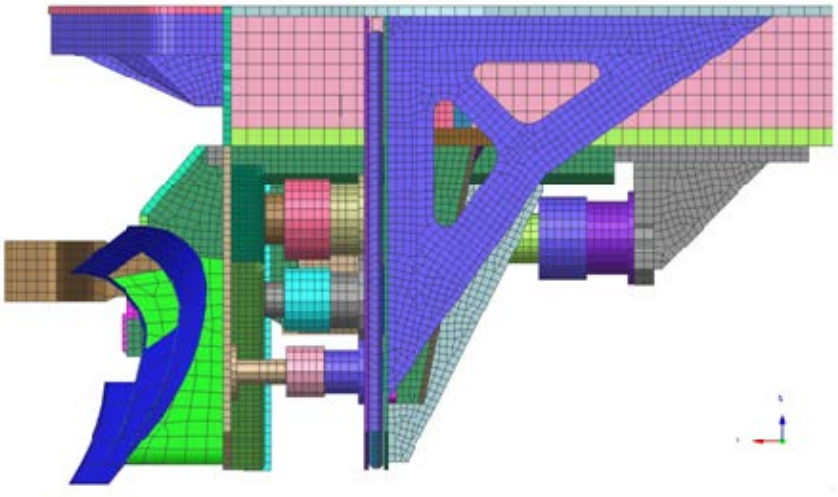

Figure 15. Side View of the Integrated Model of the CEM System

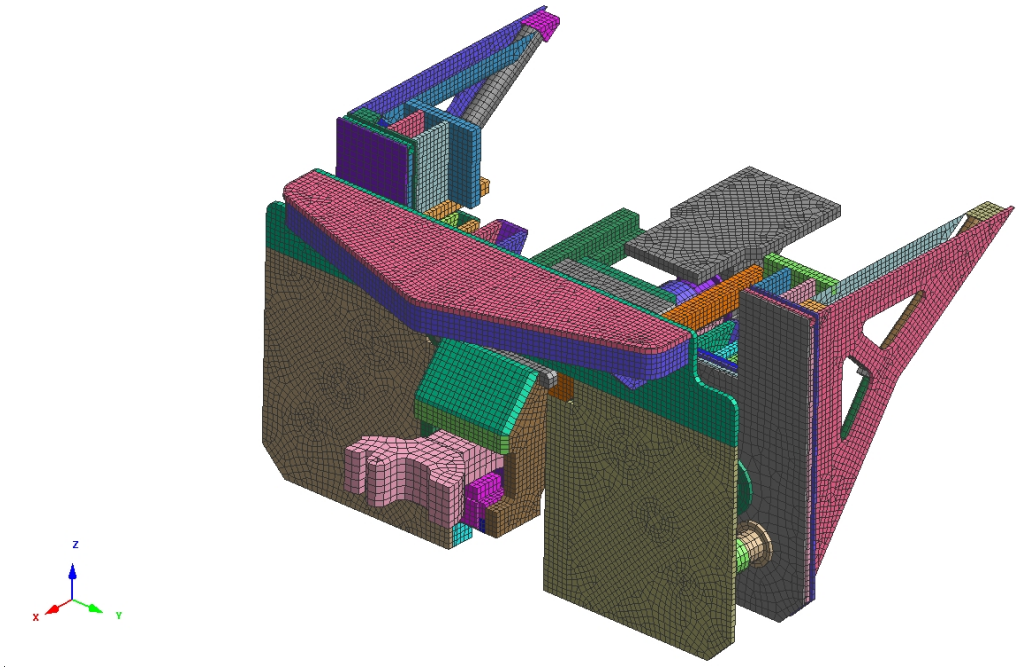

Figure 16. Isometric View of the CEM System Model (sill plate, snowplow and ladders hidden for clarity)

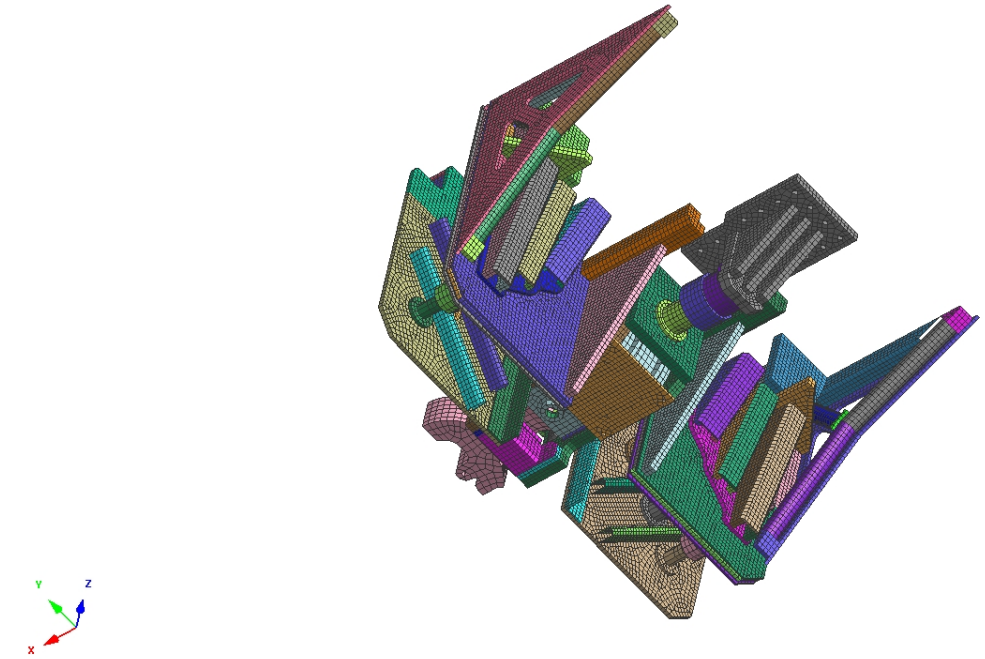

Figure 17. Typical Finite Element Meshing of CEM System Assembly (bottom view)

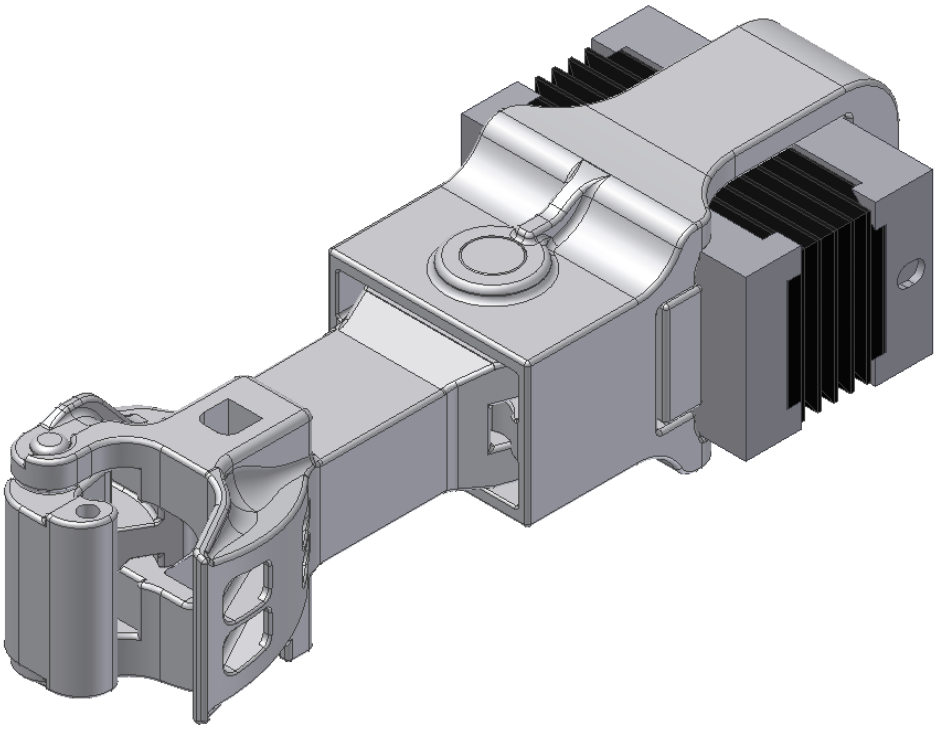

Figure 18. CAD Model of a Coupler-Draft Gear Assembly Developed and Used in FEA

3.2.2 Modeling of the Open-Top-Hopper Cars Used for Crash Simulation

Using a similar approach, the researchers developed a model for a loaded open hopper car. This model utilized available data for UP's open-top-hopper cars. The simulation used multiple copies of the loaded car throughout the consist. As described above, the model represented a consist of 35 stationary hopper cars, although only 4 are fully modeled to ease calculation (the fourth car had a simulated weight and draft gear stiffness of 32 hopper cars). The car resisting the impact had a fine-mesh structure to allow for better visualization of deformations during the simulated impact. The model used a coarser mesh version of the car in the second, third, and fourth positions. The meshing details of all four hopper cars are listed below:

The open-top-hopper car model (newly developed by QNA TSG) consisted of 50,079 nodes, 42,029 elements, and 55 parts. The empty hopper car model weighed 60,000 lb.

- First fully loaded hopper car:
  - Total number of elements = 42,029
  - Total number of parts = 55
  - Fully loaded weight = 259,600 lb

The remaining hopper cars used a coarse mesh to reduce computing time.

- Second and third fully loaded hopper cars (elements below are for each car):
  - Total number of elements = 2,016
  - Total number of parts = 42
  - Total weight = 260,000 lb

The final car used the same model as the second and third but with a higher mass.

- Fourth fully loaded hopper car simulating 32 hopper cars:
    - Total number of elements = 2,016
    - Total number of parts = 42
    - Total weight = 8,320,000 lb

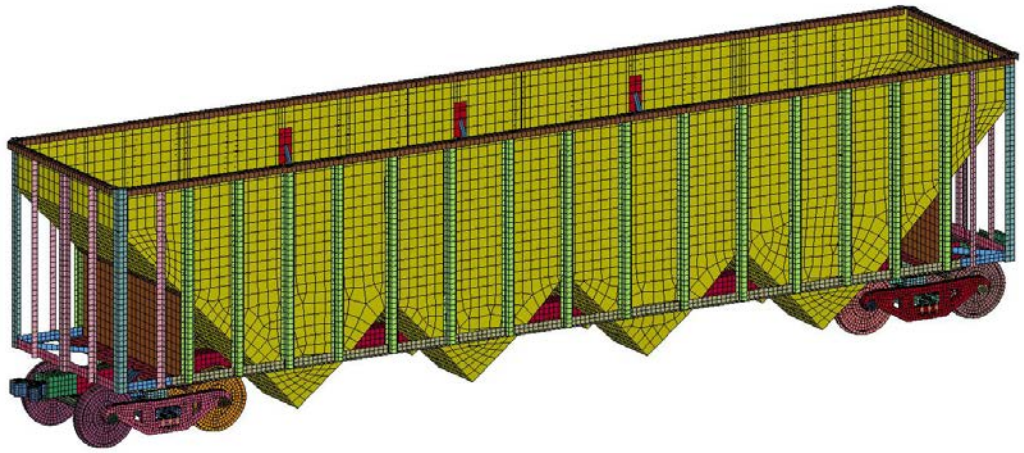

Figure 19. FEM of an Open-Top-Hopper Car Based on New CAD Model

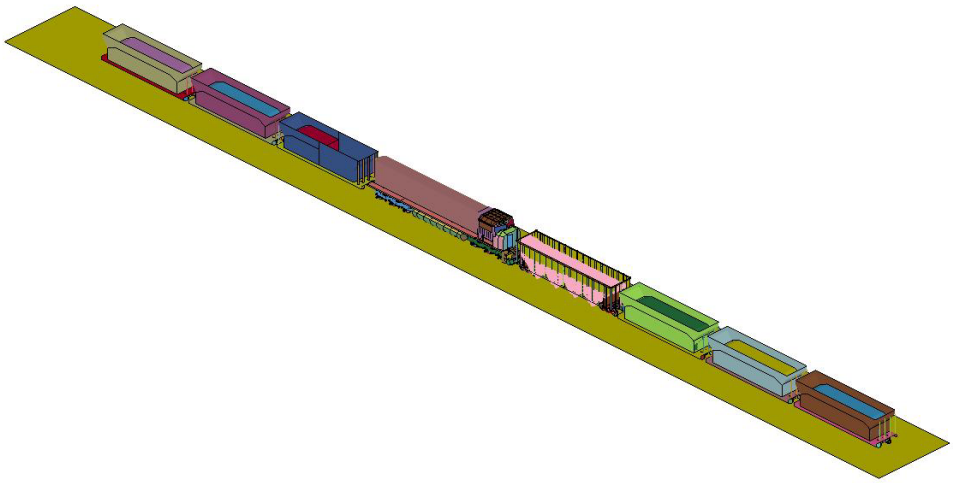

Figure 20. FEM of Freight Consists Used for Simulation of In-Line Collision

3.2.3 FEA Cases

The FEA modeled two basic scenarios. The first assumed a standard SD70MAC locomotive without any modification as tested at TTC. The second assumed a modified SD70MAC with an integrated CEM system. HyperMesh™, a multipurpose preprocessor and modeling tool, generated finite element mesh from the CAD geometry. It also served as the assembly tool for the car models to create the simulated consist. LS-DYNA, a dynamic structural analysis finite element code, was used to perform all simulations and post-processing calculations involving nonlinear elastic-plastic analyses.

The advantages of using LS-DYNA analysis code include the following:

- It is most suitable for analyzing structures in a single process. It accomplishes this by combining the dynamic, holistic modeling of the entire consist with embedded detailed models of the consist's components.
- Simulations can permit visualization of the collision process in the early stages in which:
    - Most significant locomotive structural deformations, movements, and decelerations occur.
    - 3D interactions of various components of the locomotive, including the cab and its interior, influence crew survivability.
- Models can include detailed representations of the locomotives and rail vehicles.

The objectives were to evaluate the effectiveness of the CEM system toward improving the crashworthiness and risk mitigation of a locomotive override in the event of an in-line collision with a large consist of hopper cars. The FEA involved several analysis cases including scenarios with different closing speeds. These are described in the following text.

Case I. Standard SD70MAC collision with loaded hopper car consist

This simulation used the standard SD70MAC model, hauling three loaded hopper cars. Simulations provided results at closing speeds of 20, 32.1, and 40 mph. The 32.1-mile per hour closing speed matched the test data from TTC. The locomotive consist collided with the four car consist simulating a consist of 35 stationary loaded hopper cars (see Section 3.2.2).

Case II. Modified SD70MAC (with CEM) collision with loaded hopper car consist

This case simulated a collision using an SD70MAC with the integrated CEM system. These modifications included the stiffened transfer structure, separable pilot plate and draft gear pocket, and seven energy dissipation elements dispersed within the structure. The stationary hopper car consist was identical to the Case I simulation. Comparison of results at various impact speeds allowed for determination of the safe speed to prevent override. Speed variations for Case II were identical to Case I allowing for direct comparison between the two cases to determine CEM system performance.

3.3 FEA Simulation of SD70MAC (without CEM) Collision with Stationary Hopper Car Consist

Figure 21 shows the simulation and full-scale crash test for the standard SD70MAC front end before impact, and 300 and 600 ms after impact, respectively. Impact speed was 32.1 mph to match TTC data. At 300 ms, the pilot plate deformed over the hopper car trucks, and override was under way. Comparing the deformation and progression of override in these frames, it is evident that the simulation accurately represented the collision dynamics.

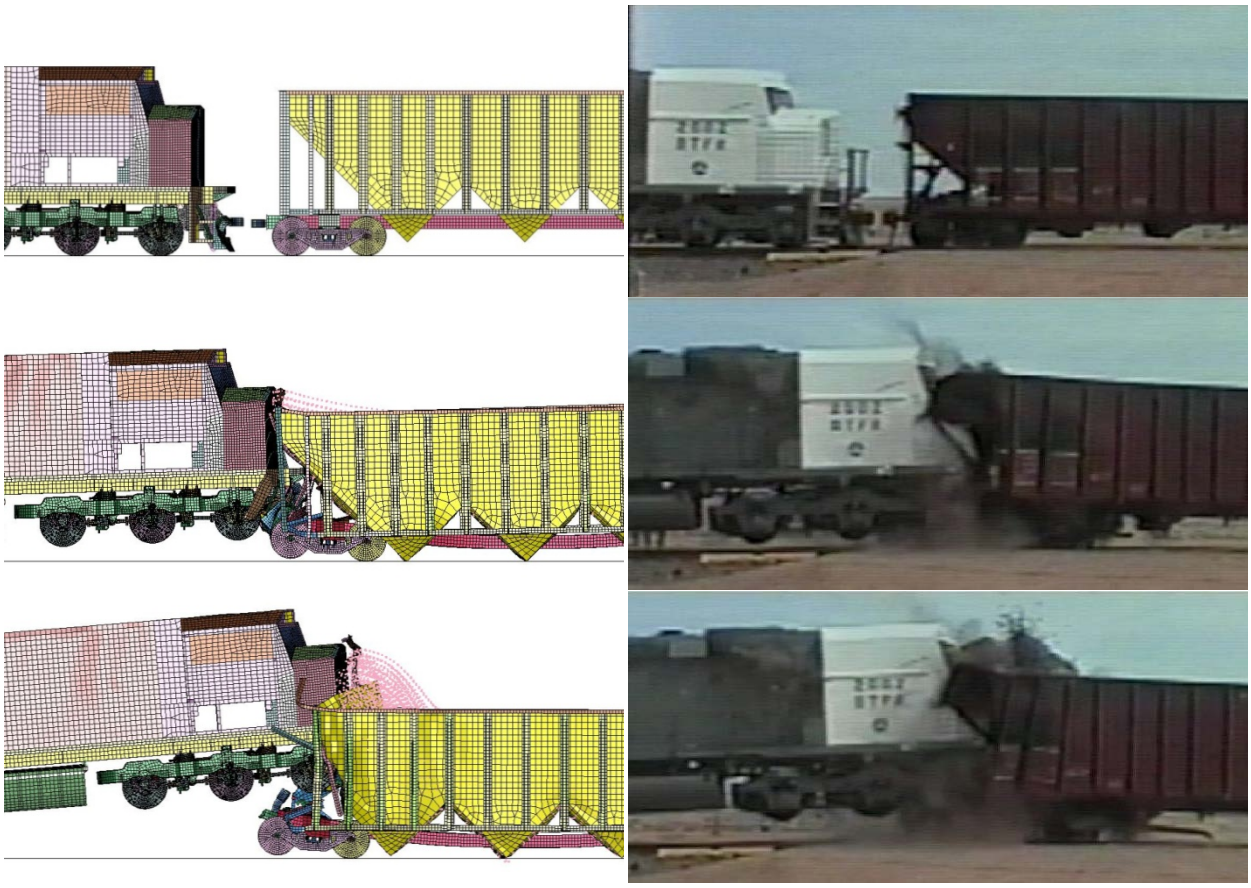

Figure 21. Simulation and Full-Scale Test Results and Comparison of the SD70MAC without CEM System

3.4 FEA Simulation Results for EMD SD70MAC with CEM System

The modified SD70MAC model incorporated the CEM system in its fore-body, allowing for the control and dissipation of collision energy. The CEM system consisted of two sets of three SEAs on both sides of the draft gear, located between the modified pilot plate and the stiffened reaction plate. The model included a final, large-capacity SEA behind the draft gear pocket and supported under the sill plate. The model assumed each SEA was a spring element, with each unit having a different critical peak force and stroke. Figure 22 shows the sequence of the collision simulation for the CEM system case.

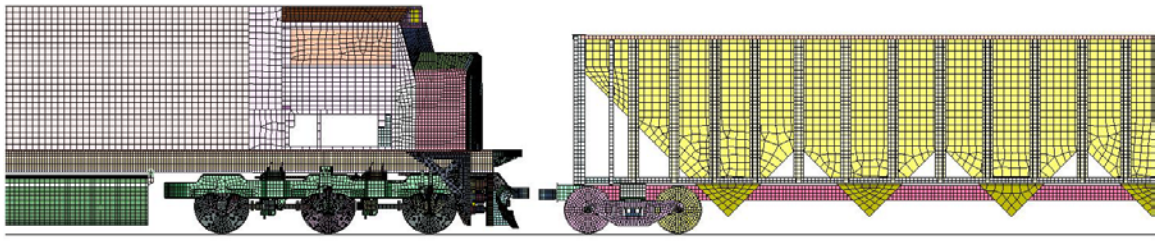

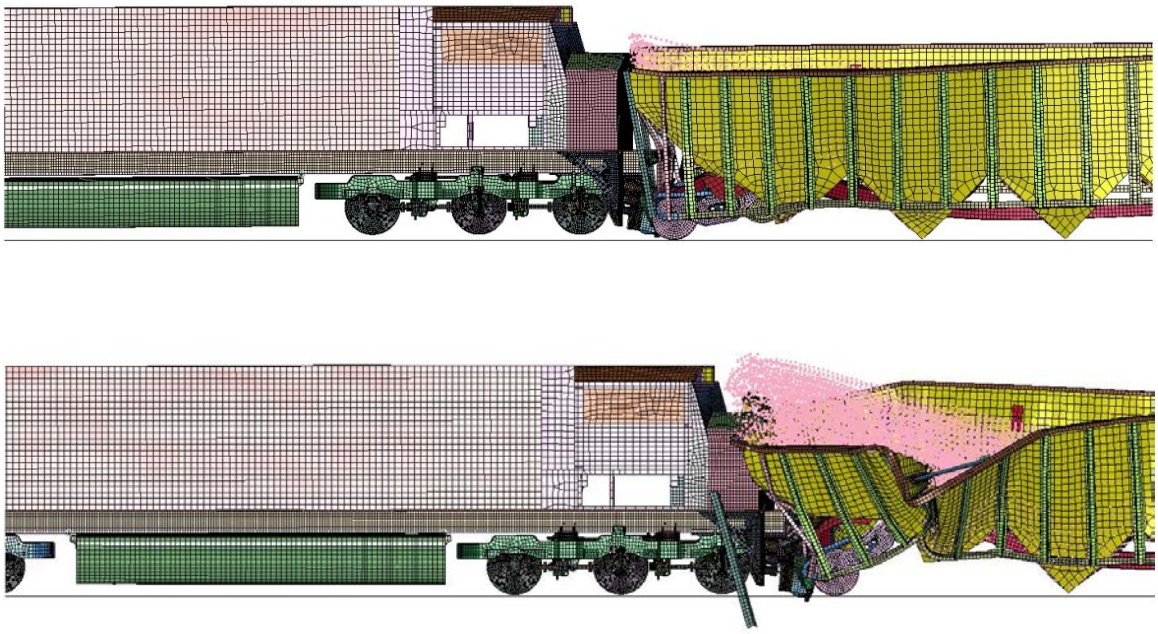

Figure 22. Simulation Results of the SD70MAC with CEM

Figure 22 shows that the dissipation and deformation control has maintained in-line motion, creating large deformation in the impacted hopper car. The broken pilot plate does not form a ramp-like structure ahead of the locomotive's front truck. This appears to prevent the locomotive from riding onto the hopper car. The locomotive wheels have lifted slightly from the rails, but by the 600-millisecond mark, the wheels have returned to the rails. The locomotive nose is largely intact but has severely damaged the hopper car structure and spilled the simulated load. At this point in the simulation, the locomotive has slowed to approximately 15 mph.

3.5 Assessment of CEM System Performance and Key Design Parameters

On the basis of the survey of the National Transportation Safety Board reports of locomotive override cases following in-line collisions, override typically occurs when closing speeds are in the range of 30-40 mph. The evaluations described here use speeds covering that range, namely 20, 32.1, and 40 mph. The closing speed of 32.1 mph was specifically chosen (instead of 30 mph) to correlate the results of FEA simulation with those obtained from a past full-scale collision test conducted at TTC as described above.

At each selected collision speed, the stationary consist remained the same, whereas the speed of the locomotive configuration was altered. Initial simulations utilized a standard front-end configuration. Subsequent simulations utilized a model with an integrated CEM system. Figure 23 shows the locomotive forward velocity (y-axis) for each of the six simulations. At higher speeds, the graphs end abruptly at some time after the impact but before the consist has come to rest. This is a result of FEA program termination because of numerical instabilities resulting from extreme deformations in the model.

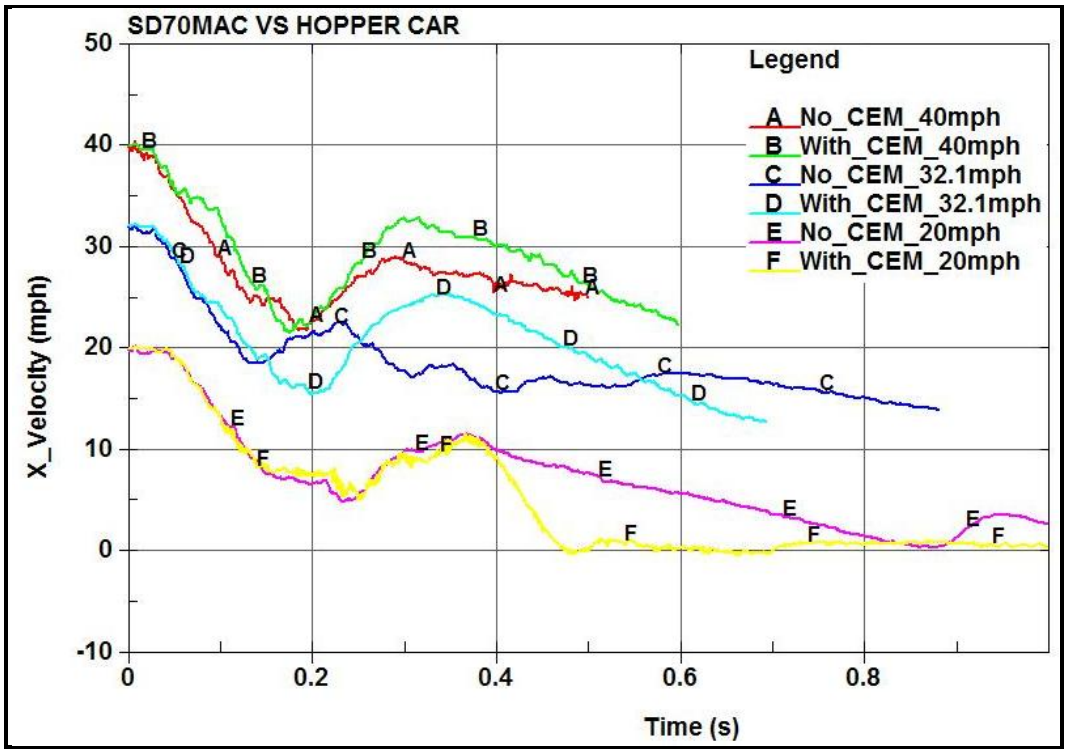

Figure 23. Post-collision Locomotive Forward Speed vs. Time

In each simulation, the axial velocity of the locomotive climbs slightly after the 200-millisecond mark. For cases with CEM, this rise is sharper than for the non-CEM case. The axial velocity drops more quickly in the non-CEM cases, because this point marks the onset of override and more of the momentum is being transferred to gain vertical displacement.

Figure 24 shows the vertical displacement for the same six simulations. In each of the non-CEM cases, the vertical displacement rises sharply at the 200-millisecond mark. The sharpest rise (and highest subsequent override) occurs for the 32 mph test case. This appears to be the peak override speed, because the total rise for both the 20 and 40 mph hour cases are lower.

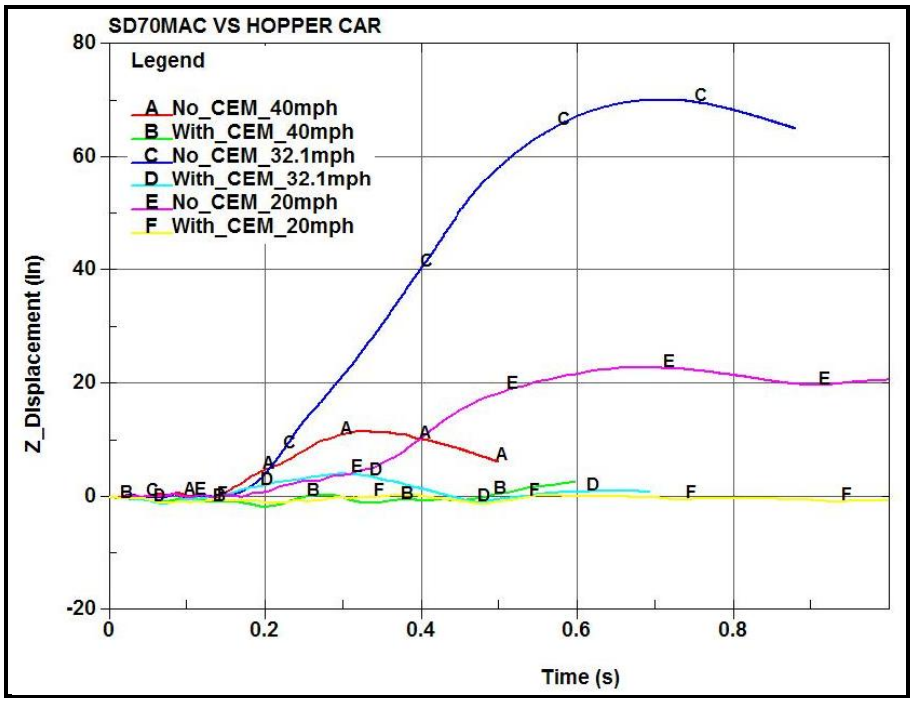

Figure 24. Vertical Displacement of Locomotive Anticlimber vs. Time following Collision

Extracted FEA data on post-collision time, distance, velocity, and average acceleration values over the time interval is shown in Table 2.

Table 2. Summary Data from FEA for SD70MAC Locomotive with and without CEM

V (mph)	With CEM	Time (s)	V_0 (in/s)	V_{AC} (in/s)	S_{AC} (in)	V_{CG} (in/s)	S_{CG} (in)	A_{AC} (in/s^2)	A_{CG} (in/s^2)
40	No	0.500	704	441	247.02	452.77	248.12	-609.5	-585.6
40	Yes	0.599	704	393	308.03	393.06	308.25	-553.8	-553.3
32.1	No	0.882	564.96	245.99	287.84	243.90	291.07	-449.3	-446.1
32.1	Yes	0.694	564.96	223.87	254.22	221.38	251.05	-529.2	-538.1
20	No	0.877	352	5.86	119.18	5.91	119.99	-519.7	-516.2
20	Yes	0.479	352	0	84.10	0	84.20	-736.6	-735.8

Legend: AC (node on anticlimber); CG (node closest to CG of sill plate)

Figure 25 shows a comparison of the FEA-simulated average decelerations for the SD70MAC with and without the CEM system for all three collision speeds. As expected, the average deceleration values for the SD70MAC with the integrated CEM system are generally higher than those for the standard front-end configuration.

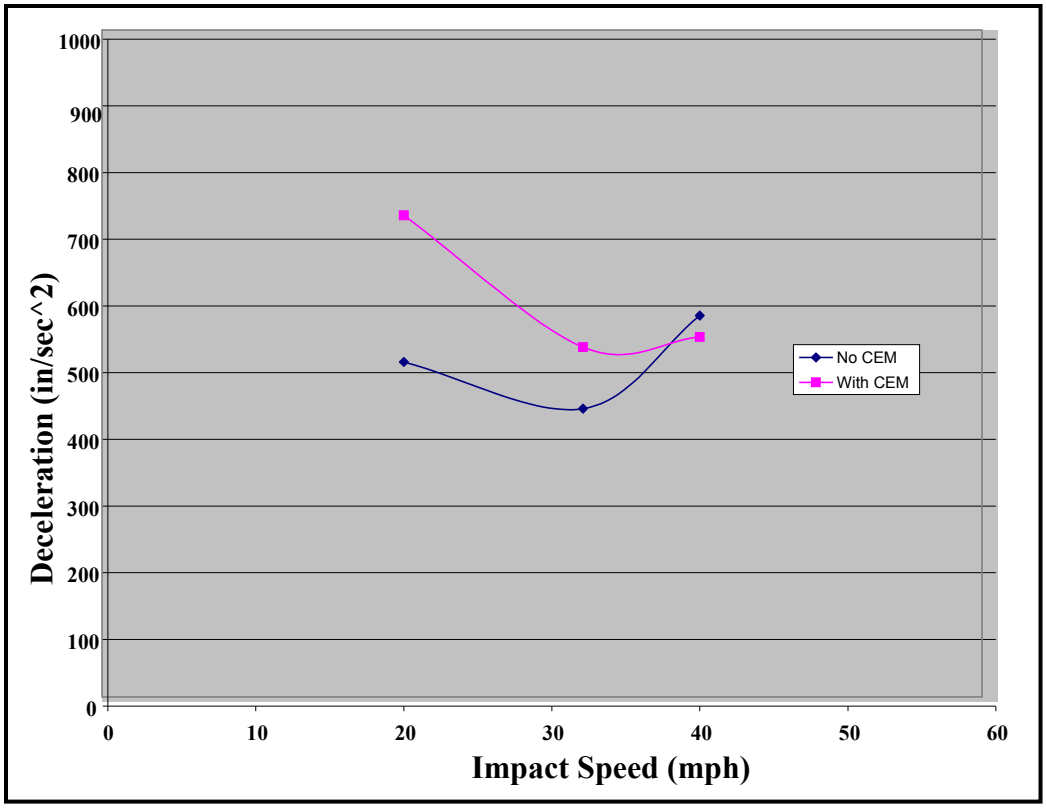

Figure 25. Computed Average Decelerations at CG of SD70MAC during Crash Event for All Cases

To assess the amount of energy dissipation attributable to the CEM system, we compared the KE status at computed time intervals for the SD70MAC consist with and without the CEM system considering the 32.1-mile per hour collision case.

(a) SD70MAC without CEM system – collision at 32.1 mph:

On the basis of the data shown in Table 1 and Figure 23, the forward velocity of the SD70MAC dropped from 47.08 ft/s at the point of collision to 20.5 ft/s within a time interval of 0.882 s. At this time, the locomotive traversed a distance of 23.98 ft, partially crushing the rear end of the hopper car. The corresponding average value of forward deceleration over this time interval was 37.44 ft/s^2 or approximately 1.16 g.

Initial KE of the SD70MAC consist = 0.5 × (1,195,000/32.2) × (47.08^2) = 41.1294 × 10^6 ft-lb.

At T = 0.882 s following collision, remaining KE = 7.798117 × 10^6 ft-lb.

The average magnitude of crash force over the duration, F = (1,195,000/32.2) × 37.44 = 1.389 × 10^6 lb.

Following the law of conservation of energy, the difference in KE = (41.1294 – 7.798117) × 10^6 = 33.331 million ft-lb energy was expended by the crash force. This occurred via energy expenditure through fracture and structural deformations; energy expenditure also occurred through raising the CG of the locomotive above the track onto the hopper car during override.

(b) SD70MAC with CEM system – collision at 32.1 mph:

In this case, the forward velocity of the SD70MAC dropped from 47.08 ft/s at the point of collision to 18.6 ft/s within a time interval of 0.694 s. At this time, the locomotive traversed only a distance of 21.185 ft, partially crushing the rear end of the hopper car. The corresponding average value of forward deceleration over this time interval is 44.1 ft/s^2 or approximately 1.37 g.

Initial KE of SD70MAC consist = $0.5 \times (1{,}195{,}000/32.2) \times (47.08^2) = 41.1294 \times 10^6$ ft-lb.

At T = 0.694 s following collision, remaining KE = 6.4196×10^6 ft-lb.

The average magnitude of crash force over the duration, $F = (1{,}195{,}000/32.2) \times 44.1 = 1.636 \times 10^6$ lb.

Therefore, the difference in KE = $(41.1294 - 6.4196) \times 10^6 = 34.7098$ million ft-lb energy. In this scenario, the energy was expended not only through the hopper car and locomotive fracture and structural deformations but also via the CEM system. The latter prevented any override of the SD70MAC.

Since the initial conditions just prior to the collision with the hopper car consist were identical for these two cases, the SD70MAC with the CEM system appears to have dissipated much more KE within a shorter time interval and while traversing a shorter distance compared with that of the SD70MAC without the CEM system. The resulting deceleration and average crash forces for the SD70MAC with the CEM system are also higher as would be expected. As a first approximation, we can assess the energy dissipation potential of the CEM system by evaluating the difference between energy spent in decelerating the SD70MAC through structural deformations and fracture in both cases. The difference in energy dissipation equals 1.3788 million ft-lb (more than 1.0 MJ), which is higher in the case of an SD70MAC with the CEM system. This is despite the added KE conversion to physical energy. The CEM system offers controlled deformations and high-energy dissipation because of phase transformation of UHMWPE materials above critical stress values within SEA units.

Evaluation of the animated crash sequences indicates that the most significant contribution to crash energy dissipation occurs in the central shock absorber, located behind the draft gear pocket. This is due to initial impact at the coupler, followed by transfer of force to the plunger of the central SEA. Subsequently, the truck of the hopper car impacts on the pilot plates on both sides of the locomotive that in turn cause plunger displacement into the remaining SEA units. The contribution of these units in preventing override comes from their coupled actions and extremely high stiffness inhibiting the pilot plate from becoming a ramp ahead of the front trucks.

4. Design and Testing of a Solid-State SEA

One method of locomotive override prevention is to dissipate KE via deformation or absorption within the cab's structure. This approach both reduces the level of impact force magnitude and delays the force transmission to the impacted object. Given the high levels of energy present in the collision, the absorption devices must have sufficient capacity. Typical damping devices are gas-oil cylinders with orifices in the piston (oleo-pneumatic type). These devices provide resistance through viscous forces within the piston. The basic devices come in a range of capacities and are commercially available. However, there is a limit to the amount of energy dissipation capacity in these devices. The capacity is a function of the diameter and stroke of the piston, along with the viscosity of the internal fluid.

This section describes an alternate approach. The device described is a QNA TSG innovation using a solid-state damping device. This device, based on the deformation of a solid polymer, has the capability to absorb significant amounts of impact energy in minimal lateral space. During impact, the forces in the polymer produce a phase transition from solid to viscous fluid offering high damping above a compressive stress threshold.

A preliminary attachment technique of the cylinders to the underframe of the locomotive is also proposed. On the basis of these concepts, the researchers defined a prototype test article along with coupler, draft gear, and SEA devices sandwiched between the pilot and reaction plates.

4.1 Background

Traditional applications of UHMWPE and HDPE materials are reserved for designs with the following requirements: low-friction-coefficient, high-wear, high-flexural, and impact resistance. Through FRA sponsorship, QNA TSG developed an innovative use of UHMWPE to provide KE absorption. With a steel cylindrical containment and a penetrating plunger, energy is transferred through the UHMWPE by a combination of stress induced flow and deformation. By scaling and optimizing the configuration, TSG developed a SEA to meet the needs of a CEM system. The SEA is capable of dissipating sufficient energy to limit override during in-line locomotive collisions.

4.2 Basic Design Approach

Generally, SEAs are made of oleo or oleo-pneumatic type dampers in which a viscous fluid flows through orifices within a cylinder-piston arrangement. Fluid resistance creates pressure as the impacting force and motion of the cylinder attempt to push or pull the cylinder through a defined stroke. The resistance damps the relative motion between the cylinder and piston, attenuating the applied force. The physical dimensions of such SEAs greatly increase in proportion to the magnitude of the impacting force and the KE to be absorbed. When used in a CEM system, the physical dimensions limit the amount of dissipation or force capacity available during an event. In the case of freight locomotives or other rolling stock, there is very little space available, thereby limiting the energy capacity. To make best use of available space, the researchers developed a solid-state damping device. This device uses commercially available UHMWPE as the primary dissipation material. The material is inert, remaining in a solid state during no-load conditions. Under high-impact energy, the material becomes plastic, extruding along any containment and provides a mechanism for energy transfer.

Traditionally, UHMWPE and HDPE materials provide low-friction and high-wear surfaces for moving parts. Water transportation system docks and locks use UHMWPE as an impact buffer, where it provides flexural stiffness and energy absorption capability against lateral impacts. For this program, researchers explored the use of cylindrical UHMWPE within a containment to absorb KE. Similar to oleo-pneumatic dampers, the system has a moving portion (a conical plunger) and a fixed portion (the containment cylinder), with the relative motion providing a path for energy transfer. Appropriately scaled and optimized, the configuration provides the primary dissipation element of the proposed CEM system for locomotive crashworthiness applications. Figure 26 shows a section view of the device.

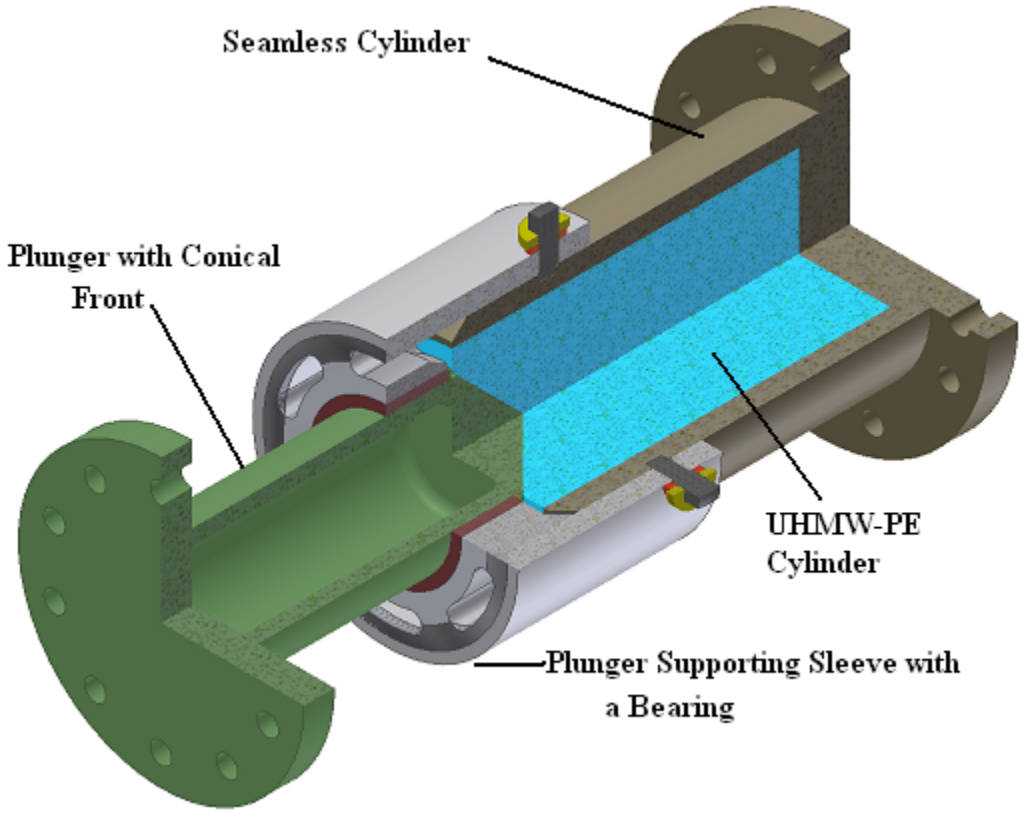

Figure 26. Schematic Drawing of a Typical Compact High-Energy Shock Absorber

The device contains very few machined parts. As seen in Figure 26, a steel cylinder contains the UHMWPE material. A steel plunger with a conical face pushes on the face of the material, applying load during an impact event. An external support sleeve provides a linear bearing to guide the plunger and retains the UHMWPE. Openings in the sleeve provide a path for material extrusion.

In a typical application, the geometry of the SEA defines the limits of impact force magnitude. Specific parameters such as piston diameter and stroke determine the maximum energy absorbed. With the components of the system mounted to the locomotive underframe, the device dissipates loads while transferring them to the stiffest portions of the structure.

During the development, the researchers tested the conceptual designs, scaling up in size and impact speed. Initial investigations used quasi-static loading to determine material performance. Small-scale-impact tests provided data on performance at near design speeds. Larger-scale tests

demonstrated the ability to predict performance based on size and provide a basis for the full-scale prototype tests.

At impact, force applied to the plunger face transfers to the conical UHMWPE end within the cylinder. When stress in the UHMWPE reaches a critical magnitude, the material undergoes a reversible-phase transition from solid to a viscous fluid state. This phase transition occurs only within a confined space and at or above the critical compressive stress. The viscous surface allows the plunger to penetrate under load, providing resistive force against the impact. Once the impulse force drops to 0, the material returns to a solid state. Moreover, the resistive force remains relatively constant after the initial rise. This is due to the constant stress level at the interface during the viscous phase. Total energy absorbed by the SEA during the event is equal to the work done by the plunger on the UHMWPE cylinder.

4.3 Quasi-Static Testing

Quasi-static testing was the method of preliminary investigation of the UHMWPE device. The Instron test machine is capable of providing controlled load-displacement measurement with applied loads of up to 50,000 lb. This testing demonstrated the existence of two distinctly different regimes of deformation behavior under compression loading. Figure 27 shows a typical quasi-static test setup, and Figure 28 shows the final position of the plunger at the end of its compression stroke in the test machine.

Figure 27. Test Setup for Quasi-Static Compression Test in Instron 8502 Test Machine

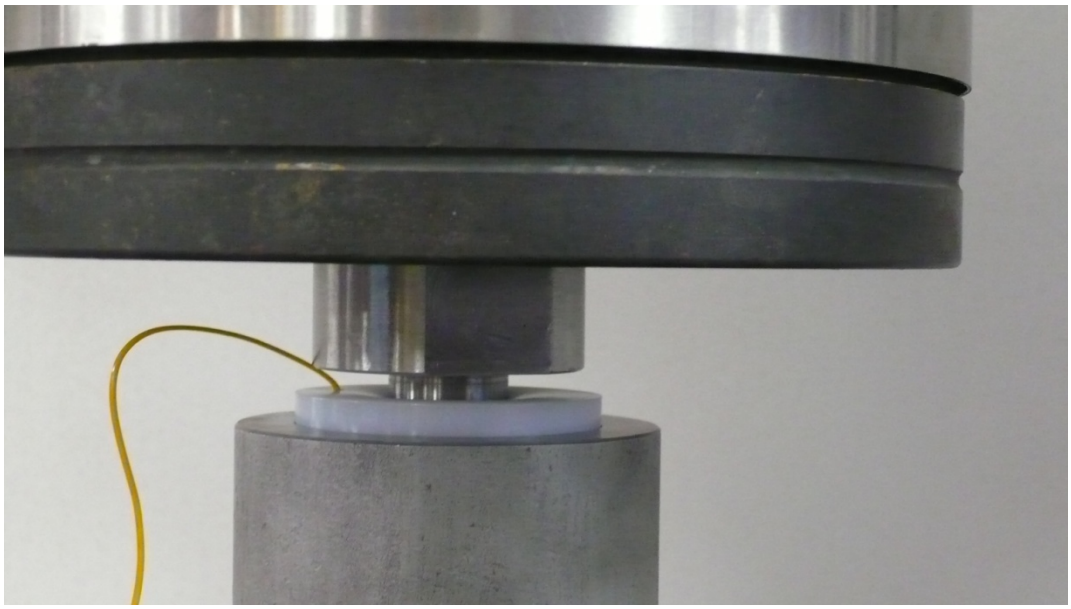

Figure 28. Final Position of Plunger at the End of Its Compression Stroke into UHMWPE

Figure 29 shows the force-displacement curve of a flat-ended fully threaded plunger during quasi-static testing. The test evaluated the critical flow stress for phase transition of UHMWPE from solid to viscous fluid state. During the viscous stage, the UHMWPE offers consistent-load, high-damping characteristics. The displacement rate for this test was 0.25 inches per minute (in/min). By performing several exploratory tests, the researchers confirmed that a reversible-phase transition takes place under high-compressive 3D stress states within the confines of the containment cylinder. The transition is reversible in the sense that upon removal of the applied load, the material regains its solid state. As seen in Figure 29, the UHMWPE behaves as an elastic low-modulus material up to a compressive stress level of approximately 25,000 pounds per square inch (psi). For this test, the stress corresponded to a compressive force of 20 kilopounds (kip). Beyond this point, the material behaves as a plastic material with no or very little further increase of load or stress level. Figure 30 displays the result of another test, utilizing a plunger with a conical front, pushed at a slightly higher displacement rate of 10 in/min.

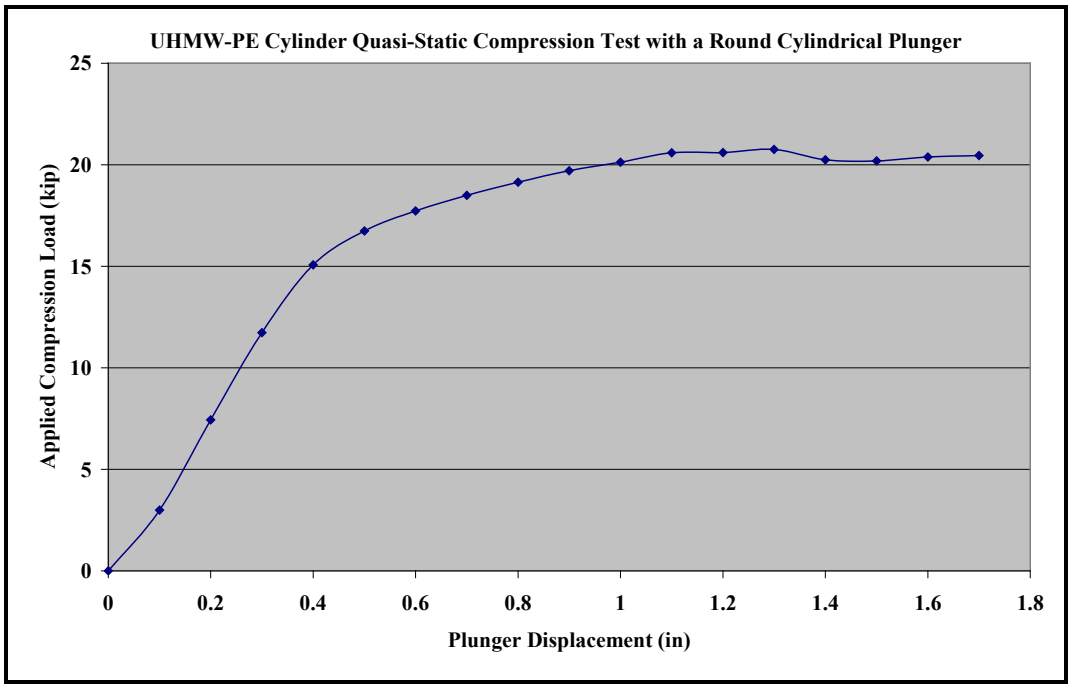

Figure 29. Quasi-Static UHMWPE Deformation with Threaded Flat-End Cylindrical Plunger

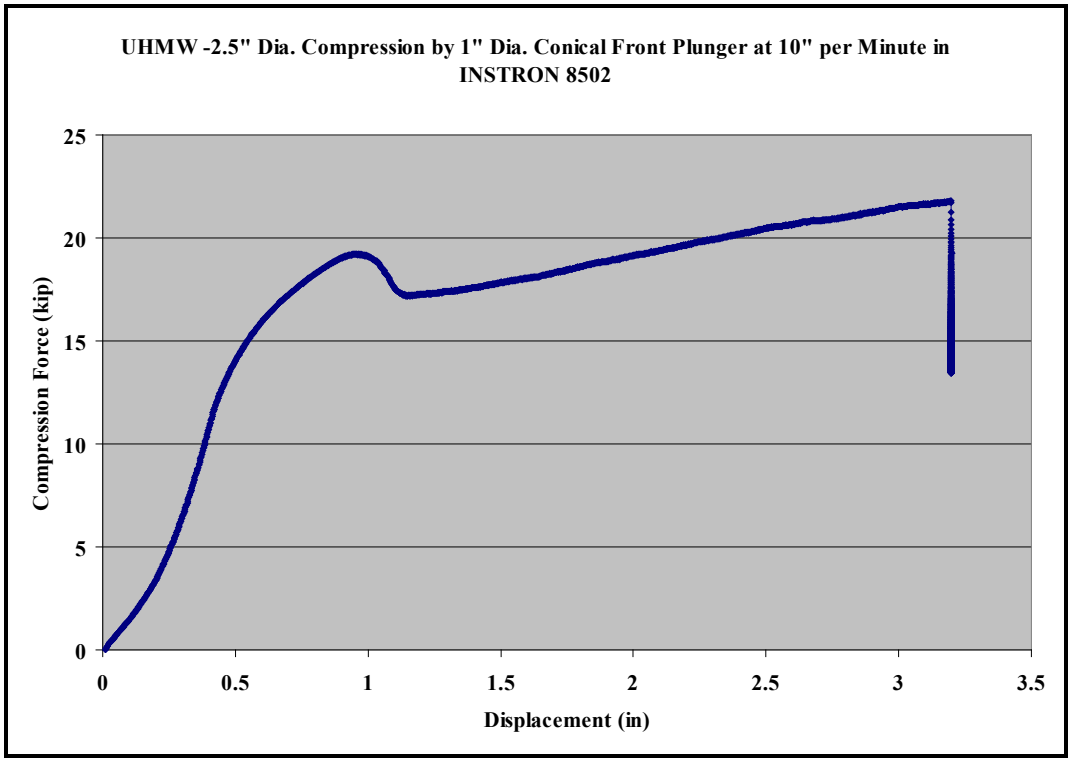

Figure 30. Quasi-Static UHMWPE Deformation with Conical Front Plunger

Evidence of the phase transition came from a test using a flat-faced cylindrical plunger. In this test, the Instron test machine forced a section of threaded steel rod with flat ends into the UHMWPE cylinder. The material deformed around the threads, allowing the core of the material

to remain in a stressed state. Following the test, the researchers sliced the cylinder axially while its core in front of the plunger was still under stressed condition. As the cylinder separated, the threaded steel rod popped out, and some UHMWPE material expanded (oozed out) in a triangular zone just ahead of the end of the bar. Once the applied stress abated, the material solidified in both halves of the sliced cylinder. Figure 31 shows a photograph of the sliced halves of the UHMWPE cylinder and the threaded steel bar used in the test. The flow of material at the moment of separation offers evidence for the transition from solid to viscous fluid under load. The solidified material offers evidence of the phase transition from viscous state to solid state upon stress relieving.

Figure 31. Test Sample with Thread Impressions and Solidified Face Material

On the basis of this information, along with data from the direct load displacement tests, the researchers considered the compressive stress of 25,000 psi as a critical quasi-static compressive stress for the UHMWPE material. Above this stress, the material begins to behave as a viscous fluid under continued loading, maintaining a constant force throughout displacement.

Computation of energy absorption from force versus displacement curves of quasi-static test showed potential for its application as a SEA. To be useful, however, the behavior must be consistent during the high-strain-rate conditions of an impact. During high-strain-rate events, materials can display different properties, appearing stiffer or softer than traditional published data. Researchers planned further testing using high-velocity impact loading to evaluate the UHMWPE for the conditions of the in-line collision.

4.4 Pendulum Impact Test Setup and Instrumentation

For the initial high-rate test, the researchers used a large radius pendulum housed at QNA TSG's Transportation Research Center to generate speed in a known impact mass. Figure 32 shows a schematic of the test setup. The base of the containment cylinder mounts horizontally at the lowest point of pendulum swing. Release height of the pendulum determines impact speed. The apparatus allowed for speeds of 15-20 ft/s, approximately half of the predicted in-line collision case (25-30 mph or 40 ft/s). A 200-kilopound compression load cell provides load measurement. The load cell mounts to a vertical post to provide a rigid backstop. The steel plunger of the SEA extends beyond the cylinder in the path of the pendulum. The plunger has a conical front end (vertex angle of 90°) guided with a linear bushing to move horizontally. Upon impact, the

plunger moves coaxially and makes contact at the centerline of the UHMWPE specimen within the containment steel cylinder.

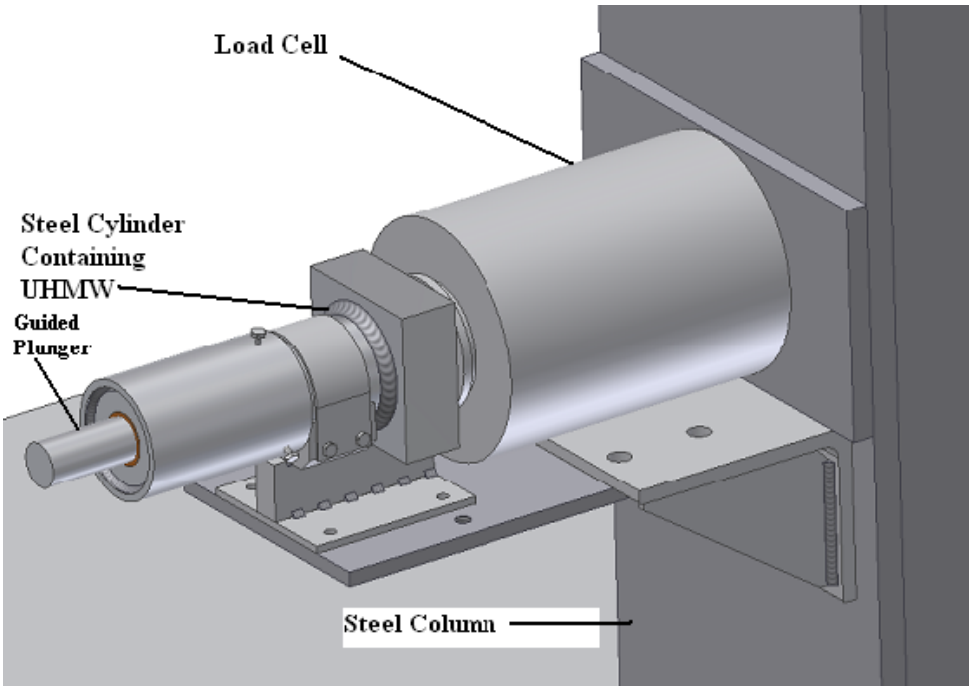

Figure 32. Schematic of Pendulum Impact Test Setup for HSR Evaluation

The swinging pendulum hangs from a cross beam approximately 20 ft above the impact point. This provides a large radius of motion, with the lowest point of the arc coinciding with the rear end of plunger. The impacting mass is a lead-filled, heavy-walled steel box with a total weight of 175 lb.

Test personnel used a block and tackle to raise the impacting mass to a specific height above the ground. A release pin allowed the mass to separate from the lifting device, causing the mass to accelerate under gravity to the impact point. By varying the release height, the test personnel could vary the impact velocity. Figure 33 shows the pendulum raised to the release height prior to a test. The maximum test height was approximately 7 ft (84 in) above ground. From conservation of energy, the theoretical impact velocity from this height is 16.9 ft/s.

Figure 33. Pendulum Impact Test Setup with Mass Raised to a Height of 84 in above Ground

Figure 34 shows the actual test setup. The flat ruler mounted just behind the plunger allows for displacement measurement via high-speed video. The severe shadows are due to the high-intensity light source needed for video capture. The load cell is visible at the left edge of the frame. Figure 35 shows a high-speed video camera, a high-intensity light source, and a data acquisition laptop computer. For the pendulum tests, the camera recorded at the rate of 10,000 frames/s, allowing study of the progressive motion of the plunger and the pendulum mass at uniform time intervals of 100 microseconds (μs).

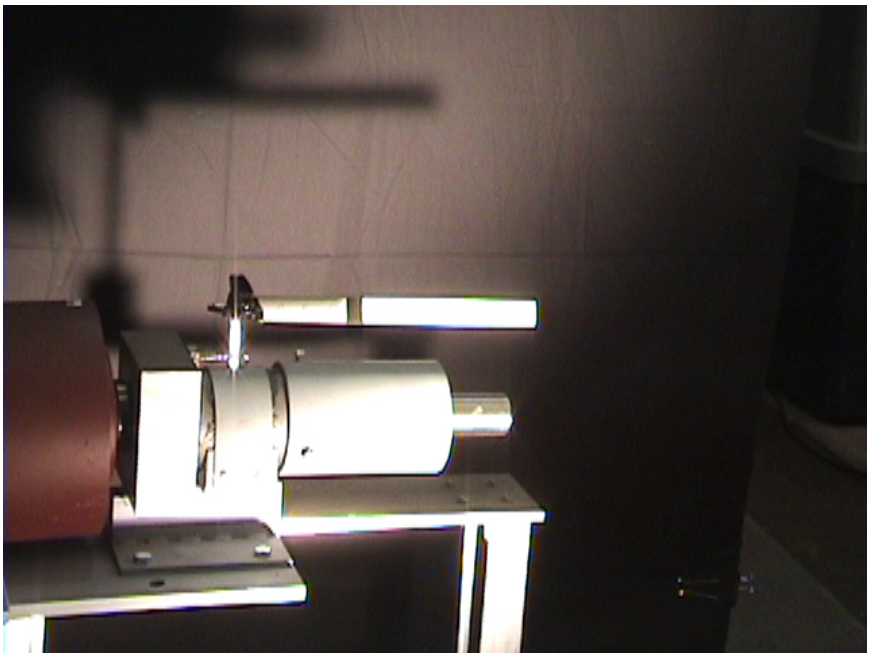

Figure 34. Test Setup Used in the Pendulum Impact Test

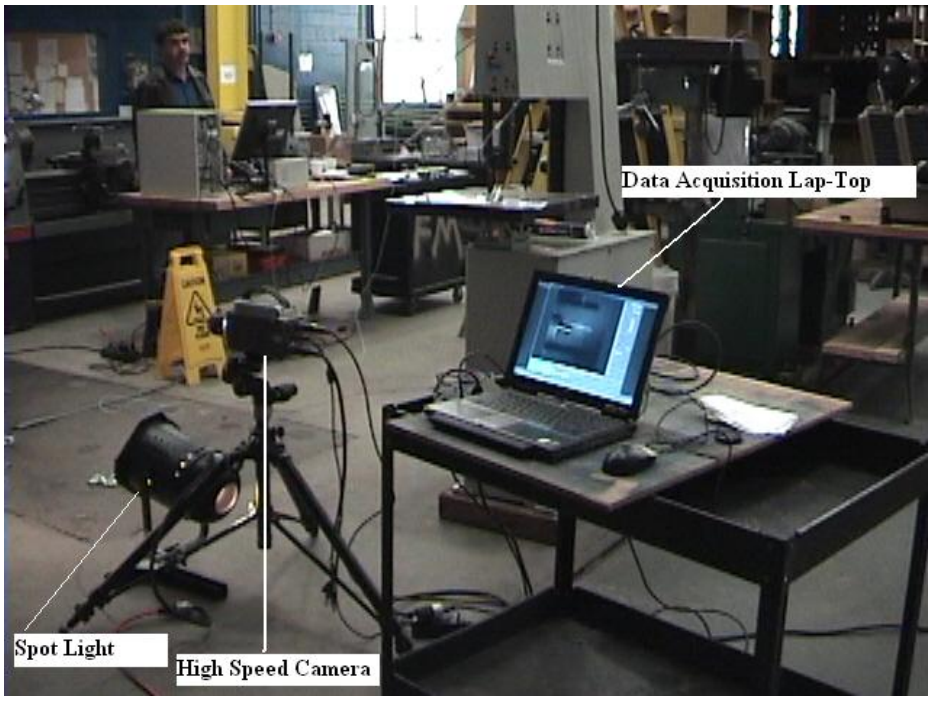

Figure 35. High-Speed Camera and Video Data Acquisition Setup

Accelerometers on the cylinder and pendulum collected motion data during the test. The load cell measured impact forces. LabView® software and associated hardware collected electronic data. Postprocessing of the high-speed video provided displacement data and verification of impact speed. Figure 36 shows the test sample and load cell.

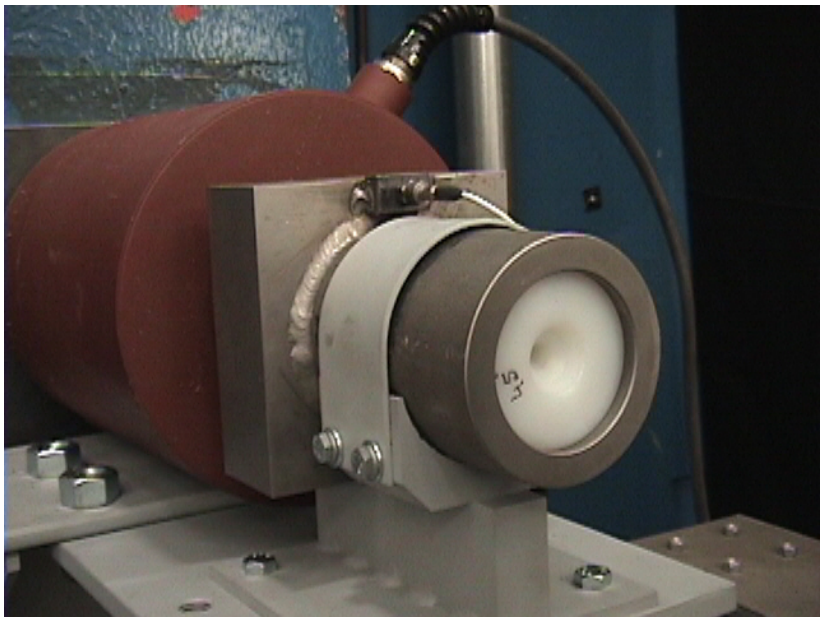

Figure 36. Accelerometer Location for Post-impact Acceleration Measurement

4.5 Test Procedure

Before each test, test personnel zeroed the sensor signals and verified connections. Before pendulum release, the camera operator turned on the light source and set the camera to record for 2 s after triggering. The camera captured video at 10,000 frames/s.

Test personnel manually released the pin holding the pendulum immediately following activation of the data collection system. Pendulum impact drove the plunger into the UHMWPE coupon, absorbing the associated KE. On several tests, the cylinder stopped the pendulum without rebound. Test personnel downloaded and saved sensor data for future analysis. Similarly, test personnel saved frame-by-frame video data via image processing software.

4.6 Analysis of Test Data

Image processing required calibration of each video file. Distances along either the flat ruler or damper cylinder provided fixed distance for calibration. The impact velocity of the pendulum with the plunger was determined by noting position over several frames before impact. Time was determined from the frame rate at video capture. Derived pendulum velocity was 16.7 ft/s.

A motion analysis module of the video capture software provided a means of determining the device stroke as a function of time. The elapsed time represents the duration from pendulum impact to the point of complete stroke. The positional change of the pendulum edge provides distance measurement. Using this data and the force/time data collected from the load cell, test personnel computed instantaneous values of plunger position, velocity, and the crush force magnitudes. Figure 37 shows the variation of pendulum inertia force with time from the instant of the pendulum mass striking the plunger. Figure 38 shows the corresponding impact force versus displacement plot.

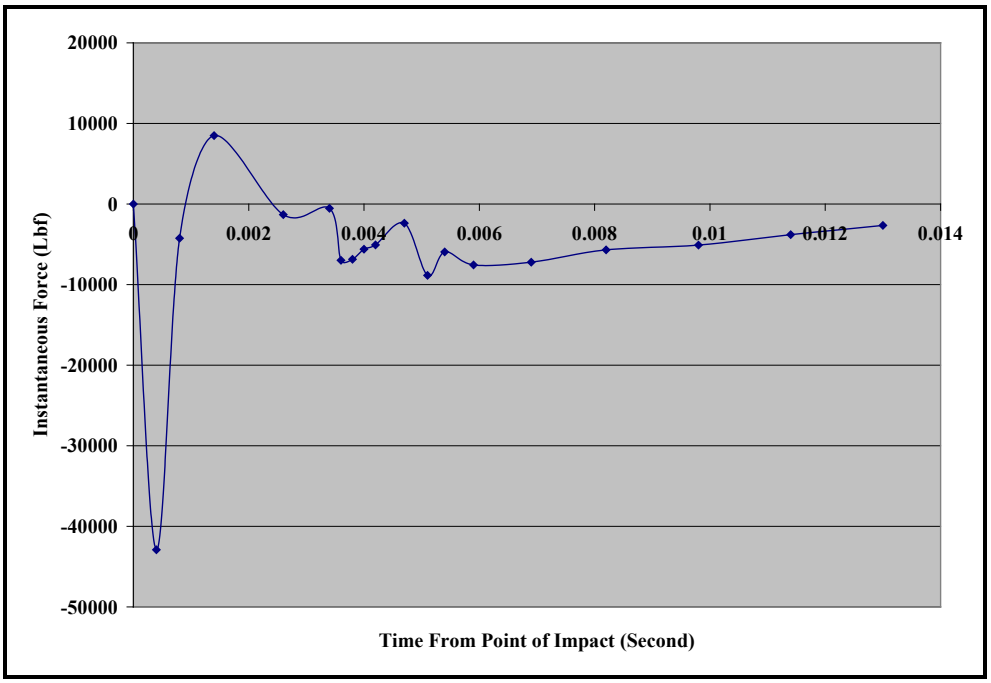

Figure 37. Instantaneous Inertia Force in Pendulum vs. Time

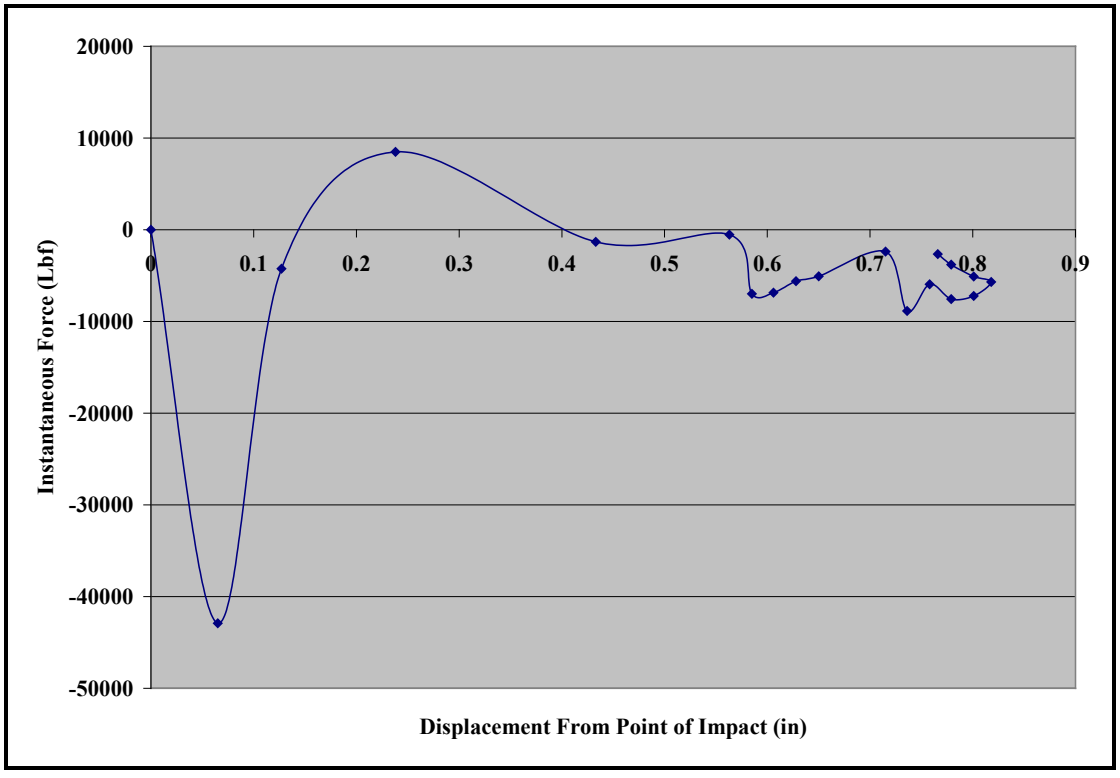

Figure 38. Instantaneous Inertia Force vs. Plunger Displacement

The peak instantaneous inertial force 42 kip develops over the first 0.065 in (Figure 38) or within 0.4 ms from impact (Figure 37). Beyond this point, the plunger deforms and penetrates the UHMWPE for a total displacement of 0.8 in. During this portion of the event, the UHMWPE offers a lower resistance (inertial forces less than 10 kip). This indicated the efficacy of the

UHMWPE material as a shock absorbing material under a high-strain rate. However, the plunger did not penetrate the UHMWPE material completely, causing the pendulum to bounce back from the plunger.

During this test series, the researchers determined that the high-capacity load cell was not sensitive enough to resolve force versus displacement data. However, the tests did indicate that the SEA provided significant damping.

On the basis of these results, the researchers concluded that the available KE in the pendulum was inadequate to drive the plunger completely into the UHMWPE cylinder. Subsequent tests utilized a plunger diameter of 0.5 in to lower the required force. These tests also utilized a more sensitive dynamic load cell with a peak capacity of 10 kip. The test matrix allowed evaluation of geometric parameters described in the following section.

4.7 Evaluation of Effects of Geometric Parameters

To evaluate the effects of plunger size and material area, researchers developed a simple test matrix for the next set of pendulum impact tests. This test made use of the original test setup but used an additional steel liner inside the cylinder to reduce the cylinder inner diameter (ID) to achieve the desired cross-sectional area ratio. Researchers also evaluated the effects of a cone angle at the end of the steel plunger, using both 90° and 60° faces. Table 3 shows the matrix for tests performed on May 21, 2009, at QNA TSG's Transportation Research Center facility in Fitchburg, MA.

Table 3. Test Matrix Used for Evaluation of the Effects of Geometric Parameters

Test No.	Plunger Diameter (in)	Plunger Frontal Cone Angle	UHMWPE Diameter (in)	Area Ratio*	Remarks
1	0.5	90°	2.5	25	UHMWPE snug-fit inside cylinder
2	0.5	60°	2.5	25	UHMWPE snug-fit inside cylinder
3	0.5	90°	1.25	6.25	Steel liner of 1.25" ID used within cyl.
4	0.5	60°	1.25	6.25	Steel liner of 1.25" ID used within cyl.

***Area ratio refers to the ratio of cross-sectional area of UHMWPE to that of cylindrical plunger.**

The test setup and procedure were the same as described in Sections 4.4 and 4.5. The pendulum mass and swing radius remain unchanged. Slight variations noted in pendulum release height resulted in slight variations of impact velocity. Data collection and video capture remained at a 10-kilohertz frequency, with data recorded on the data acquisition PCs. These data required postprocessing to derive useful information. Figure 39 shows a picture of the test setup used for the pendulum impact test.

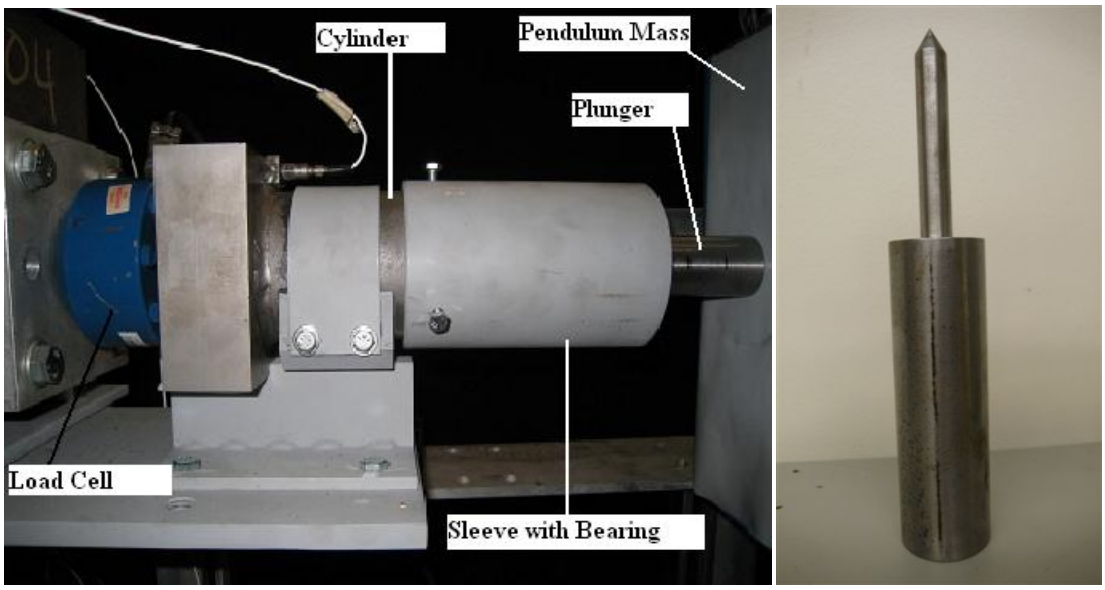

Figure 39. Test Setup Used for the Pendulum Impact Test and the 0.5-Inch-Diameter Plunger

4.7.1 Test 1

Researchers computed the strike velocity at the point of impact between pendulum and plunger via image processing software. Impact velocity for Test 1 was 17.025 ft/s. Figure 40 shows the impact point along with the references used for calculation.

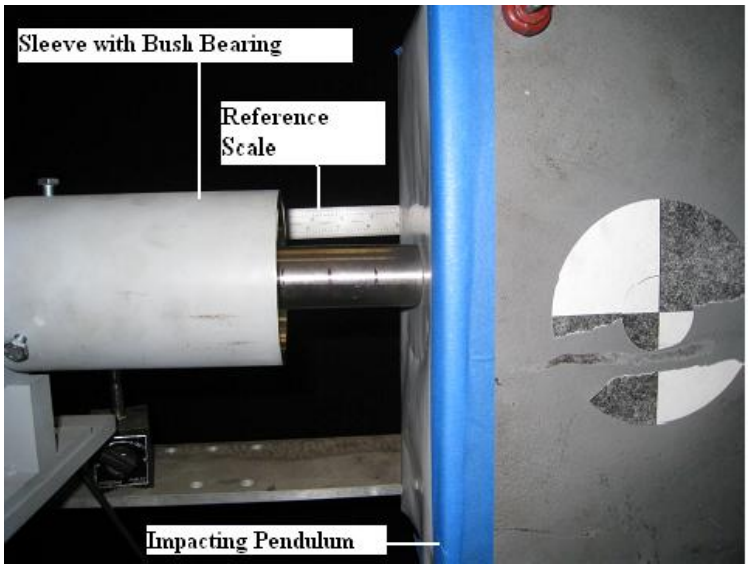

Figure 40. Reference System Used for Displacement and Velocity Evaluation

The video record indicates that the plunger penetrated the UHMWPE material within the first 5 ms of impact. Physical limitations allowed for only 2.25 in of plunger stroke. Figure 41 shows the variation of compressive force experienced by the load cell (resting against the base of cylinder) and displacement of the plunger with time following the impact event.

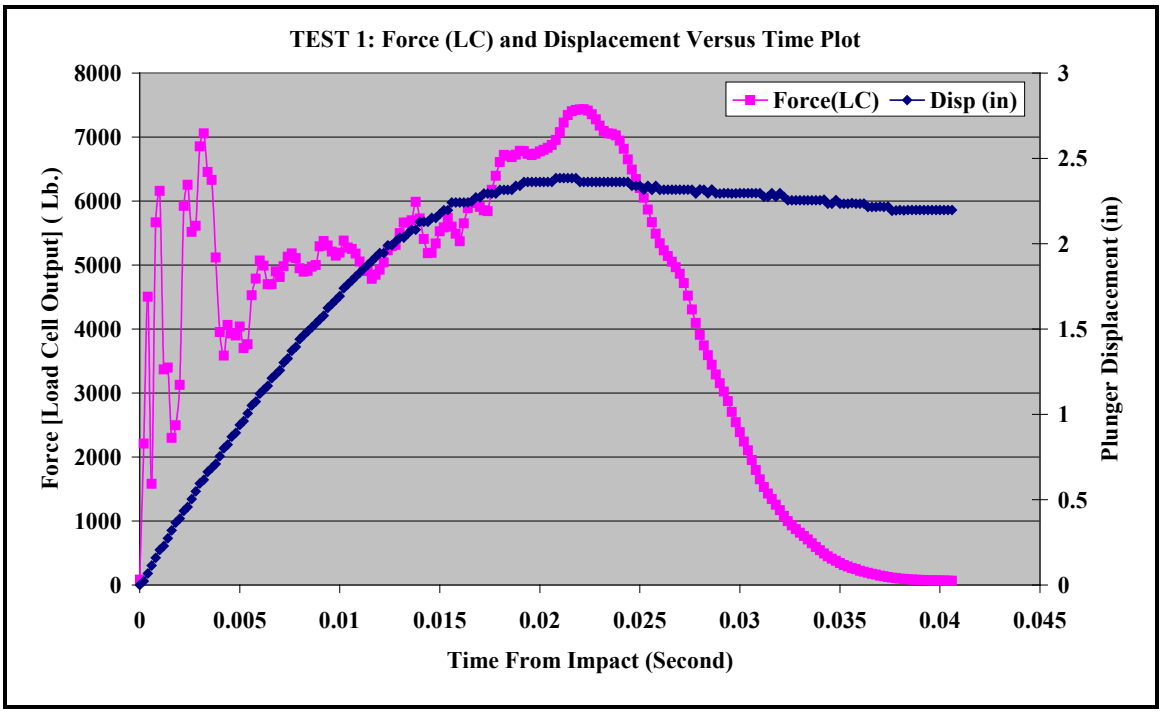

Figure 41. Plunger Force and Displacement vs. Time after Impact (Test 1)

During the initial impact, the plunger experiences transient dynamic forces with peak amplitude of approximately 7,000 lb (Figure 41). At the 5-millisecond mark, the UHMWPE material at the plunger face reaches critical compressive stress, transitioning from solid to viscous state. After this, the resistive force from the UHMWPE drops below 4,000 lb, increasing slowly as the plunger travels farther. At the 22-millisecond mark, the force peaks at approximately 7,500 lb because of the high-squeezing effect on the UHMWPE as it accommodates the added volume of the plunger.

Figure 42 shows the force displacement curve for Test 1. The area under this curve represents the work done by the plunger during the event. Motion analysis of the high-speed video provided plunger displacement data. The striking velocity of pendulum on the plunger was 17.025 ft/s, and the corresponding KE of pendulum (at 175 lb) was 787.64 ft-lb. (9,451.6 in-lb). The estimated work, based on the area under the curve in Figure 42, was 9,422 in-lbf.

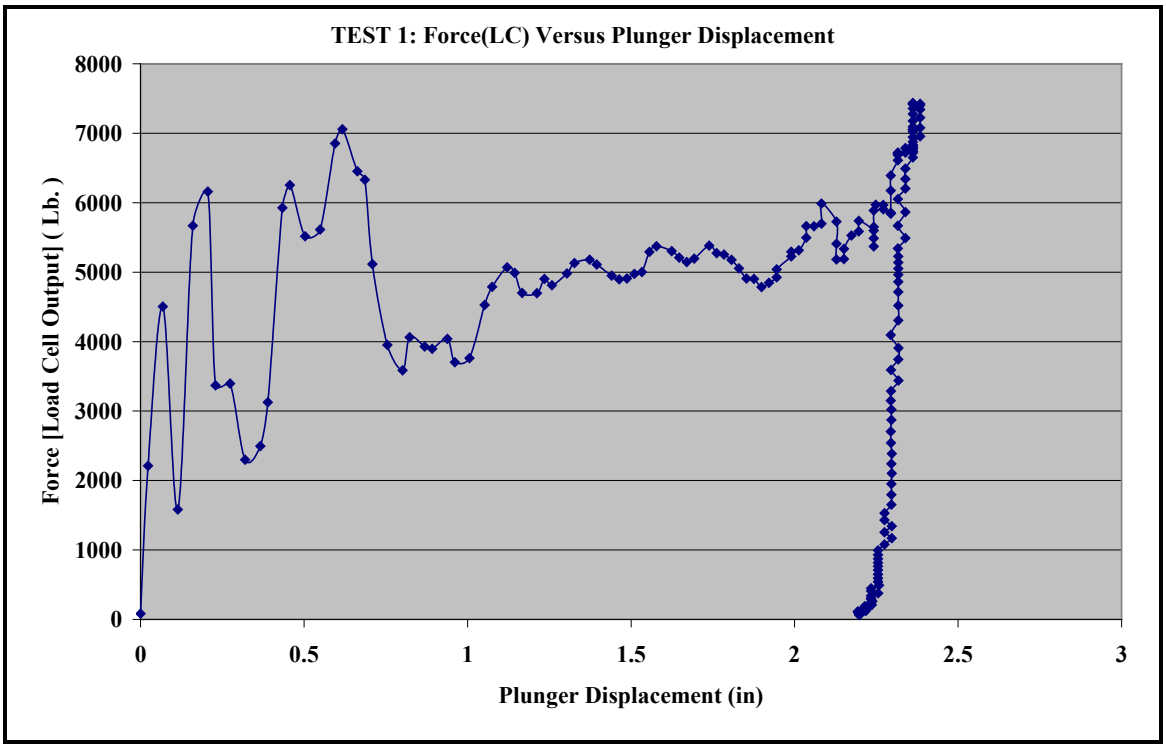

Figure 42. Force vs. Displacement Curve for the Plunger (Test 1)

4.7.2 Test 2

Using the same procedure, researchers determined the impact velocity for Test 2 at 17.14 ft/s. Before the pendulum struck the plunger, the KE of the pendulum was 798.44 ft-lb (9,581.25 in-lb). Variations in plunger configuration allowed the maximum plunger stroke to increase to 2.475 in. Figure 43 shows the variation of compressive force experienced by the load cell and the displacement of the plunger with time following impact.

Figure 44 shows the corresponding force experienced by the plunger and its displacement into UHMWPE cylinder in the process of absorbing the KE through doing work. The estimated work, based on the area under the curve in Figure 44, was 9,211 in-lbf.

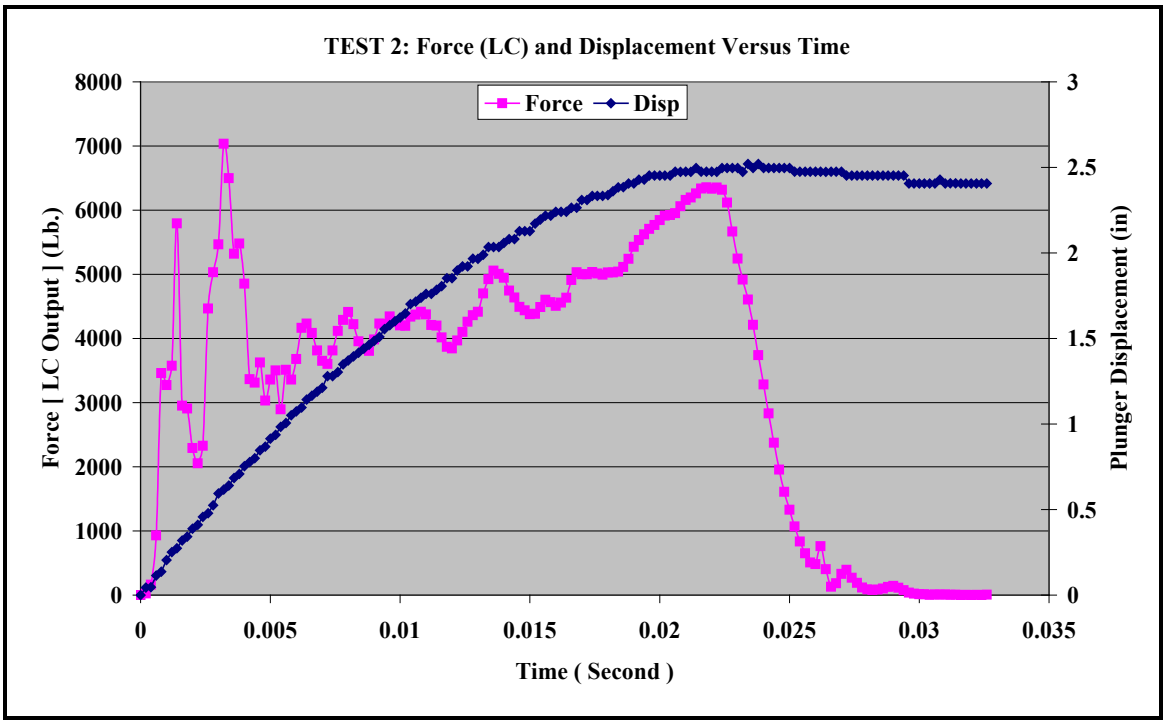

Figure 43. Plunger Force and Displacement vs. Time after Impact (Test 2)

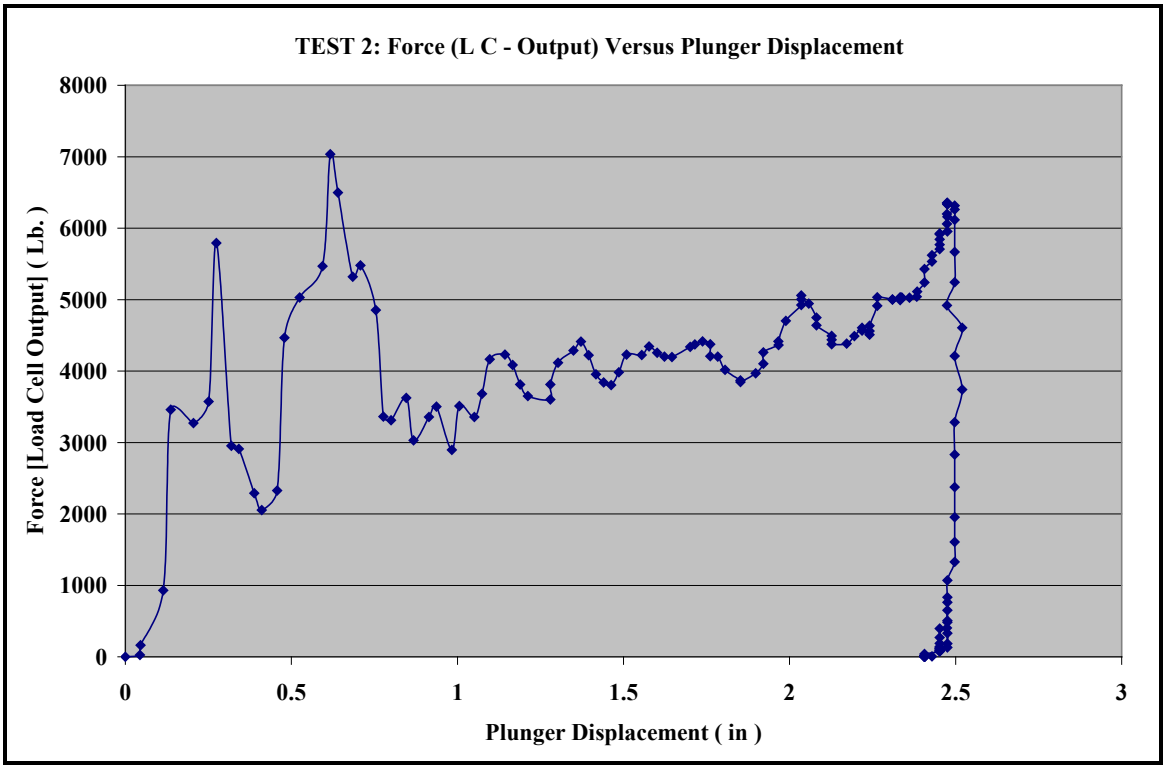

Figure 44. Force vs. Displacement Curve for the Plunger (Test 2)

4.7.3 Test 3

Using the same procedure, researchers determined the impact velocity for Test 3 at 16.94 ft/s. Before the pendulum struck the plunger, the KE of the pendulum was 779.48 ft-lb (9,353.75 in-lb). Variations in plunger configuration limited the maximum plunger stroke to 2.151 in. Figure 45 shows the variation of compressive force experienced by the load cell and the displacement of the plunger with time following impact.

Figure 46 shows the corresponding force experienced by the plunger and its displacement into the UHMWPE cylinder in the process of absorbing the KE through doing work. The estimated work, based on the area under the curve in Figure 46, was 9,349 in-lb.

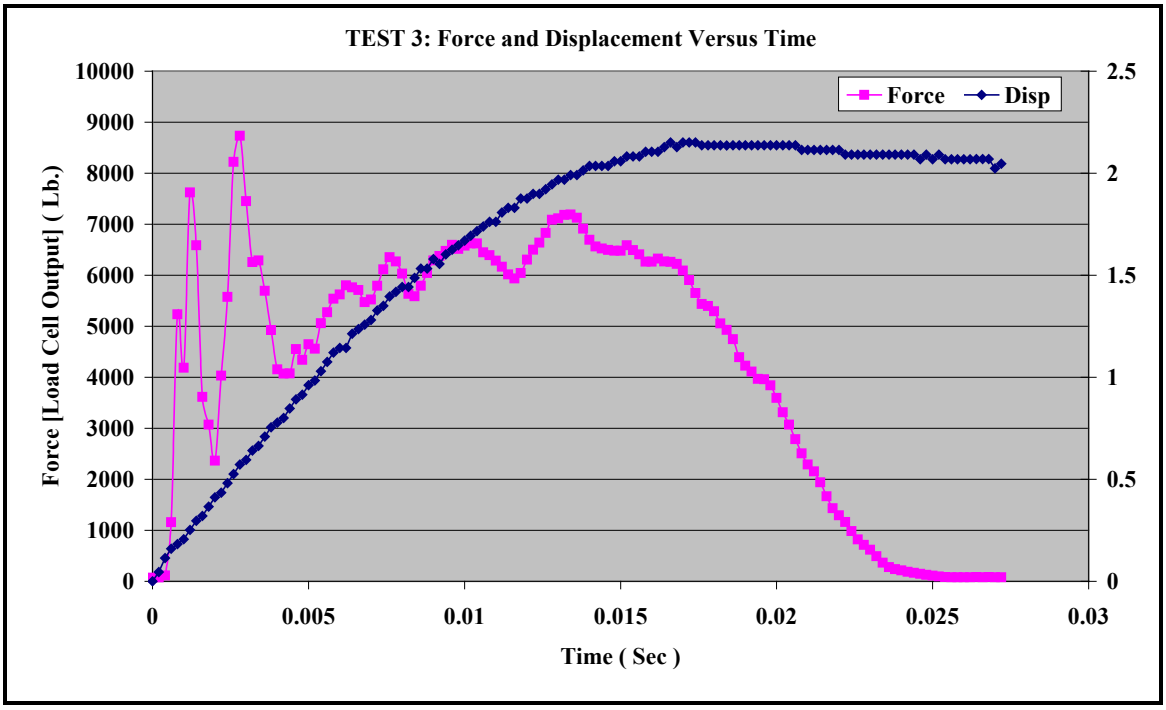

Figure 45. Plunger Force and Displacement vs. Time after Impact (Test 3)

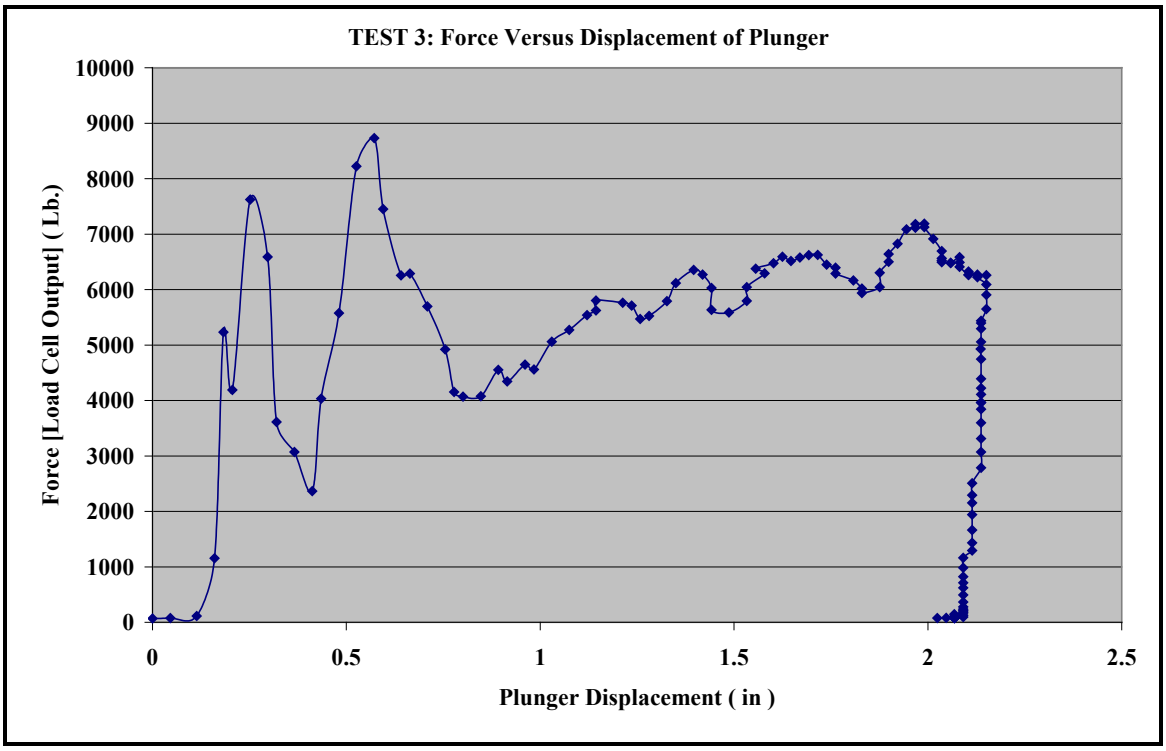

Figure 46. Force vs. Displacement Curve for the Plunger (Test 3)

4.7.4 Test 4

Using the same procedure, researchers determined the impact velocity for Test 4 at 17.13 ft/s. Before the pendulum struck the plunger, the KE of the pendulum was 797 ft-lb (9,564 in-lb). Variations in plunger configuration allowed the maximum plunger stroke to increase to 2.251 in. Figure 47 shows the variation of compressive force experienced by the load cell and the displacement of the plunger with time following impact.

Figure 48 shows the corresponding force experienced by the plunger and its displacement into UHMWPE cylinder in the process of absorbing KE of impact through doing work. The estimated work, based on the area under the curve in Figure 48, was 9,234 in-lb.

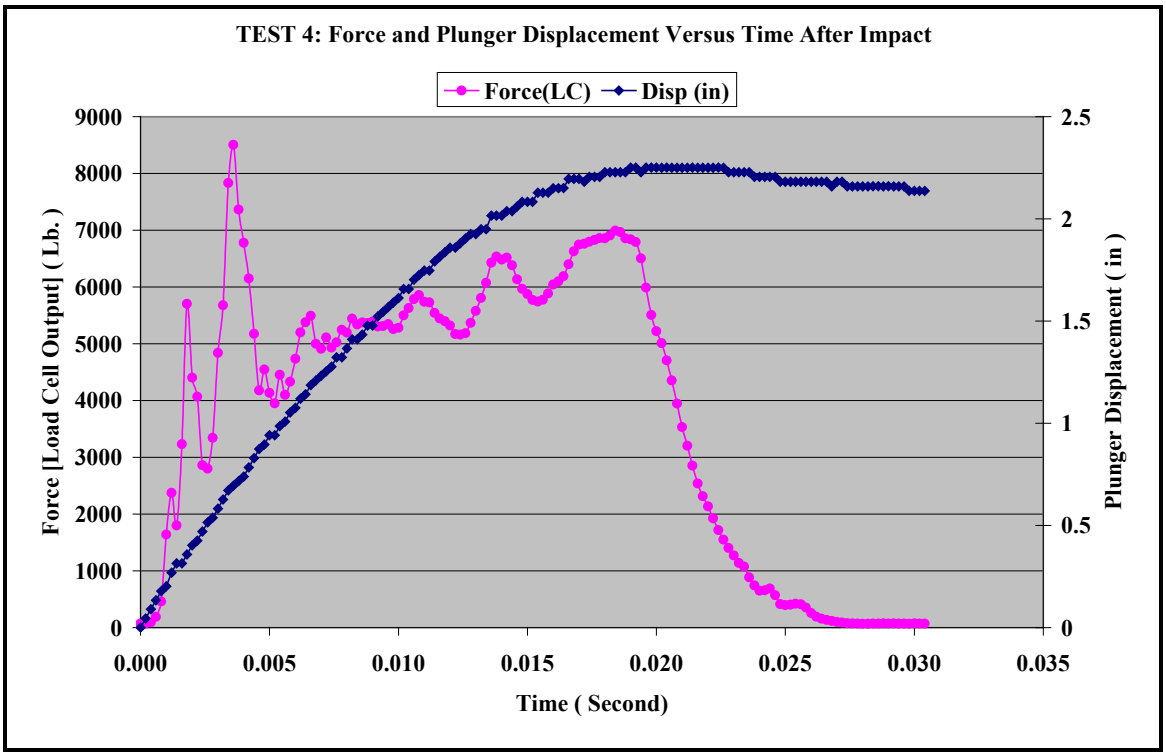

Figure 47. Plunger Force and Displacement vs. Time after Impact (Test 4)

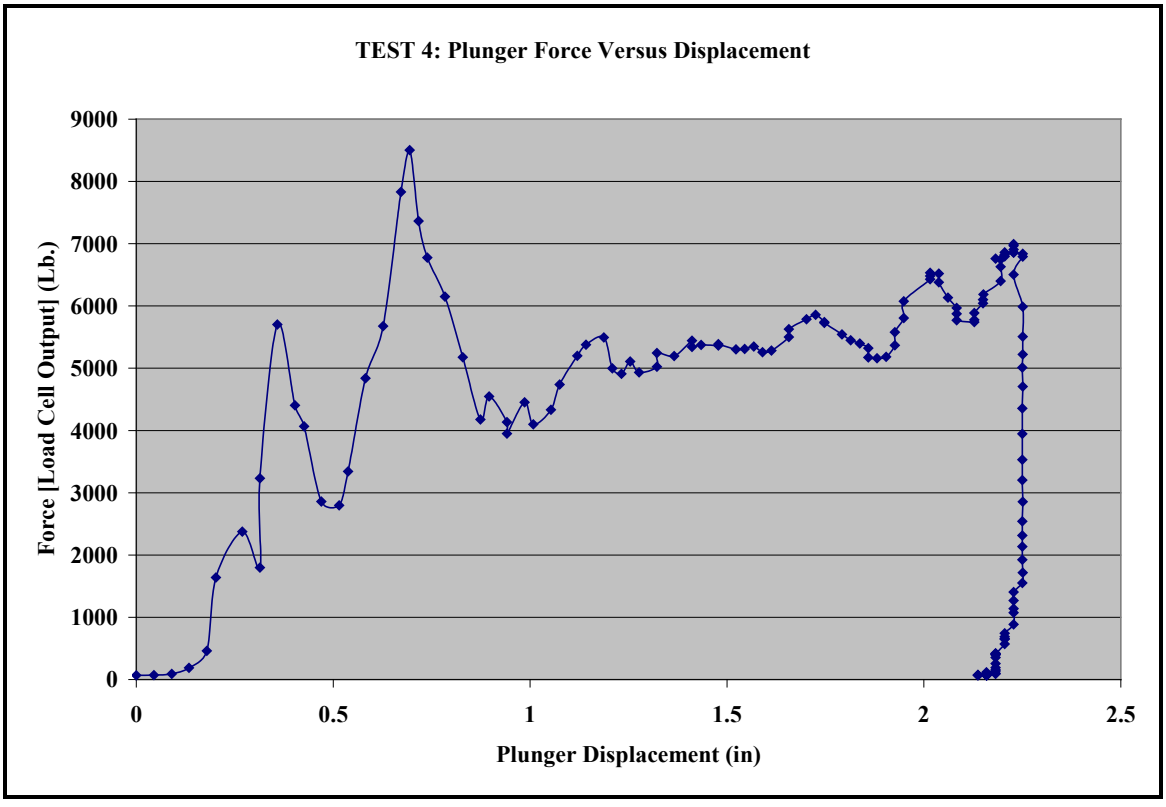

Figure 48. Force vs. Plunger Displacement following Impact Event (Test 4)

In summary, all four pendulum impact tests demonstrate the effectiveness of the solid-state shock absorption concept. Furthermore, the tests determine two important geometric parameters that govern the energy absorption and transitional force level. The primary parameter is the diameter of the plunger and the cross-sectional area ratio of the UHMWPE cylinder to that of the plunger.

A secondary parameter is the cone angle of the plunger face. Figure 49 shows a comparison of impact force vs. time between Test 1 and Test 2. For these two tests, the plunger diameter was 0.5 in and the area ratio was 25. However, the cone (vertex) angles of plunger were 90° and 60° respectively. Note that the drive force on the 60° plunger drops by 10 percent during the penetration phase of the event.

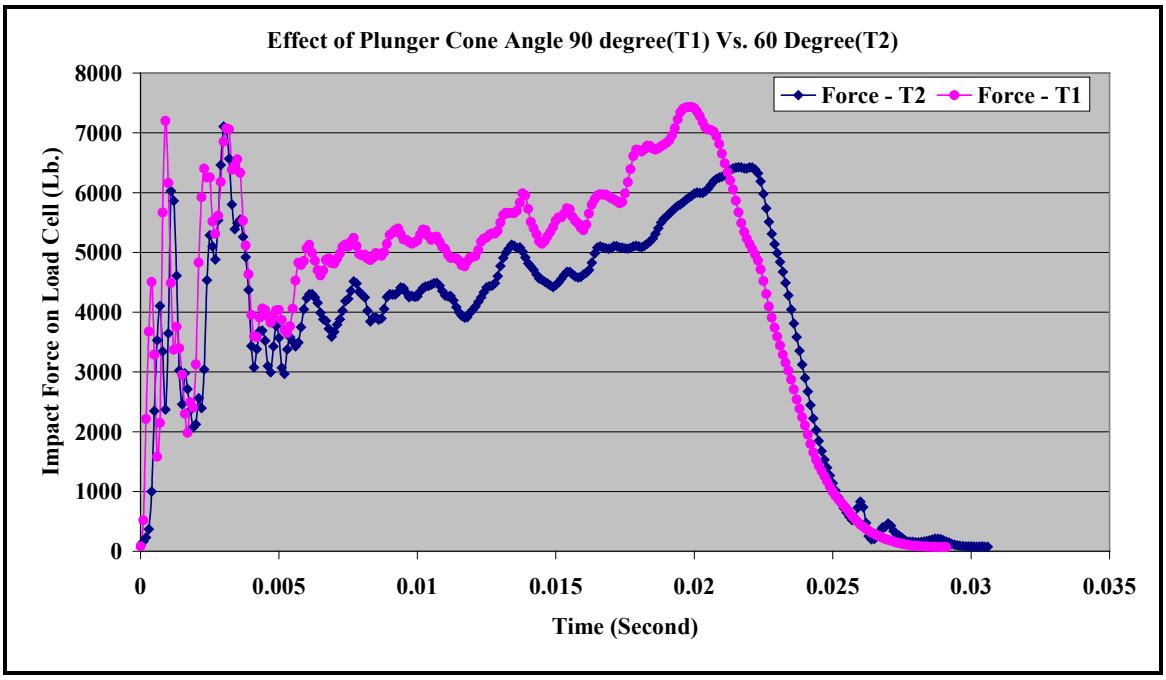

Figure 49. Force Response vs. Time for 90° and 60° Plungers (area ratio = 25)

Figure 50 shows a comparison of impact force variation versus time between Test 3 and Test 4. For these two tests, the plunger diameter was 0.5 in, and the area ratio was 6.25. A UHMWPE core of 1.25 inches in diameter allowed for reduction in area ratio. A steel sleeve compensated for the difference between the core and containment cylinder diameters. Cone (vertex) angles of the plunger were 90° and 60°, respectively.

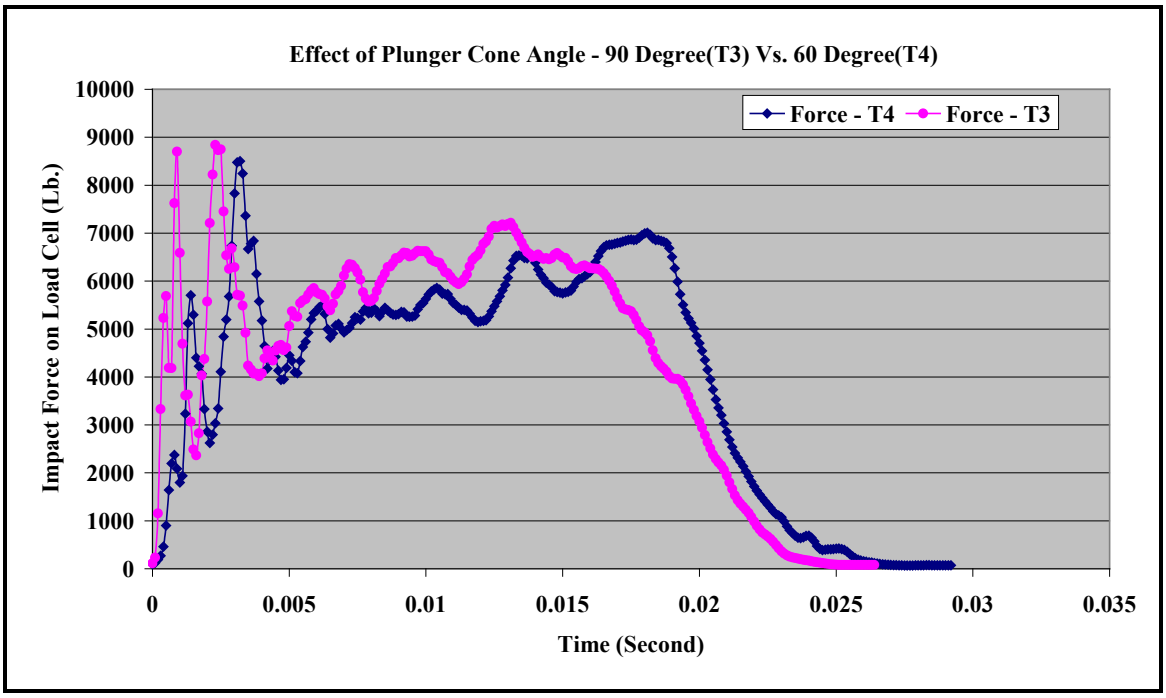

Figure 50. Force Response vs. Time for 90° and 60° Plungers (area ratio = 6.25)

Note that at this area ratio, there is no significant change in the drive force with cone angle, but the peak drive force increases by 30 percent from 7,000 to 9,000 lb. In addition, the duration of the event increases by about 10 msec.

Comparing the results from Figure 49 and Figure 50, we observe that the peak dynamic force magnitudes drop slightly with cone angle for a given area ratio.

Figure 51 and Figure 52 show comparisons of area ratio for cone angles of 90° and 60°, respectively.

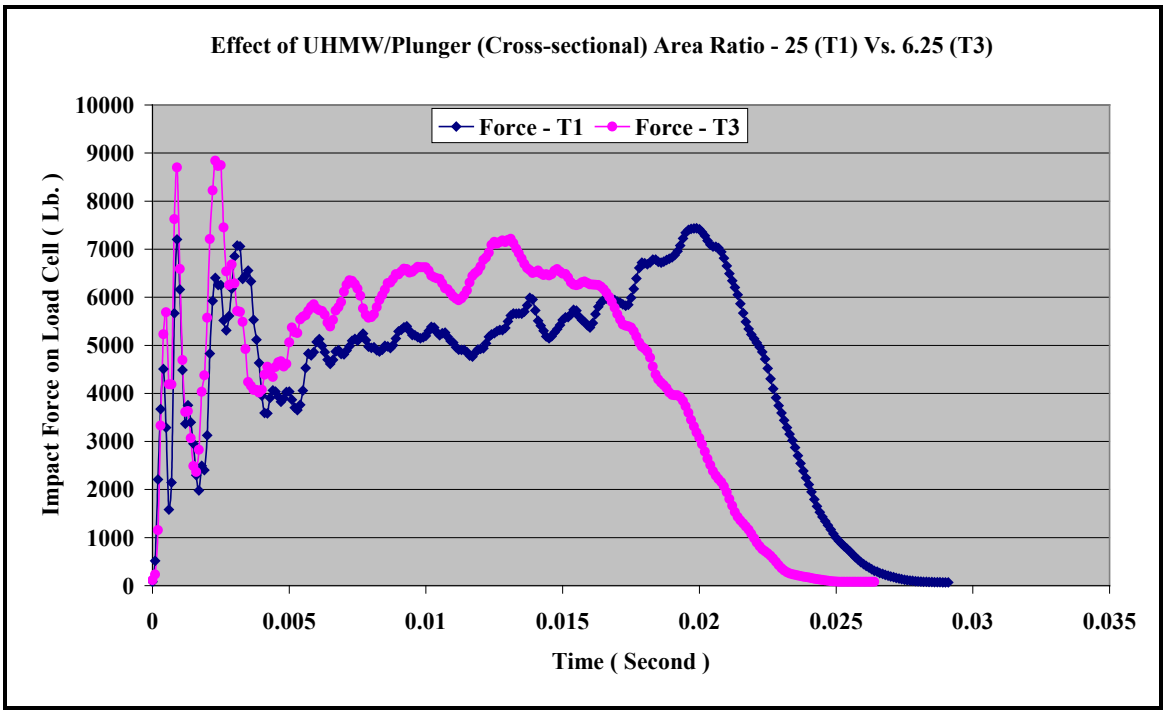

Figure 51. Force Response vs. Time for 90° Plunger for Area Ratios of 25 and 6.25

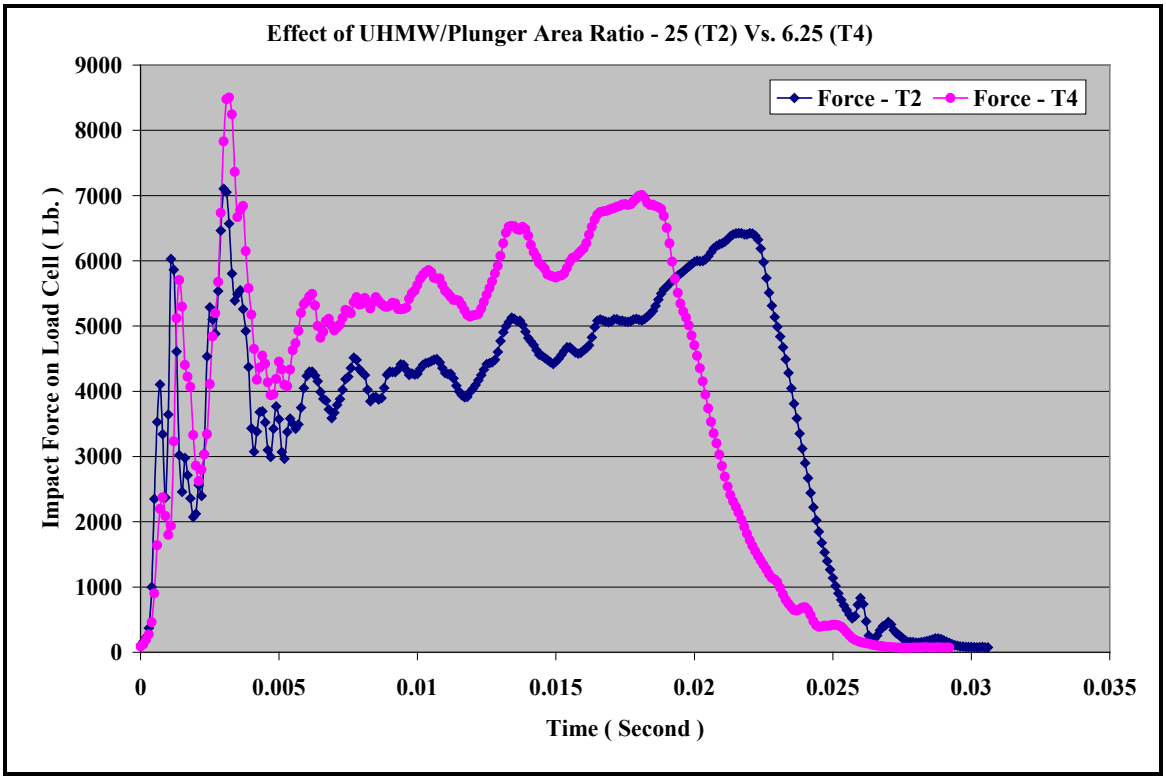

Figure 52. Force Response vs. Time for 60° Plunger for Area Ratios of 25 and 6.25

From the above two figures, it is seen that for the larger area ratio (25), the peak dynamic force magnitude is almost 7,000 lb, whereas for the smaller area ratio (6.25), it increases to approximately 9,000 lb. Area ratio, therefore, has a significant effect on the impact force requirements. Control of these two parameters—the plunger diameter and the ratio of core area to plunger area—permits controlled design of a compact CEM system. Varying the cone vertex angle does not make a difference to the peak impact force for a given area ratio but does lengthen the duration of the event slightly.

Previous quasi-static test results in the Instron test machine demonstrated the critical stress magnitude of 25,000 psi for solid to viscous transition. The speed in that test series was limited to 10 in/min by the equipment. Impact tests using HSR demonstrated a similar behavior, which is not available in the open literature. In these HSR tests, the maximum velocity of impact was approximately 17 ft/s, typical of low-speed train collisions. Using the peak dynamic force recorded during HSR tests, the researchers calculated a DSMF. The DSMF accounts for the strain rate effects in each of the four tests by factoring the specific peak stresses to the quasi-static critical stress of 25,000 psi. Table 4 provides a summary of test results. Note that the DSMF varies inversely with area ratio but is consistent for a given ratio.

Table 4. Summary of Pendulum Impact Test Results

	Test No.			
	1	**2**	**3**	**4**
Impact velocity (ft/sec)	17.025	17.14	16.94	17.126
KE of impact (in-lbf.)	9,451	9,581	9,353	9,564
Peak dynamic force on UHMWPE [from load cell] (lb) / Peak stress (psi)	7,000/ 35,651	7,000/ 35,651	8,800/ 44,818	8,700/ 44,308
Maximum plunger travel (in)	2.225	2.475	2.151	2.251
Approx. energy absorbed (in-lbf)	9,422	9,211	9,349	9,234
Cross-sectional area ratio	25	25	6.25	6.25
DSMF	1.43	1.43	1.79	1.77

4.8 Low-Temperature Effects on UHMWPE Deformation Behavior

To ensure that the proposed technology would function properly in a railroad environment, researchers performed a series of tests to evaluate the performance at low temperature. In this series of tests, the test personnel cold saturated the UHMWPE cores at 0° F for 7 days before testing with the pendulum apparatus.

Pendulum mass and release height (and, therefore, impact velocity) remained unchanged from the previous testing. Area ratios matched Tests 1 and 2 described above. To ensure that the core temperature remained as low as possible, test personnel removed the core from the freezer just before the test. The temperature of the UHMWPE test article inside the cylinder was 4.5° F just before the pendulum impact.

The plunger penetration at low temperature was identical to the previous room temperature testing. Upon removal of the plunger, the core revealed evidence of the deformed hole surface and phase transformation seen in room temperature tests. Furthermore, according to the material manufacturer, UHMWPE deformation behavior remains similar at both room and cryogenic temperatures. Thus, researchers theorize that the new SEA will be effective at low temperatures normally encountered in railroad operations in winter months.

4.9 Design and Impact Testing of a Prototype SEA

For railroad applications, the ability to scale up the design to practical dimensions is critical. To accomplish this, the researchers designed and fabricated a prototype unit having geometric dimensions as shown in Figure 53. ASF-Keystone evaluated this device at its Camp Hill, PA, facility.

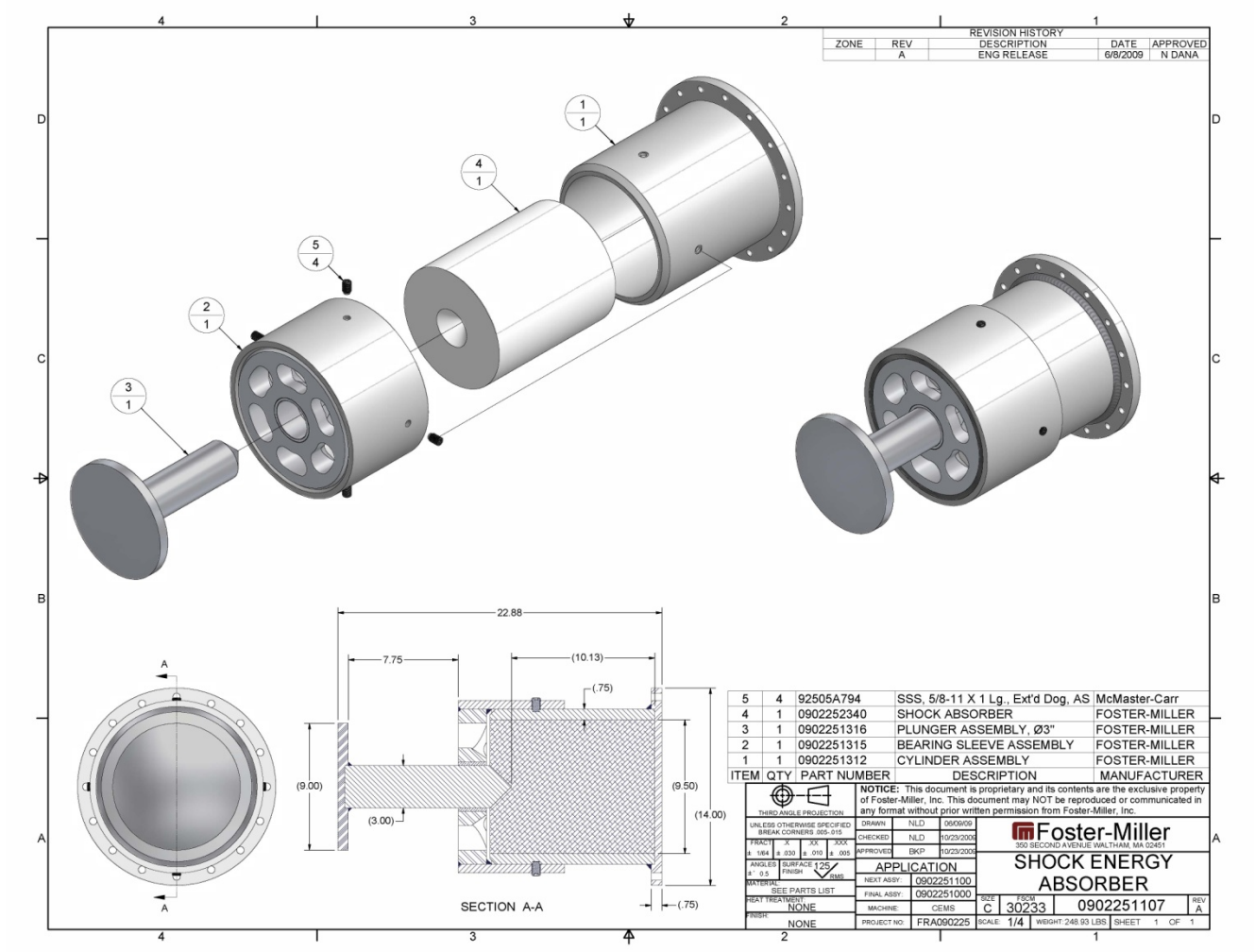

Figure 53. SEA Prototype Tested at AFS-Keystone

The components of the SEA include a seamless cylinder and the plunger fabricated to close geometry tolerances from 4140 steel. Heat treatment of these components raises the ultimate tensile strength up to 148 kilopounds per square inch (ksi). For testing, researchers also fabricated two UHMWPE cores. Figure 54 shows the assembled SEA prototype.

Figure 54. Picture of an Assembled SEA Prototype Fabricated for Drop Hammer Testing

The SEA prototype validation occurred on November 23, 2009. Researchers recorded all tests using commercial, real-time video. Testing utilized Keystone's 27, 000-pound nominal weight drop hammer. Keystone provided data collection equipment, including linear position and applied load. Figure 55 shows the AFS-Keystone drop hammer test facility and its high-speed data acquisition system.

Figure 55. AFS-Keystone Drop Hammer Test Facility and Data Acquisition System

For the first test, the initial drop height selected was 20 in. Measured plunger travel following impact was 4.5 in. Figure 56 shows the resultant force and displacement versus time. Note that during the event, there was a slight rebound from displacement, with the final plunger position remaining at 4 in.

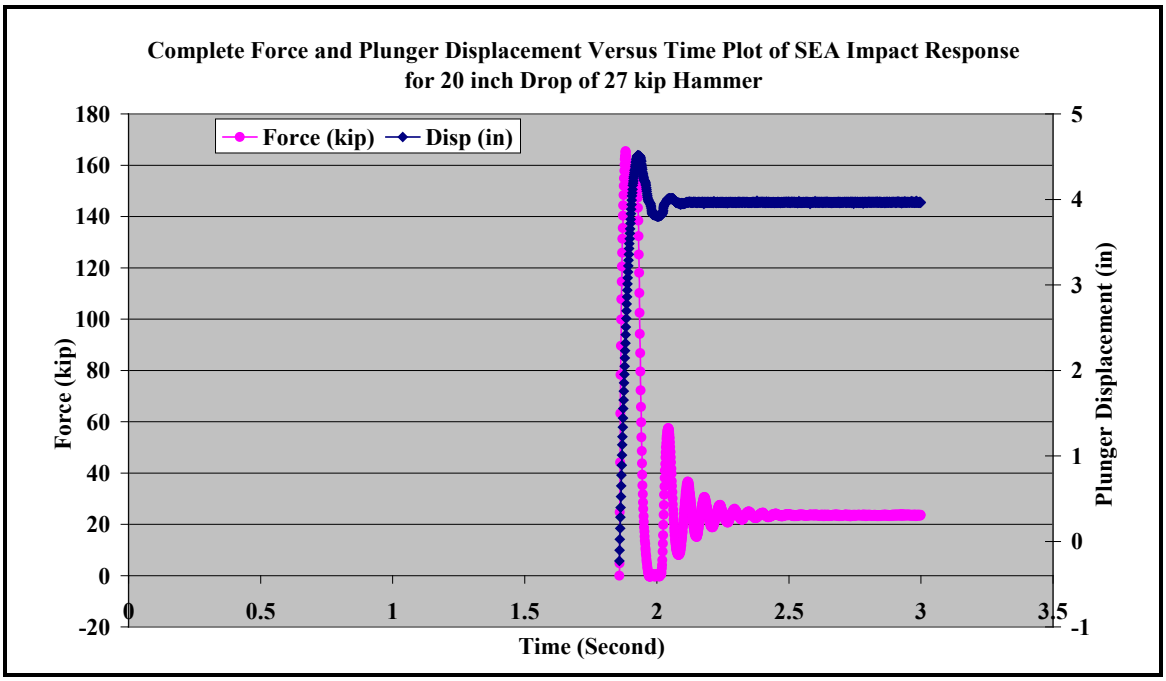

Figure 56. Force and Displacement vs. Time for 20-Inch Hammer Drop

Researchers determined that there was sufficient capacity for a second test with this core. A second drop of 8 in resulted in an additional plunger displacement of 1.5 in. Figure 57 shows the corresponding force and displacement versus time.

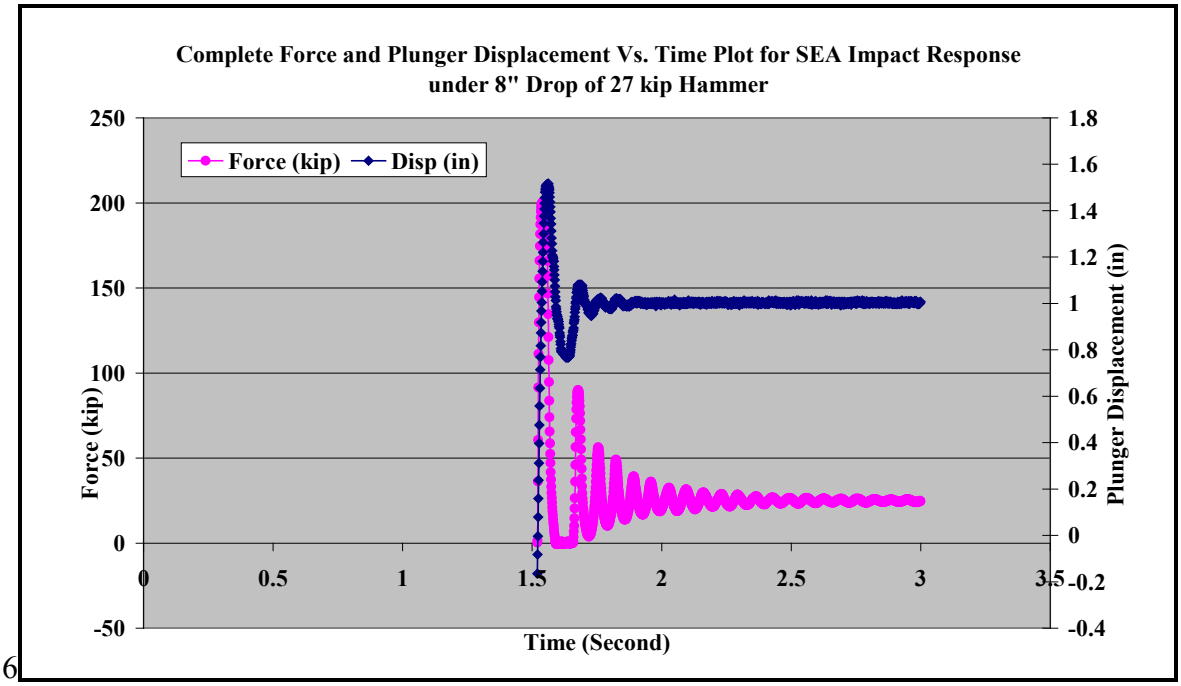

Figure 57. Force and Displacement vs. Time for 8-Inch Hammer Drop

Considering both the impact events, the total travel of the plunger was 6 in, and the total KE absorbed by the sample #1 was approximately 77,000 ft-lb.

Test personnel then replaced the core, and a third test was performed, dropping the hammer from 30.133 in above the top surface of the plunger. The plunger traveled 6.39 in, which corresponds to an energy absorption level of approximately 82,260 ft-lb. Figure 58 shows the force and displacement versus time for the 30-inch hammer drop.

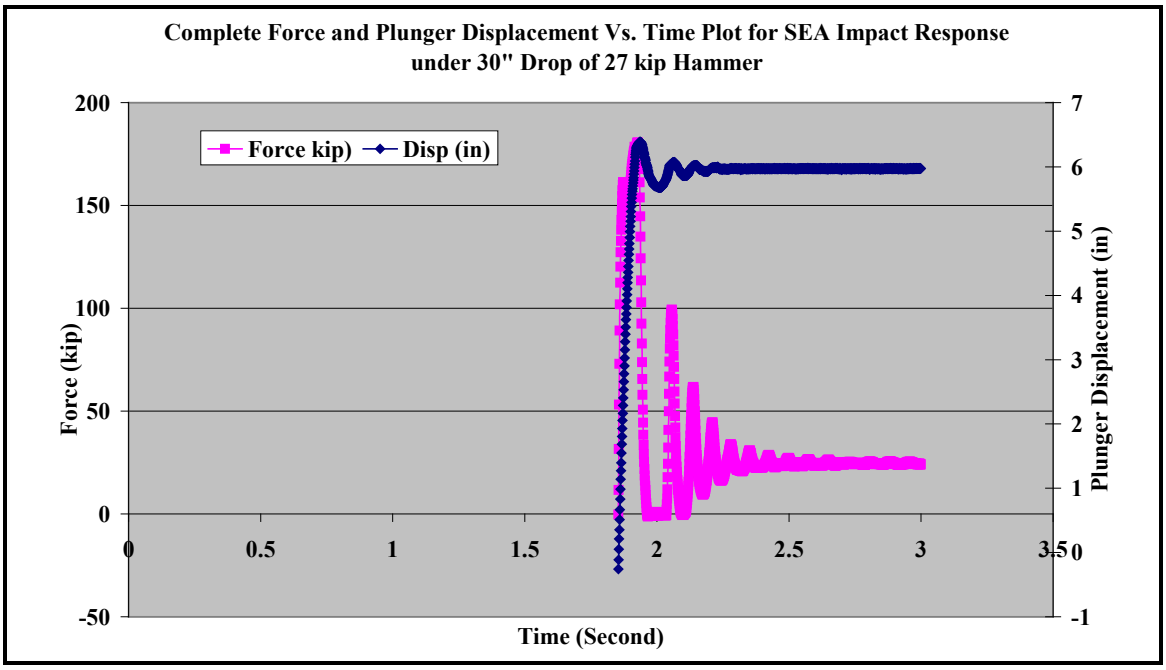

Figure 58. Force and Displacement vs. Time for 30-Inch Hammer Drop

Figure 59 shows the photographs of the SEA unit at the drop hammer test facility before and after the impact by the 27-kilpound hammer. Figure 60 shows the force versus displacement curve for the 30-inch drop used to calculate the total energy absorbed.

Figure 59. Prototype before and after Impact for 30-Inch Hammer Drop

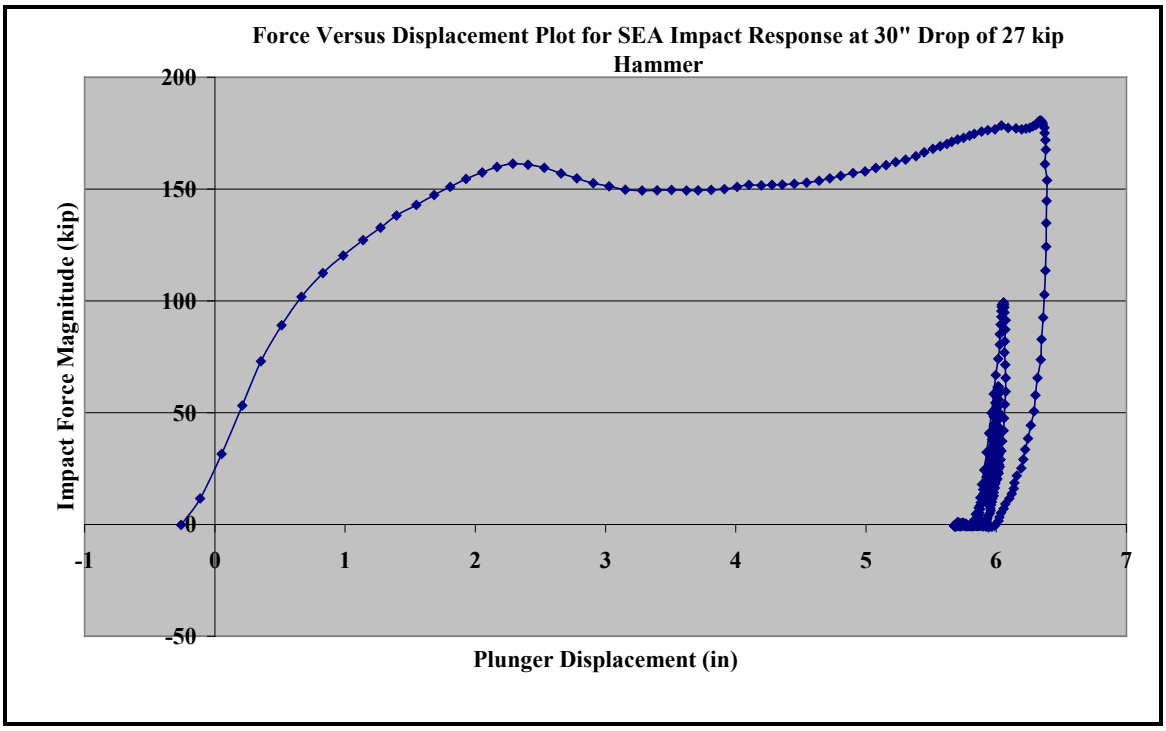

Figure 60. Force vs. Displacement Response of SEA following 30-Inch Hammer Drop

For each of the tests performed with a 27-kilopound hammer, the response of the SEA is similar. As the drop hammer strikes the top surface of the plunger, the UHMWPE resists the movement of the impact hammer applying a resistive force that peaks between 160 and 200 kip over the first 25-30 ms of the event. On reaching the critical stress magnitude for phase transition, the reaction force on the plunger drops to zero as the plunger and hammer bounce upward because of highly compressed viscous fluid at the bottom end of cylinder. With the stress on UHMWPE relieved below the critical value, the molecular bonds within the UHMWPE reestablish under the reversible-phase transition process. Next, when the plunger moves downward again, the semi-viscous solid UHMWPE develops reaction force (up to almost 100 kip as seen from Figure 60 for the case of 30 in drop) to oppose plunger motion. Each of the tests display this downward and upward bouncing motion of the plunger with progressively smaller magnitudes over a few cycles. The resulting reaction force recorded by the load cell at the end of the oscillating events was found to be the dead weight of the drop hammer resting on the top of plunger.

4.10 Analysis the SEA

The effectiveness of the CEM system described in Section 2 presupposes a SEA of a specific capacity. To enable design of a CEM system to meet the requirements of a specific locomotive, the researchers developed an analytical model of the SEA. The FEM allows for tailoring of geometric design, scaling, and dynamics to meet specific locomotive requirements. For the analysis, the researchers modeled the SEA designed for use between the front pilot plate and the reaction plate of an SD70MAC locomotive as described in Section 3. This SEA most closely resembles the unit described in Section 4.9, allowing for comparisons between model and actual test results.

4.10.1 FEM Details

Researchers created the FEM directly from geometric data generated from CAD files. The full SEA model consists of approximately 482,700 nodes, 47,600 solid, thick shell elements and 421,200 SPH particles. The model represents a SEA with a 3-inch plunger and an area ratio of 10. Computations performed in LS-DYNA provided both graphical and numerical results for analysis.

The flange-end of the cylinder has zero displacement along the direction of simulated impact. Contact interfaces defined between plunger, bush bearing, sleeve, cylinder, and UHMWPE parts allow for plunger motion into the core. The core material assumes a piecewise-linear plasticity model with yield stress of 4.8 ksi and ultimate stress of 8.0 ksi for 50 percent elongation and contraction according to available data. Total impacting mass was set at 27,000 lb, and the initial impact velocity was set at 12.69 ft/s to match the 30-inch drop test. Figure 61 shows the SEA model mesh. Figure 62 shows a section view of the model. The computational time step involved in this drop test simulation was 0.4 μs.

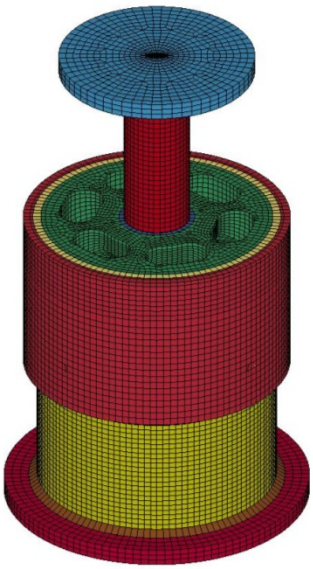

Figure 61. FEM of SEA Considered for the Analysis

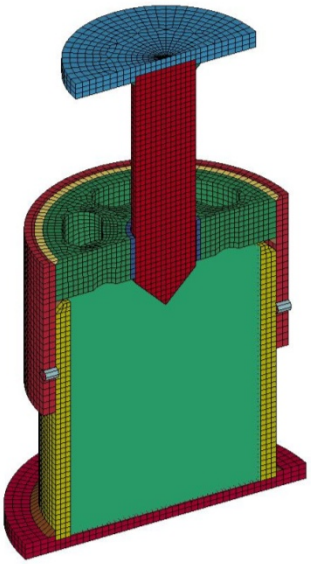

Figure 62. A Cross-Sectional View of the FEM Showing Meshing of Components

For the analysis, researchers assigned material parameters for the cylinder, plunger, outer sleeve, bush bearing, and the UHMWPE, based on published data. Because of the extremely high-strength requirement, the seamless cylinder and the plunger are high-strength low-alloy 4140 steel. This material provides tensile yield strength of 140 ksi (minimum) and an ultimate strength of 165 ksi at 18 percent elongation after heat treatment. The outer sleeve supporting the bush bearing inside was made of cold-drawn 1045 steel with a yield strength of 70 ksi, an ultimate strength of 91 ksi, and an elongation at break of 10 percent. The UHMWPE material characteristics assumed a bilinear confined compression stress-strain curve with yield stress of 4.8 ksi and the ultimate stress of 8.0 ksi. Where needed, the material data included the DSMF

derived from the quasi-static and pendulum testing describe in Sections 4.3 and 4.4. Researchers used the piecewise-linear plasticity material model for the UHMWPE to compensate for the sudden drop in the stress value and gradual stress rise observed in pendulum impact tests.

4.10.2 Results of Simulation and Analysis

Impact of the weight dropped at 12.69 ft/s generated extremely high compressive stress at the nose of the plunger. This resulted in failure of those elements in the FEM of the UHMWPE material. As nodes fail, LS-DYNA excludes them from calculation in subsequent time steps. This phenomenon was progressively replicated as the plunger penetrated into the UHMWPE material. Maximum displacement of plunger during the simulation was 6.91 in, occurring over the first 100 ms. The compressed UHMWPE then pushed back slightly on the plunger, forcing it upward against the resting weight. Figure 63 through Figure 68 show graphical results of the simulation.

Figure 63 shows a plot of plunger vertical velocity versus time over the entire event. Figure 64 shows the corresponding vertical displacement of plunger versus time.

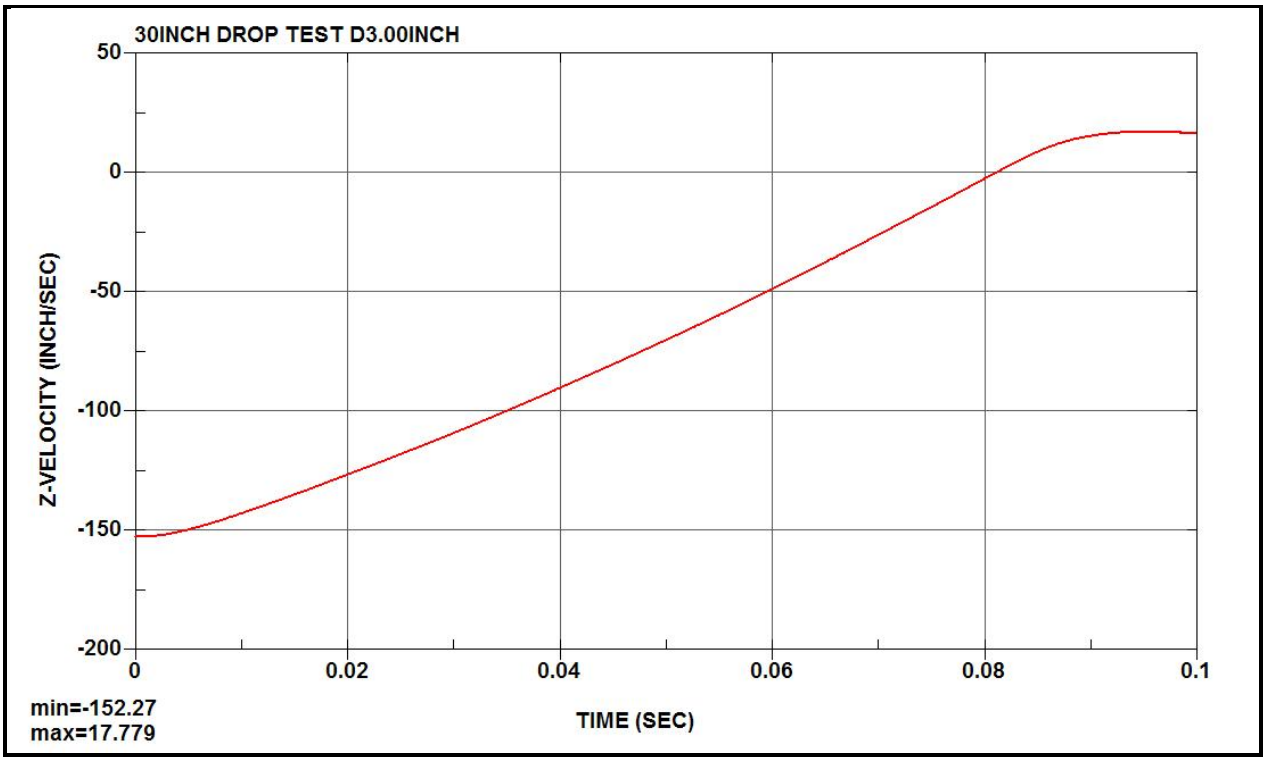

Figure 63. Plunger Vertical Velocity vs. Time

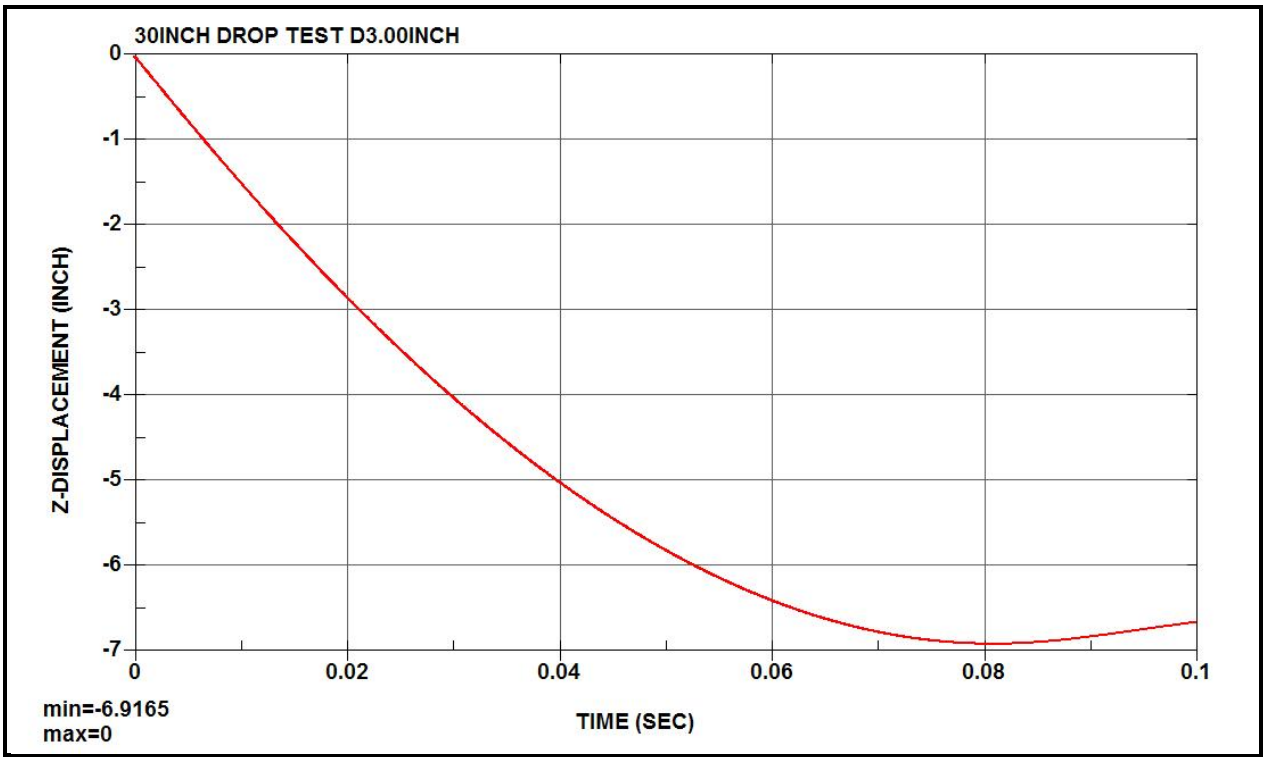

Figure 64. Plunger Vertical Displacement vs. Time

Figure 65 shows in a cross-sectional view the final position of the plunger within the cylinder at 100 ms after impact. The plunger pushed away SPH particles of UHMWPE material at the cone tip. A similar plastic zone formed around the plunger. In reality, the highly compressed zone of UHMWPE material transforms from solid state to a viscous fluid state. Fully modeling this requires a more complex two-phase computational fluid dynamics analysis that is beyond the scope of present FEA. Figure 66 shows the effective von Mises stress contours at 50 ms after impact. Figure 67 shows the effective plastic strain contours of UHMWPE at 100 ms.

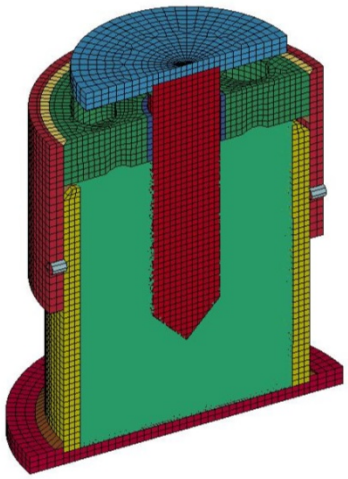

Figure 65. Simulation Result Showing Position of Plunger at 100 ms after Impact

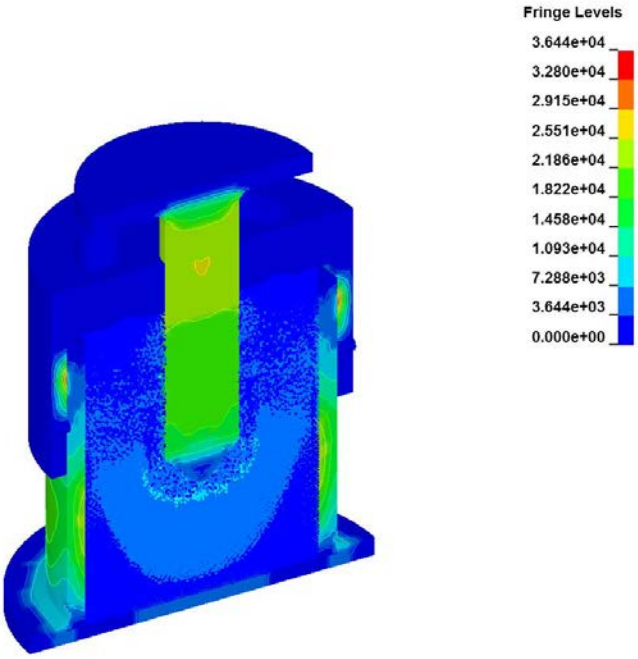

Figure 66. Effective Stress (von Mises) Contours at 50 ms after Impact

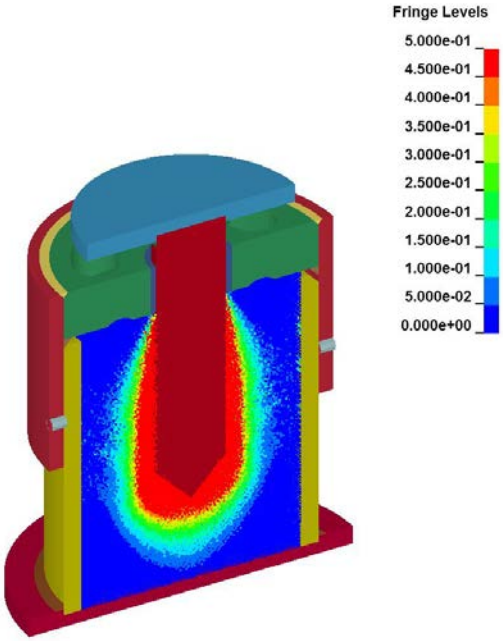

Figure 67. Effective Plastic Strain of UHMWPE at 100 ms after Impact

Figure 68 shows the post-impact axial force on the plunger versus axial displacement. This force represents the resistance offered by the UHMWPE material while crushing within the cylinder. The axial force is a calculated value, derived from the cross-sectional area of the plunger and the

corresponding stress magnitude. The red line in Figure 68 shows the actual drop test result for comparison.

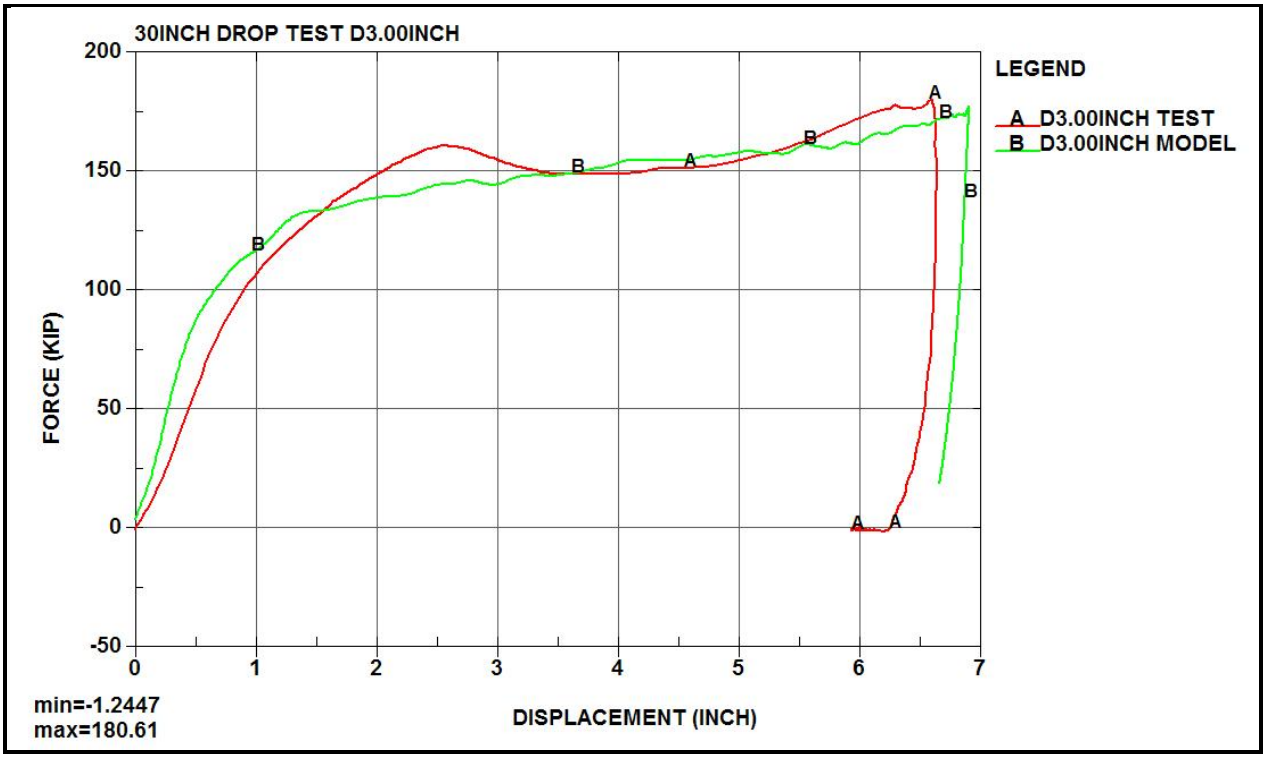

Figure 68. Axial Force vs. Axial Displacement of the Plunger

The area under the graph in Figure 68 represents the amount of KE and gravity work absorbed by the UHMWPE during the event. Over the same time period, the plunger velocity drops from 12.69 ft/s to zero within the total plunger penetration of 6.91 in. The area under this curve represents the work done by the plunger during its total displacement. The approximate area under the curve is 971,070 in-lb. As a comparison, the total energy available from the 27,000-pound weight dropping 36.57 in is 987,390 in-lb. The remaining energy dissipates through the frictional force generated as the plunger drives through the core. In the FEA, dynamic coefficient of friction between the UHMWPE and the steel plunger is 0.12, based on data available from the UHMWPE manufacturer. This comparison of FEA results with those obtained from the prototype test permits calibration of the FEM to aid in reasonable performance prediction of similar SEA with different dimensions.

5. Results and Recommendations

The overall goal of the program is to develop a cushioning system that minimizes the risk of post-collision locomotive override. To accomplish this, the researchers studied the effects of innovative cushioning systems during in-line collisions. Comparisons of FEA simulations at 20, 32.1, and 40 mph demonstrate that CEM systems will mitigate override during an in-line collision. Simulations used the current SD70MAC configuration with no CEM system in place.

In addition, researchers developed an innovative SEA that provides superior capacity compared to current railroad CEM systems. The device is a solid-state damper that undergoes a viscoelastic-phase transformation during HSRs. During plastic deformation, the device provides capacity in excess of 82,000 ft-lb using only 6 in of total stroke.

5.1 Crash Energy Management

The CEM system demonstrates that deformable and energy dissipative elements can be integrated within the current SD70MAC geometry. The inclusion of high capacity-damping elements within the chassis provides sufficient energy absorption to reduce impact speeds, and it improves load transfer throughout the chassis and underbody. As part of the approach, the CEM system controls the deformation of the pilot plate, limiting the likelihood of bending under the chassis, and mitigating the potential for override.

5.2 FEA Simulation Results

Analysis of the CEM system demonstrated that the configuration is effective in mitigating override. Simulations at three discreet speeds, 20, 32.1, and 40 mph, showed that CEM will limit the likelihood of override by controlling the impact dynamics, compensating for stiffness mismatches between cars, and dissipating energy over a wider area than current designs. The closing speed of 32.1 mph allowed for direct comparison to full-scale collision test data from previous research at TTC.

Comparisons of accelerations with and without CEM indicated that speed reductions of 15 mph or more are possible from moderate collision speeds (<40 mph). More importantly, the CEM system demonstrated dramatic reductions in vertical speeds—particularly at lower impact speeds (<35 mph)—because of the elimination of override.

5.3 Design of a SEA Device

To achieve the desired levels of energy absorption required to meet the CEM analysis, the researchers developed a solid-state SEA. The device uses a UHMWPE core as its primary dissipative element. This allows for a low-cost, low (or no)-maintenance device suitable for rail operations.

The development included laboratory testing of the device under a variety of conditions. This included low and HSR testing, low-temperature evaluation, and development of scaling parameters. A full-scale, full-speed test demonstrated the effectiveness of the design under laboratory conditions.

5.4 Applications to Railroad Industry Safety and Recommendations

Based on the team's experiences with the design and FEA from this research, it is conceivable that considerable improvements to the crashworthiness in a collision are possible for a variety of railroad vehicles. The research presented in this report focuses on locomotive applications, but the methods used are applicable to other rolling stocks as well. Crumple or crush zones at both ends of passenger coaches are now common practice within the industry. Integrating the high-capacity SEA device described in this report into the CEM system provides a means of reducing the length of the crush zones and increasing the passenger space without compromising safety. The SEA unit limits peak impact forces and prevents serious injuries to passengers. Optimization of the device allows for maximum dissipation capacity within the constraints of peak force and available stroke in the carriage.

Another potential application of the SEA-based CEM system is in hazardous material (HAZMAT)-carrying tank cars. Because of past records of accidents and release of toxic inhalation hazard chemicals near populated areas, USDOT's Pipeline and Hazardous Materials Safety Administration and FRA recently released rules that include new safety measures for transportation of dangerous materials in tank cars. In addition, European rules state that the side buffer capacity of HAZMAT-carrying tank cars be 2,212.8 in-kip (250 kJ) for older tank cars and 3,540 in-kip (400 kJ) for tank cars manufactured after 2007. On the basis of the research results obtained, similar high-capacity SEA units as part of CEM system can be used at each end of the tank car as well as at the matching end of rolling stock attached to the tank cars in a freight consist.

5.5 Further Development and Testing

To date, evaluations of the solid-state SEA are limited to analysis and laboratory testing. Evaluations of a full-scale damper at ASF-Keystone demonstrated the scalability of the system under laboratory conditions. To best evaluate the potential of a full CEM system in an in-line collision, a full-scale and full-speed test of an integrated SEA is required.

6. References

1. Mayville, R. A., Stringfellow, R. G., Rancatore, R. J., and Hosmer, T. P. (1995). *Locomotive Crashworthiness Research, Volume 1: Model Development and Validation*. Report No. DOT/FRA/ORD-95/08.1. Washington, DC: Federal Railroad Administration.
2. Kentner, P., Brundige, B., Thorpe, J. C., and Winfield, J. (Eds.). (1997). *The Car and Locomotive Cyclopedia (6th ed.).* New York: Simmons-Boardman Publishing Corp.
3. American Welding Society. (1980). Structural Welding Code, D1.1-80. Miami, FL: American Welding Society.
4. HyperMesh Users' Manual, Version 9.0. (2008). Troy, MI: Altair Computing, Inc.
5. LS-DYNA Users' Manual, Version 97.1. (2008). Livermore, CA: Livermore Software Technology Corporation.

Abbreviations and Acronyms

3D	three- dimensional
AWS	American Welding Society
CEM	crash energy management
DSMF	dynamic stress multiplying factor
FEA	finite element analysis
FEM	finite element model
FRA	Federal Railroad Administration
HAZMAT	hazardous material
HSR	high strain rate
ID	inner diameter
KE	kinetic energy
kip	kilopound(s)
ksi	kilopound(s) per square inch
µs	microsecond(s)
min	minute(s)
PE	physical energy
psi	pound(s) per square inch
QNA	QinetiQ North America
SEA	shock energy absorber
TSG	Technology Solutions Group
TTC	Transportation Technology Center
UHMWPE	ultrahigh molecular weight–polyethylene
UP	Union Pacific Railroad
USDOT	U.S. Department of Transportation